Aging and the Fluctuation-Dissipation Relation in Colloidal Glasses and Gels

ACADEMISCH PROEFSCHRIFT

ter verkrijging van de graad van doctor
aan de universiteit van Amsterdam
op gezag van de Rector Magnificus
prof. dr. J.W. Zwemmer
ten overstaan van een door het college voor promoties
ingestelde commissie, in het openbaar te verdedigen
in de Aula der Universiteit
op vrijdag 16 maart 2007, te 14:00 uur

door

Sara Jabbari-Farouji

geboren te Bandar-Abbas, Iran

Promotiecommissie:

Promotores:	prof. dr. D. Bonn and prof. dr. G.H. Wegdam
Co-promotor:	dr. E. Eiser
Overige leden:	prof. dr. L. Cugliandolo
	prof. dr. D. Frenkel
	prof. dr. F. C. MacKintosh
	prof. dr. W. K. Kegel
	dr. Th. M. Nieuwenhuizen
	dr. R. Sprik
	prof. dr. H. B. van Linden van den Heuvell

Faculteit der Natuurwetenschappen, Wiskunde en Informatica

Paranimfen: Alessia Gasparini
Salima Rafaï

This work is part of the research programme of the 'Stichting voor Fundamenteel Onderzoek der Materie (FOM)', which is financially supported by the 'Nederlandse Organisatie voor Wetenschappelijk Onderzoek (NWO)'.

Cover: Laponite gel in blue (Jakub Otwinowski, Sara Jabbari-Farouji, Stan Konings, Salima Rafaï and Nazly Sedghinegad)

Contents

1.

General Introduction

1.1 Introduction

Materials such as slurries, pastes, gels, clay suspensions, foams, emulsions and granular media are widespread in our everyday life. These substances share common properties that defy the classical definitions of solids and liquids. These complex fluids behave like solids when left to themselves, but will flow like a liquid when we exert a sufficiently large stress on them, as occurs for instance in toothpaste. In recent years, the paradigm of *soft glassy material* has been used to describe such diverse range of materials exhibiting strong local disorder and slow mesoscopic rearrangements.

This is in contrast to the textbook description of glassy systems which is often limited to that of simple molecular glasses, such as vitreous silica or polymeric glasses. Conventionally, glasses are defined as mechanically solid-like materials without any long-range order characteristic of crystalline structures: the most prominent feature of them being their enormous viscosity (10^{13} Pa.s). Over the last decade or so, however, it has become increasingly evident that the much broader concept of *soft glassy material* provides an interesting bridge between complex fluids and glasses. In this view, all systems with a relaxation time longer than or comparable to experimental timescales can be considered as glassy [1, 2]. This has recently prompted many researchers to investigate glassy behavior of this large variety of substances, characterized by relaxation times longer than typical experimental time scales of observation. Another common feature of glassy systems is *aging*, meaning that the system's properties depend on the time elapsed since the quench into a glassy state, notably the relaxation time of

the system grows in time. Understanding the nature of the glassy state and its non-equilibrium behavior (aging) remains one of the outstanding challenges in condensed-matter physics. As was pointed out by the Nobel prize winner Philip Anderson in 1995: "The glass transition remains the deepest and most important unsolved problem in solid-state physics".

Despite various experimental and theoretical studies of glasses and non-equilibrium systems in general, a unified statistical physical description of such non-equilibrium systems is still missing. One of the most interesting recent developments along these lines is the proposal to generalize the fluctuation dissipation theorem to non-equilibrium situations [3]. The fluctuation dissipation theorem relates the response of a system to a weak external perturbation to the relaxation of the spontaneous fluctuations in equilibrium [4]. The response function is proportional to the power spectral density of thermal fluctuations with a prefactor given by the temperature. This suggests a generalization for systems out of equilibrium, in which the (non-equilibrium) fluctuations are related to the response via a time-scale-dependent *effective temperature*. In this thesis, we measure the effective temperature of a few soft glassy materials: colloidal glasses and gels.

Significant progress in understanding the physics of glasses has been achieved through the use of colloids to model atoms or molecules. Like atomic glasses, colloidal systems may undergo a glass transition. However, instead of lowering the temperature to form a glass, the particle volume fraction is increased. The key advantage is that time and length scales in colloidal systems are much more readily accessible experimentally than in atomic and molecular glasses. The colloidal system that we focus on in this thesis is a synthetic clay called Laponite. It is a white powder that is easily dispersed in water. When dissolved in water, it evolves from an initially liquid-like state to a solid-like state which looks like a transparent gel. We aim here to get a better understanding of the non-equilibrium behavior of this soft glassy material.

The nature of non-ergodic states of Laponite suspensions has been the subject of discussion: both colloidal gel and colloidal glass formation have been invoked and are thought to be mutually exclusive. In this thesis, we provide experimental criteria for distinguishing gels and glasses and show that gel and glassy states of Laponite both exist and are well-defined in the limit of low and high concentrations.

Furthermore, Laponite has various applications in industry, for instance it is used in cosmetic products, hair gel and toothpaste. Therefore, understanding its flow properties is of crucial importance both during processing as well as for applications. Part of our study is devoted to the studies of flow properties of Laponite suspensions. From a more fundamental point of view, it is interesting

to be able to have 'glassy' and 'gel' states of the same material and compare their mechanical properties.

1.2 Phenomenology of glasses

Traditionally glasses are obtained by supercooling a liquid below its glass transition temperature so rapidly that the particles can not find their equilibrium configuration: the crystal. Therefore, the liquid falls out of equilibrium. The slow degrees of freedom no longer relax on the experimental time scale and the relaxation time of the supercooled liquid and the viscosity grow several orders of magnitude over a relatively small temperature interval. The temperature at which the relaxation time of the liquid becomes longer than the observation time is called the glass transition temperature T_g. Experimentally T_g is defined as the temperature at which viscosity reaches 10^{13} Pa.s or the relaxation time larger than 100 s. The determination of T_g depends however on the experimental procedure such as the cooling rate. Another equivalent definition is that T_g marks the transition from ergodic to non-ergodic behavior, i.e. the temperature at which the density-density correlation does not decay to zero on the experimental time scale. In equilibrium, the system's configurations in phase space are distributed with a probability given by the Boltzmann-Gibbs distribution. A system is said to be ergodic if the configurations that the system can explore do not depend on the initial condition, i.e. the whole phase space can be visited according to the Boltzmann-Gibbs distribution at that temperature. As a consequence, the ensemble-average of a measured quantity is equal to its time-average. To the contrary, non-ergodicity means that after a given (long) time (denoted as waiting time t_w), only a limited region of the phase space, close to the initial configuration has been accessed during the evolution of the system. As a result the system is trapped in a metastable state. In such a situation, the time and ensemble average are not necessarily equivalent. In general the ergodicity-breaking in glasses is said to be weak. This means that the system does not fall into a unique metastable state with an extremely long life-time. To the contrary, in a finite time the glass is able to access part of the phase space and escape from the metastable state in which it was initially vitrified to find itself in another metastable state.

The fact that the system spends a large amount of time exploring local minima of the free energy and does not relax towards the stable state corresponding to the global minimum of free energy leads to aging effects, as will be explained in the following.

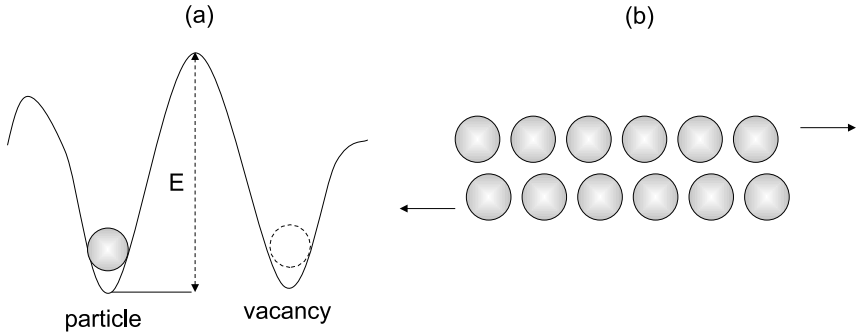

Figure 1.1: Phenomenological pictures of viscosity and diffusion coefficients a)Diffusion is proportional to the chance to jump from site to site. b) The viscosity coefficient is related to the lifetime at each site [i.e, (1/(chance to jump)].

1.2.1 Qualitative relation between viscosity and diffusion

A glass can be viewed as a material in which a slowing down of diffusive motion of the particles by many orders of magnitude with respect to the liquid state has occurred. The slowing down is most conveniently expressed in terms of the relaxation time τ which is proportional to the inverse of the diffusion coefficient $\tau \sim 1/D$. τ characterizes the time scale on which the slowest measurable processes (e.g. changes in particle positions) relax to equilibrium.

The slowing down of motion is concomitant with an enormous increase of viscosity, so that the material can not flow on experimental time scales anymore. To a certain approximation, the viscosity is connected with the relaxation time τ by the mechanical Maxwell equation $\eta \approx G_g \tau$. Here G_g is the glass modulus of the order 10^{11} Pa [5]. Consequently, the viscosity is inversely proportional to the diffusion coefficient $\eta \sim 1/D$.

A phenomenological view based on a cage-diffusion picture provides an intuitive way of relating the two transport coefficients (diffusion and viscosity) in a liquid [6].

In this phenomenological model, each particle in a liquid can be thought of as trapped in a cage, i.e. a potential well created by the constraints imposed by neighboring particles. For a particle to move, the cage has to be broken open, creating an empty space (vacancy) in which the particle can move. Classically, there is an energy barrier associated with such a rearrangement. This is illustrated very schematically in Fig. 1.1a: A certain activation energy E is needed to escape from the cage. Thus the chance to jump from one site to another is proportional

to $\exp(-E/kT)$ and this must be proportional to the diffusion constant, so that

$$D = D_0 \exp(-E/kT) \tag{1.1}$$

where D_0 is a constant.

The shear viscosity is related to the time an atom remains at a given site, since in dense liquid it is governed by the rate at which shear can take place between two layers of atoms. This is illustrated in Fig. 1.1b. The viscosity is proportional to the reciprocal of the chance for a jump from site to site, or to $\exp(E/kT)$, i.e the inverse of the diffusion coefficient.

$$\eta = \eta_0 \exp(E/kT) \tag{1.2}$$

where η_0 is a material constant.

A system following this type of behavior is said to show "Arrhenius behavior". A large number of materials show Arrhenius behavior for temperatures above T_g. Such substances show small jumps in their specific heat across the glass transition. They are known as strong glass forming liquids. Examples of these materials are SiO_2 (window glass) and GeO_2.

On the other hand, there are materials that show large deviations from the Arrhenius law and the viscosity changes with T are described by the so called Vogel-Fulcher-Tammann law [7, 8, 9]:

$$\eta = \eta_0 \exp(\frac{AT_0}{T - T_0}) \tag{1.3}$$

These materials are referred to as fragile glass formers and the constant A characterizes the degree of fragility of the material. They usually present a big jump in heat capacity at T_g. Some examples of fragile glass formers are o-Terphenyl, toluene, chlorobenzene and polymers. The proportionality of relaxation time and viscosity fails near the glass transition, as there have been for instance reports of violations of the Stokes-Einstein relation in structural glasses [10, 11].

1.2.2 Aging

Properties of non-equilibrium systems such as glasses may evolve in time as the system slowly evolves towards its equilibrium configuration, although never reaching it. As a result the observables of the system such as the correlation and response functions not only depend on the delay time, as is the case for a time-translation invariant system, but also on the waiting time or sample age t_w defined as the time elapsed since the sample is quenched into the non-equilibrium state.

In "hard" condensed matter systems, the quench is realized by means of a temperature quench. In soft glassy materials such as colloidal systems and foams, this can be achieved by increasing the volume fraction of, for instance, particles or bubbles. Examples of correlations that can be measured are density fluctuations measured by dynamic light scattering in soft glassy materials or magnetization correlations in spin glasses. Examples of typically measurable response functions are the mechanical response from rheological measurements and the magnetic response in spin glasses. Usually, a two step decay of the form below is observed in the correlation and the response functions of glassy systems [12, 13, 14]:

$$C(t, t_w) \simeq C_\infty(t - t_w) + C_{ag}(t, t_w) \tag{1.4}$$

$$R(t, t_w) \simeq R_\infty(t - t_w) + R_{ag}(t, t_w) \tag{1.5}$$

where $C_\infty(t - t_w)$ and $R_\infty(t - t_w)$ describe the fast decay of the correlation and the response which are time-translational invariant and do not depend on the age of the sample. $C_{ag}(t, t_w)$ and $R_{ag}(t, t_w)$ are the slow, aging parts which depend on the age of the sample and can evolve quite dramatically during aging. Depending on the system, the aging parts behave quite differently. For instance for spin glasses a behavior of the form $R_{ag}(t, t_w) \sim f(t/t_w)$ has been observed (see [15] and references therein). Some dipolar glasses, close to a ferroelectric transition, however show a very different behavior of the form $R_{ag}(t, t_w) \sim At/t_w^\mu$ in which $0 < \mu < 1$ [16, 12].

An appealing approach for understanding the complex dynamics of glassy systems such as a non-exponential two step decay is to consider the influence of a system's free-energy landscape on its relaxation processes. The dynamics of the system is viewed as the motion of the "state point" (described by the coordinates of all the particles) in the 6N dimensional configuration space. The free energy of the system as a function of particle coordinates and momenta defines a complicated 6N-dimensional surface or landscape. We may partition this phase space into basins such that the local minimization of the free energy maps any point in a basin to the same minimum. The properties of the system at a given state are then dictated by the basins sampled and their mutual accessibility.

The complicated free energy landscape, with many local minima of the free energy [17, 18] provides a natural framework for understanding aging. The interpretation of the time evolution of the system is that at early times after the quench to the glassy state, the system is able to access at least part of the phase space, and can get out of local minima by thermal activation. However, as time goes on, the system finds deeper and deeper minima, that are more difficult to escape from, and consequently the relaxation of the system is slower. Because of this, the system cannot reach thermodynamic equilibrium: it is non-ergodic.

During this aging, the viscosity increases and the diffusion coefficient of the particles decreases. This suggests that the trapping of particles in cages, formed by the constraints that neighboring particles impose, in real space is equivalent to arrest of the state-point in a local minimum of the free energy.

In theory and simulations, it is usually the potential energy landscape which is calculated. The free-energy landscape is difficult to access, since it is hard to compute the entropic contributions [19]. An example of a theoretical model based on energy landscape, which predicts aging successfully is the trap model originally developed in the context of spin glasses [17] by Bouchaud. This model illustrates the basic mechanism behind aging. In the trap model, non-interacting particles evolve through a hopping mechanism in an energy landscape with wells of depth E. Trap model was further generalized by Sollich et. al. to obtain the mechanical response and the aging of soft glassy materials [20].

1.2.3 Dynamical heterogeneity

Another fundamental feature of slow dynamics that is of great current interest in supercooled fluids and glasses is dynamical heterogeneity [21, 22, 23, 24]. Dynamical heterogeneity means that there exist mesoscopic regions in the sample that transiently relax with a very different dynamics from the average one. Dynamical heterogeneities can in principle be both spatial and temporal. Spatial heterogeneity means that at a given time different regions relax with different rates. Temporal heterogeneity suggest sudden rearrangements occurring somewhere in the sample which lead to large fluctuations in the time series of some global measured quantity.

The existence of dynamical heterogeneities in supercooled liquids and glasses has been suggested on the basis of experiments performed using different techniques [21, 22, 23, 25]. Experimentally, soft materials provide a unique opportunity to study temporal and spatial heterogeneity in supercooled fluids and glasses in great detail, because the relevant length and time scales are more easily accessible than for hard condensed matter systems. Typical experiments that can detect heterogeneity in soft matter are performed using time-resolved confocal microscopy [26] or for instance the recently introduced "time-resolved light-scattering technique" that allows temporal heterogeneities to be measured [27].

In confocal microscopy one reconstructs the trajectory of each particle in a three dimensional colloidal suspension made of several thousand particles. Using this technique Kegel and van Blaaderen [28] showed that supercooled liquids and glasses of hard spheres show regions of fast moving particles in a sea of more

slowly moving particles. The dynamical heterogeneities are manifested as a non-Gaussian distribution of particle displacements, i.e. the self-part of the van Hove correlation functions $G_s(x,\tau)$

$$G_s(x,\tau) = \frac{1}{N}\langle\sum_{i=1}^{N}\delta[\mathbf{x}+\mathbf{x}_i(0)-\mathbf{x}_i(\tau)]\rangle \tag{1.6}$$

where $\mathbf{x}$ is the distance from a given particle center. The lowest order deviation of $G_s(x,\tau)$ from a Gaussian distribution is quantified by

$$\alpha_2(\tau) = \frac{< x^4(\tau) >}{3 < x^2(\tau) >^2} - 1 \tag{1.7}$$

Furthermore, they showed that $G_s(x,\tau)$ could reasonably well described by a sum of two Gaussians: a wide one for the most mobile fraction of the particles, and a narrow one for the slowest fraction.

The time-resolved light-scattering technique [27] has been developed with the aim of testing large temporal fluctuations in the two-time correlations of intensity $I(t)$, i.e. $C(t+\tau,t) =< I(t+\tau)I(t) >$. Using a multi-speckle collector, $C(t+\tau,t)$ is calculated as an average over speckles of the intensity-intensity two-time correlations. Temporal fluctuations in colloidal suspensions have been studied in this way. In order to investigate the temporal heterogeneity of the dynamics, it is useful to plot $C(t+\tau,t)$ as a function of time t for a fixed lag time τ. For temporally homogeneous dynamics, one expects $C(t+\tau,t)$ to be constant (except for small fluctuations due to measurement noise). To the contrary, a large drop of $C(t+\tau,t)$ at time t would be indicative of a sudden rearrangement event occurring between t and $t+\tau$ and leading to a significant change of the sample configuration. Large drops of $C(t+\tau,t)$ have been indeed observed in time-resolved light-scattering measurements on a variety of systems, including colloidal fractal gels and concentrated surfactant phases [27, 29].

The presence of dynamical heterogeneity can explain some of the other common features such as non-exponential relaxations and translational-rotational decoupling observed in glassy dynamics. Practically all disordered systems exhibit a distribution of relaxation times. Often enough, this distribution of time constants is observed in terms of a non-exponential normalized autocorrelation functions of for instance density which are well described by a Kohlrausch-Williams-Watts (KWW) function which is the stretched exponential function $\exp(-(t/\tau)^{\beta})$. Both numerical simulations and experiments suggest that the origin of the non-exponential relaxation in super-cooled liquids are the so called dynamical heterogeneities, i.e. a superposition of different relaxation processes [21, 22, 23].

The coefficients of rotational and self-diffusion in the viscous regime of glass-formers are accessible via NMR measurements [11, 30, 31]. Interestingly, these studies have shown that the temperature dependence of translational diffusion $D_t(T)$ differs from that of rotational diffusion $D_r(T)$ for temperatures $T < 1.2T_g$, while $D_t(T)$ and $D_r(T)$ display the same behavior at elevated temperatures, $T > 1.2T_g$. In the lower temperature regime, $D_t(T)$ displays a weaker temperature dependence relative to $D_r(T)$ and, accordingly, translational diffusion is enhanced over rotation when compared with the higher temperature situation. Within this picture of spatially distributed timescales τ, one can argue that the average timescale of rotational motion is governed by the slower contributions within the (spatial) distribution of relaxation times, $D_r(T) \propto < \tau >^{-1}$, while the faster times are more relevant in determining the average translation time with $D_t(T)$ being approximated by $< \tau^{-1} >$[32]. As a consequence of this explanation, the extent of translational enhancement is expected to correlate with the width of the relaxation time distribution and should disappear as the correlation function approaches a single exponential upon increasing temperature [33].

1.3 Fluctuation-dissipation relations

In equilibrium, the connection between the random fluctuations in a system and the response to an external perturbation is provided by the fluctuation-dissipation theorem (FDT). In statistical physics, the fluctuation dissipation theorem states that in thermodynamic equilibrium the response of a system to a small external perturbation is the same as its response to a spontaneous fluctuation. In other words, the physics governing the response of a system that is taken out of equilibrium (e.g. dragging a sphere through a liquid) can be described entirely in terms of its fluctuations about the equilibrium state ("out-of-equilibrium" in the above sentence should be understood as close to equilibrium or stationary states). This is the fundamental observation behind the fluctuation-dissipation theorem and the somewhat earlier Regression Hypothesis made by Onsager [34]. The fluctuation-dissipation theorem was proved in general by Callen and Welton in 1952 [35], although special cases of it were understood much earlier [34]. A comprehensive review article about FDT and its applications in thermally equilibrated systems has been written by Kubo [4]. Here, I first briefly review the FDT at the level which is used in this thesis. Second, I will discuss the extensions of the fluctuation-dissipation relation to strongly non-equilibrium systems like aging systems as proposed by Cugliandolo et. al. [3].

1.3.1 Fluctuation-dissipation theorem in equilibrium

Consider a system which is disturbed by an external field $f(t)$ which is weak relative to the particle interaction potential so that rates of relaxation are not affected by the applied field. Let B be some macroscopic thermodynamic variable conjugate to the perturbing field and A be another macroscopic observable whose relaxation we are interested in. Then the change in the Hamiltonian of the system is $\Delta\mathcal{H} = -fB$. The perturbation leads to a change of $< \Delta A(t) >= \int dt' R_{AB}(t,t') f(t')$ in the observable A. Therefore, the mutual response of the observable B to the external force f results as

$$R_{AB}(t,t') = \frac{< \delta A(t) >}{\delta f(t')}|_{f=0} \tag{1.8}$$

Within the linear response theory, the response function is related to the correlation function of observables A and B defined as $C_{AB}(t,t') =< A(t)B(t') > - < A(t) >< B(t') >$. Therefore, the FDT relates the response to the correlation function in equilibrium with a prefactor that is inversely proportional to the system's temperature.

$$R_{AB}(t,t') = \frac{1}{k_B T} \frac{\partial C_{AB}(t,t')}{\partial t'} \tag{1.9}$$

Note that in equilibrium, as a result of time translational invariance, both the two-time correlation and response function only depend on $s = t - t'$, i. e. $C(t,t') = C(t-t')$ and $R(t,t') = R(t-t')$.

Equivalently the FDT can be Fourier transformed and represented in the frequency domain. Note that due to causality $R(s)$ is only defined for positive times. Therefore the Fourier transforms of the response and the correlation function are one-sided:

$$\begin{aligned} \alpha(\omega) &= \alpha'(\omega) + i\alpha''(\omega) = \int_0^\infty ds R(s) \exp(i\omega s) \\ \tilde{C}(\omega) &= \Re \int_0^\infty ds C(s) \exp(i\omega s) = \frac{1}{2} S(\omega) \end{aligned} \tag{1.10}$$

where here $S(\omega) = \int_{-\infty}^{\infty} C(s) \exp(i\omega s) ds$ is the power spectrum of the correlation function. Consequently the FDT in Fourier space would read

$$\alpha'(\omega) = -\frac{\omega}{k_B T} \tilde{C}(\omega) = -\frac{\omega}{2k_B T} S(\omega). \tag{1.11}$$

Kramers-Kronig relations

Due to causality the response function $R(t)$ vanishes for $t < 0$. This means that the Laplace transform of response function $\alpha(z)$, which is a function of the complex variable z, is actually analytic in the upper half plane ($\Im z > 0$). Thus, we can apply the Cauchy theorem for complex functions. Through this identity, we can connect the real part of the response function to its imaginary part and vice versa, leading to the Kramers-Kronig relations.

$$\begin{aligned} \alpha'(\omega) &= \frac{2}{\pi} P \int_0^\infty \frac{\omega' \alpha''(\omega')}{\omega'^2 - \omega^2} d\omega' \\ \alpha''(\omega) &= \frac{2}{\pi} P \int_0^\infty \frac{\omega' \alpha'(\omega')}{\omega'^2 - \omega^2} d\omega' \end{aligned} \tag{1.12}$$

The Kramers-Kronig relations express the fact that the functions α' and α'' are not independent of each other. Indeed, one can completely recover one from the other via such a transformation knowing the full frequency behavior. This has practical consequences for the microrheology techniques which we are using in this thesis, as will be explained in the next chapter.

Explicit examples of the FDT

Einstein relation
As an explicit example, we first look at the Brownian motion of a particle in a viscous fluid, which has a direct application in the microrheology technique used in this thesis. The equation of motion of particle in the surrounding liquid is

$$m\ddot{x}(t) + \int \xi(t - t')\dot{x}(t')dt' = F_{ext} + \zeta(t) \tag{1.13}$$

Here ξ is the friction coefficient of the drag force exerted on the Brownian particle by the surrounding fluid, and ζ is the stochastic random force imparted to the particle through the thermal motion of molecules of the surrounding fluid.

The linear response $\alpha = \alpha' - i\alpha''$ of a sphere embedded in an isotropic medium and subjected to an applied oscillatory force $\mathbf{f}(\omega)$ is

$$x(\omega) = \alpha_{xx}(\omega) f(\omega) \tag{1.14}$$

where $x(\omega)$ is the resulting displacement of the particle. Therefore, in this case the FDT takes the form

$$\alpha''_{xx}(\omega) = \frac{\omega}{2k_B T} < |x^2(\omega)| > \tag{1.15}$$

which is known as the Einstein relation in frequency space.

Similarly, we can write a FDT relation for the velocity of a Brownian particle and its mobility $\mu(\omega)$.

$$\mathbf{v}(\omega) = \alpha_{vx}(\omega) f(\omega) = \mu(\omega) f(\omega) \tag{1.16}$$

Multiplying both sides of Eq. (1.14) by $i\omega$, we find that $\mu(\omega) = i\omega\alpha_{xx}(\omega)$. Knowing that $< |v^2(\omega)| >= \omega^2 < |x^2(\omega)| >$, we arrive at the following relation between the velocity correlation and mobility:

$$\mu'(\omega) = \frac{1}{2k_B T} < |v^2(\omega)| > \tag{1.17}$$

For a purely viscous liquid, we have $\alpha(\omega) = -i\alpha''$ and $\mu(\omega) = \mu' = 1/\xi = \omega\alpha''$.

If we take $f(\omega) = \zeta(\omega)$ in Eq. (1.16), we can obtain the relation between the power spectrum of the random force and the drag coefficient $\xi(\omega) = 1/\mu(\omega)$. From Eq. (1.16), we have $< |v^2(\omega)| >=< |\mu^2(\omega)| >< |\zeta^2(\omega)| >$, replacing this in the FDT relation Eq. (1.17), we get

$$< |\zeta^2(\omega)| >= 2k_B T \frac{\mu'(\omega)}{< |\mu^2(\omega)| >} = 2k_B T \xi'(\omega) \tag{1.18}$$

This relation shows that the drag force that a particle experiences in the fluid at a microscopic level is due to the randomly fluctuating forces acting on the particle at finite temperature. These random forces are at the origin of macroscopic dissipation.

Nyquist theorem

Another important example of the FDT with important applications is simple electrical circuits is Nyquist theorem. There, an electric current satisfies an equation similar to that of a particle in a dissipative medium:

$$(R + iL\omega) I(\omega) = V_{ext}(\omega) + \zeta(\omega) \tag{1.19}$$

where L is the inductance, I is the current. V_{ext} represents a (constant or slowly varying) external applied field, R is the resistance, and ζ is the fluctuating voltage related to dissipation. Taking the ensemble average of this equation yields the familiar law relating the voltage, current, and resistance $V_{ext} = IZ$, in which $Z = R + \imath L\omega$ is the impedance. The impedance Z here is analogous to the drag coefficient ξ of a Brownian particle, and a similar analysis to what was done above leads to the FDT for the fluctuations of the noise voltage

$$Z'(\omega) = \frac{1}{2k_B T} < |\zeta^2(\omega)| > \tag{1.20}$$

This general relationship between voltage fluctuations and the impedance in a circuit is known as the Nyquist theorem. It is another special case of the FDT.

1.3.2 Fluctuation-dissipation relation in non-equilibrium

In practice, non-equilibrium behavior is observed in two typical situations. The first one is the case of an aging glassy material, whose relaxation time grows with time. The second practical way of creating a non-equilibrium situation is to drive the system by applying some external field or force, which feeds energy into it on large scales. In the latter case the system often reaches a stationary state and recovers time-translational invariance, while glassy systems are non-stationary and the time-translational invariance is broken.

Systems that are either driven by an external force or that are glassy are not thermally equilibrated because they show very slow relaxation processes. Therefore one can not define a temperature for such systems in the usual sense and the principles and theories of equilibrium statistical mechanics do not necessarily hold for them.

In aging systems time-translational invariance is broken. Therefore, the observables A are dependent on the waiting-time (t_w). The validity of the fluctuation-dissipation relations (FDR) Eq. (1.9) in non-equilibrium systems can not be taken for granted. Indeed there have been reports of violation of the FDR in theoretical models of [3, 36, 37, 38] and experiments on glasses [39, 40, 41].

Given two observables depending on the waiting time $A(t_w)$ and $B(t_w)$, their correlation function and response functions are defined in a similar manner as in equilibrium, but now due to the breaking of time translational invariance the correlation function can not be written as a function of the time difference.

$$\begin{aligned} C_{AB}(t,t_w) &=< A(t)B(t_w) > - < A(t) >< B(t_w) > \\ R_{AB}(t,t_w) &= \frac{< \delta A(t) >}{\delta f(t_w)}|_{f=0};\ t > t_w \end{aligned} \tag{1.21}$$

Then the generalization of FDR would read

$$R_{AB}(t,t_w) = \frac{X(t,t_w)}{k_B T_{\text{bath}}(t,t_w)} \frac{\partial C_{AB}(t,t_w)}{\partial t_w} \tag{1.22}$$

Values of X different from unity mark a violation of FDR . These violations can persist even in the limit of long waiting times, indicating strongly non-equilibrium behavior even though one-time quantities such as entropy and average energy may evolve infinitesimally slowly.

Cugliandolo et. al. [3] suggested an extension of the FDR to non-equilibrium systems in which the deviations from the FDR are quantified by a time-scale-dependent effective temperature, i.e. $T_{\text{eff}}(t, t_w) = T/X(t, t_w)$. This effective temperature will depend on the age of glass as well. They suggested that this temperature has properties of conventional temperature for systems that are thermally in equilibrium, i.e.

- the effective temperature associated with a time scale is the one measured in a system by a thermometer in contact with the system, whose reaction time is equal to that time scale.
- it determines the direction of heat flow within that time scale
- it acts as a criterion for thermalization

Plotting the integrated response function $\chi(t, t_w)$ versus the correlation function gives us the FD plot. The slope of this curve determines the effective temperature of the system. Therefore deviations from a straight line in the FD plot characterize the non-equilibrium nature of the system. The slope at short times gives the bath temperature, while at long times it gives an effective temperature deviating from the bath temperature.

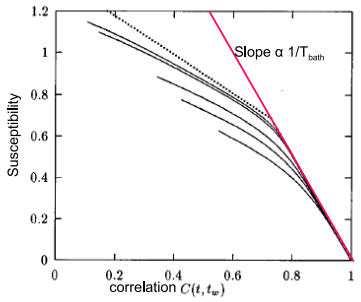

Figure 1.2: The integrated response function $\chi(t, t_w)$ vs the autocorrelation function $C(t, t_w)$ for a spin glass model at $T < T_g$. The full curves correspond to different total times t, equal, from bottom to top, to 12.5, 25, 37.5, 50, and 75, respectively ($t_w < t/4$ throughout!). The dots represent the analytical solution for $t_w \longrightarrow \infty$. Neither $\chi(t, t_w)$ nor $C(t, t_w)$ achieve stationarity. This figure is taken from ref. [3].

In systems with slow dynamics, such as spin glasses and colloidal glasses, for short delay times $\tau = t - t_w \ll t_w$, the correlation function in general first shows a fast decay from C_0 to some plateau value. This part is time translationally invariant. Consequently, at these time scales the system thermalizes with the bath and one obtains $T_{\text{eff}}(t, t_w) = T_{\text{bath}}$. Therefore the slope of the FD plot is proportional to $1/T_{\text{bath}}$ at large values of the correlation functions. On the other hand in the limit of long times $t, t_w \to \infty$ and $(t - t_w \sim t_w)$. This is the time regime for which a non-linear relation between integrated response and correlation function is predicted by some models and deviations from the FDR can be expected [3]. Fig. 1.2 shows an example of such FD plots calculated for a spin glass model taken from reference [3].

Furthermore, Cugliandolo et. al. suggested that by coupling a non-equilibrium system to a harmonic oscillator of frequency ω, the oscillator would measure the effective temperature at that frequency corresponding to the time scale $t - t_w \sim \omega^{-1}$ [3]. Therefore, it is useful to write the non-equilibrium FDR in frequency space.

$$\begin{aligned} \alpha(\omega, t_w) &= \alpha'(\omega, t_w) + \alpha''(\omega, t_w) = \int_{t_w}^{\infty} dt R(t, t_w) \exp(i\omega t) \qquad (1.23) \\ \tilde{C}(\omega, t_w) &= \Re \int_{t_w}^{\infty} dt C(t, t_w) \exp(i\omega t) = \frac{1}{2} S(\omega, t_w) \end{aligned}$$

Consequently, the FDR in the frequency domain takes the form

$$\alpha''(\omega, t_w) = \frac{\omega}{2 k_B T_{\text{eff}}(\omega, t_w)} S(\omega, t_w) \qquad (1.24)$$

In this thesis, we are going to investigate the validity of the FDR in the form of the Einstein relation for colloidal glasses and gels.

1.4 Colloidal systems

Colloidal dispersions offer a powerful testing ground for fundamental issues in statistical physics, with attention now turning to non-equilibrium phenomena such as the glass transition [42, 43]. In addition, the presence of two components, i.e. a solvent and colloids results in the emergence of new disordered states of matter such as gels which are absent in molecular systems.

Colloidal gels and glasses are two types of "jammed" states of soft condensed matter with static elasticity. They are similar in the sense that both are non-ergodic disordered states and show aging. The difference between gels and glasses

is rather clear in their ideal limits. The elasticity of a gel stems from percolated infinite network, while that of a glass stems from caging effects. In addition a gel is inhomogeneous over the characteristic length scale of the network, and has a hierarchic structural organization, while a glass is essentially homogeneous for interparticle distances a few times larger than the particle radius.

Colloidal glasses of hard spheres and fractal colloidal gels are the two limiting cases of disordered solid-like states which are relatively well understood. Colloidal glasses form at high volume fractions of hard spheres, with their solid-like properties originating from permanent trapping of particles within cages formed by neighboring particles [44, 42]. In contrast, at very low volume fractions, the presence of strong attractions between colloidal particles can lead to the formation of fractal clusters which ultimately form a space-filling network. At volume fractions between these two extremes, particles can still form non-ergodic disordered states whose nature depends on both the interaction strength and the colloid volume fraction. For example the presence of short-range attractions with high enough strengths at moderate volume fractions of hard sphere has lead to the appearance of a new type of non-equilibrium state: *attractive glass* [45, 46, 47]. The vitrification in a repulsive glass is induced by increasing the pressure and caused by steric hinderance of hard cores at high densities. While in an attractive glass it is induced by increasing the attraction strength and caused by bond formation between the particles. At this moment, a theoretical picture which unifies these limits by connecting the high density repulsive glass to the low density space-spanning network remains to be constructed.

We consider here suspensions of charged colloidal clay particles, Laponite. When a small amount of Laponite powder (weight fractions of less than a few percent) is dissolved in water, the suspension spontaneously evolves from an initially ergodic liquid-like state to a non-ergodic soft solid-like state. The isotropic non-ergodic state has recently attracted considerable attention [48, 49, 50, 51, 52, 53, 14]. It has been proposed to be a colloidal glass, but is also very often called a colloidal gel. Therefore, the nature of the non-ergodic state of this material is ambiguous. In this thesis, we provide experimental evidence for the existence both types of non-ergodic states, i.e. gel and glass. Below, we give a brief summary of our current knowledge about the non-equilibrium phase diagram of hard spheres and Laponite suspensions.

1.4.1 Hard spheres

In hard sphere colloids, it is the volume fraction instead of the temperature that plays the role of the control parameter. Upon the increase of the volume fraction

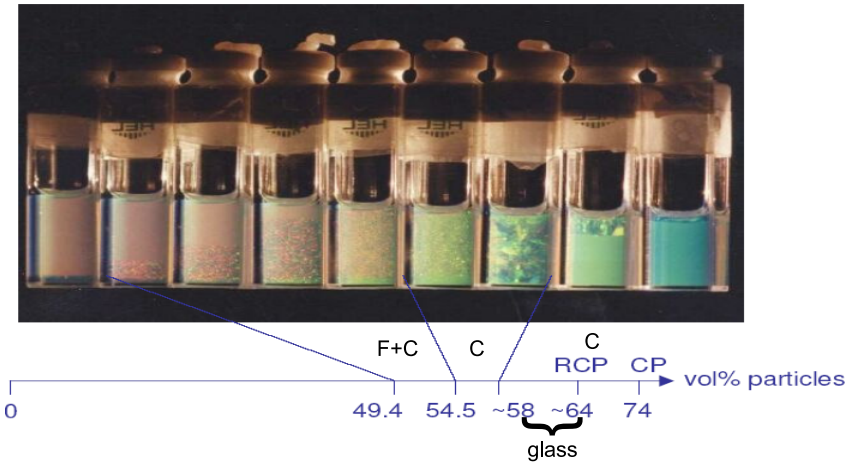

Figure 1.3: The equilibrium and non-equilibrium phase diagram of hard spheres. The figure is taken from Pusey and Van Megen [44].

of hard spheres, the system shows a full range of phase behavior from fluid → crystal → glass [44, 42]. In the range of volume fractions $0.49 < \phi < 0.545$ fluid and crystal coexist. For volume fractions $\phi > 0.545$ the crystalline solid is the stable phase of the system. The glass phase can, however, form at volume fractions between 0.58 and 0.64.

In hard spheres, the dramatic slowing down of the dynamics when approaching ϕ_g is due to the 'cage effect': the motion of any given particle is increasingly hindered by its neighbors as the particles are packed more tightly. The glass transition is therefore driven by the repulsive (excluded volume) interaction between the spheres, and the arrested phase thus formed is termed repulsive glass. Recent theoretical [54, 55, 56] and experimental [45, 46, 47] work has shown that the addition of short-ranged low energy attractive interactions can lead, surprisingly, to the melting of such a repulsive glass. This can be understood in the framework of the cage effect: particle bonding due to attractions results in the increase of the available free volume, thus loosening and eventually opening the cage. If the strength of the attraction is increased further a new arrested phase is formed, because the bonds are sufficiently long-lived to effectively confine the particles. This arrested phase is referred to as an attractive glass, although the term gel is also found in the literature. For a short general introduction to the topic of

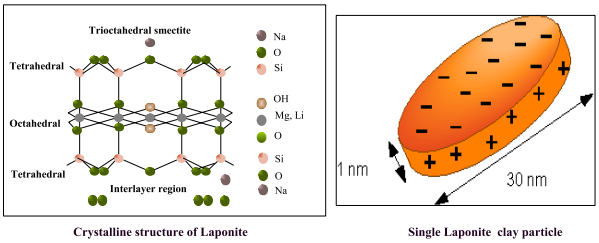

Figure 1.4: The structure of Laponite particles from Laporte company.

attractive versus repulsive glass, see [57]. A brief and clear review of the experimental work on this topic is given in [58], while reference [59] discusses recent theoretical advances.

1.4.2 Laponite

Laponite (a synthetic hectorite manufactured by Laporte Ind. Ltd, see Fig. 1.4) is a synthetic layered silicate with specific density of 2.5 g/cm^3. To a good approximation Laponite particles can be considered as rigid disks of $R \approx 15$ nm and $H \approx 1$ nm. Each particle is a mono-crystalline disk built up by three layers, two outer tetrahedral silicate layers and a central one consisting of octahedrally surrounded magnesia. Part of the magnesium in the central layer is replaced by Lithium.

Laponite comes as a white powder, and each powder particle is composed of several stacks of Laponite particles. When Laponite is dispersed in deionized water or in any polar liquid, the polar molecules penetrate between the interleaf regions (i.e. within the stacks), dissolving the interleaf cations and separating the platelet surfaces by hydration and electrostatic forces. Thus, in the final structure the particle surface has a negative charge on the order a few thousand electron charges (in water) [60], while the edges of the crystal may, depending on the pH, have small localized positive charges generated by absorption of hydroxyl groups where the crystal structure terminates [61]. This positive charge is much smaller than the negative charge at the faces and is estimated to be at most about 50e. Laponite dispersions are thus consisting of a collection of negatively charged disks and counterions, which are mainly positive sodium ions and solvent molecules.

Because of its purity and very small size, Laponite clay forms colorless and transparent suspensions which are particularly suitable for light scattering studies. In addition, Laponite suspensions form non-ergodic states at volume fractions as

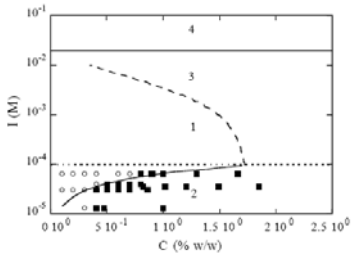

Figure 1.5: Phase behavior of Laponite suspensions as suggested in reference [62]. In this figure, I is the ionic strength with the unit (Mol/Liter) and C shows the Laponite concentration in weight percent. Region 4 is related to a macroscopic flocculation regime. The line, separating region 1 and 3, is related to the liquid/solid-like transition observed at high ionic strength. Open circles: liquid suspensions; full squares: solid-like suspensions. The full line is the prediction of the liquid-solid transition using a renormalization of the solid particle size with the Debye screening length [63].

low as 10^{-3}.

Laponite has an additional special feature which makes it more interesting from the viewpoint of non-equilibrium statistical physics. In this system, in addition to the density, time can act as a natural parameter to study the transition from an ergodic to a non-ergodic state. Since its particles are anisotropic, it also gives the possibility of studying the dynamics of the orientational degree of freedom. Furthermore, it can model a variety of natural clays omnipresent in our everyday life. In industry, it has various applications, for instance it is used as a thickener in cosmetic products.

Despite various studies on the non-equilibrium behavior of Laponite suspensions, [64, 48, 49, 65, 66, 67, 68, 53] a unified picture of the aging dynamics of Laponite suspensions and the nature of non-ergodic states is still missing. The phase diagram in Fig. 1.5 has been proposed based on experimental studies of Mourchid and Levitz et. al. [64] and Bonn et. al. [63] who proposed the existence of low volume fraction repulsive Wigner glass due to the strong electrostatic repulsions. As can be seen, at very low concentrations the suspensions are liquid (region 1). For weight fractions $C > 1$ wt%, and at ionic strengths lower than 10^{-4} M (region 2) a low volume fraction Wigner colloidal glass is formed. In region 3, corresponding to high concentrations of Laponite and moderate ionic strengths, solid-like structures are formed whose nature (being gel or glass) has been the subject of controversy. At very high salt concentrations $I > 10$ mM, flocculation

occurs (region 4). It should be noted that further experiments [52, 67, 69] show that the above phase diagram needs revision.

In this thesis, we take advantage of light scattering, rheology and microrheology to get a deeper insight into the non-equilibrium phase diagram of Laponite suspensions. We see that the above phase diagram needs to be modified according to our data, and we find evidence for a new non-ergodic state, the "attractive glass" in Laponite.

1.5 Outline of this thesis

This thesis is organized as follows:

In chapter 2 we review the experimental techniques and data analysis methods used in this thesis. The techniques which are used are light scattering, rheology and microrheology

Chapter 3 is devoted to the light scattering study of the aging dynamics of translational diffusion of Laponite particles over a wide range of concentration and salt content.

Our results suggest that there are at least two metastable minima in the free energy corresponding to gel and glass states, and that different pathways towards these non-equilibrium states exist. Furthermore, we provide experimental criteria for the distinction between gels and glasses. Finally, we present a generalized phase diagram based on our data.

Chapter 4 focuses on the study of the rotational dynamics of colloidal gels and glasses of Laponite during their evolution to a non-ergodic state. Our remarkable observation is that the slowing down of the rotational diffusion occurs at a faster rate than the translational motion. In addition, we find that aging of the rotational degree of freedom in gels and glasses of Laponite is distinctly different. Therefore the evolution of short and long time rotational diffusion supplies us with a further criterion to distinguish gels and glasses.

In Chapter 5, we investigate the validity of the fluctuation-dissipation relation in the form of the Einstein relation in hard sphere glasses and colloidal glasses and gels of Laponite at different stages of aging. We do not find any deviations from the FDR at any stage of aging in any of these systems in the frequency range 0.1-10000 Hz, contrary to previous reports [70, 41, 71].

In Chapter 6, we study the evolution of the viscoelastic properties of Laponite glasses and gels over a wide range of frequencies. Combination of one- and two-particle microrheology provides us with a strong tool for detecting spatial heterogeneities. Our measurements show that glasses are homogenous on length

scales larger than 0.5 micron. On the other hand, gels have a heterogenous structure with local shear moduli varying from one position in the sample to another. Therefore, these measurements again confirm our previous results of a distinction between gels and glasses based on light scattering studies and provide an additional criterion for discerning colloidal gels and glasses. In addition, our data show that despite the characteristic difference in structure of Laponite gels and glasses, the frequency behavior of their local shear moduli are similar. We find that for all Laponite samples the frequency-dependent complex shear modulus shows a transition from a single power law at early stages of aging to a sum of two power laws at later stages.

2.

Experimental Techniques

Experimental methods used in this thesis to probe the properties of colloidal suspensions are light scattering, rheology and microrheology. Below we describe in detail the physical basis of each of the techniques used and the information obtained by them.

2.1 Light scattering

Scattering is a general physical process in which some form of radiation, such as light, sound, or moving particles, starts to deviate from its usually straight trajectory by one or more localized non-uniformities in the medium through which it passes [72, 73, 74].

The types of non-uniformities that can cause scattering, known as scatterers or scattering centers, are too numerous to list. Some examples of them include particles, bubbles, droplets, density fluctuations in fluids, defects in crystalline solids, surface roughness, cells in organisms, and textile fibers in clothing.

In descriptions of scattering, we commonly distinguish between two general types of scattering, *elastic* and *inelastic* [72, 74]. Elastic scattering involves no (or a very small) loss or gain of energy by the radiation. Inelastic scattering does involve some change in the energy of the radiation. In this case scattering is accompanied by some *absorption* of light. Both scattering and absorption remove energy from a beam of light traversing the medium. The sum of energies attenuated by absorption and scattering processes is called *extinction*.

We will restrict ourselves here to elastic scattering. When radiation is only scattered by one localized scattering center, this is called *single scattering*. When

the radiation is scattered many times from different scattering centers we have *multiple scattering*.

Light scattering is one of the two major physical processes that contribute to the visible appearance of most objects, the other being absorption. Surfaces described as white owe their appearance almost completely to the scattering of light by the surface of the object. The absence of surface scattering leads to a shiny or glossy appearance. Light scattering can also give color to some objects, usually shades of blue as with the sky, the human iris, and the feathers of some birds.

Rayleigh scattering [72, 75] is the limiting case in which electromagnetic radiation (including light) is scattered by a small spherical volume of variant refractive index such as a particle, bubble, droplet, or density fluctuation. Scattering in this regime was first modelled successfully by Lord Rayleigh. In order for Rayleigh's model to apply, the sphere must be much smaller in diameter than the wavelength λ of the scattered wave, i.e. $(D/\lambda \ll 1)$. The upper limit is taken to be about 1/10 the wavelength. In this size regime, the exact shape of the scattering center is usually not very significant and can often be treated as a sphere of equivalent volume. The degree of scattering varies as a function of the ratio of the particle diameter to the wavelength of the radiation, along with many other factors including polarization, angle, and coherence.

The problem of electromagnetic scattering by spheres of arbitrary size was first solved by Gustav Mie and is therefore known as Mie scattering that is usually used for large particles, $D/\lambda \gg 1$ [73]. In Mie scattering, the shape of the scattering center becomes important. Although the theory is general, in practice it is only applicable for spheres, and with some modifications it can be used for spheroids and ellipsoids. Closed-form solutions for scattering by certain other simple shapes exist, but no general closed-form solution is known for arbitrary shapes.

At values of the ratio of particle diameter to the wavelength of more than about 10 $(D/\lambda > 10)$, the laws of geometric optics are mostly sufficient to describe the interaction of light with the particle, and at this point the interaction is not usually described as scattering [76].

There are two classes of research problems in scattering. One category which involves predicting how various systems will scatter radiation. The other widely studied but more difficult challenge is the "inverse scattering problem," in which the goal is to observe scattered radiation and use that observation to determine properties of either the scatterers or their interactions. An electromagnetic field impinging on a sample is scattered from inhomogeneities such as a dispersion of colloids in which the colloidal particles undergo random Brownian motion. The electric field amplitudes scattered by these different regions of sample interfere

2.1.

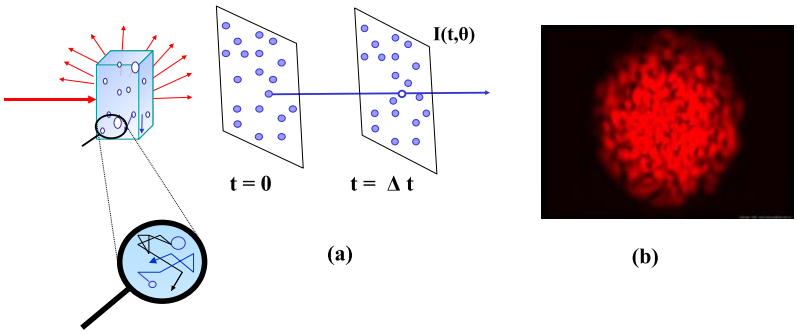

Figure 2.1: a) Schematic time-dependent speckle pattern produced from light scattered by particles undergoing Brownian motion. b) a real image of speckle pattern in light scattering experiments

and create a distribution of dark and bright regions in the far field: *a speckle pattern* (See Fig. 2.1). In fact the inverse scattering is the problem of inverting the observed speckle pattern to the real space picture. The inverse is not usually unique because several different types of scattering centers can usually give rise to the same pattern of scattered radiation, so the problem can not be solved in the general case. Fortunately, there are ways to extract some useful, albeit incomplete, information about the scatterer.

In this thesis we deal with inverse scattering problem of light from a soft glassy material (Laponite suspensions). Our aim is to obtain spatial and temporal correlations of the scatterers undergoing Brownian motion in a colloidal suspension. When illuminated with laser light, the colloids undergoing Brownian motion act as moving scattering centers. The total light scattered by an assembly of colloids produces a time and direction dependent pattern of constructive and destructive interference arising from the phase differences between elementary waves scattered from each of them. Looking at the time-averaged pattern formed by this assembly, we obtain structural information about the particles themselves and about the suspension as a whole which can then be related to thermodynamic properties. Studying this pattern is the purpose of Static Light Scattering (SLS) [77]. Studying the temporal correlation of the total scattered light at a given direction is the purpose of Dynamic Light Scattering (DLS) which gives us information about the dynamics of the colloids.

We first focus on the scattering pattern from a single particle and in the

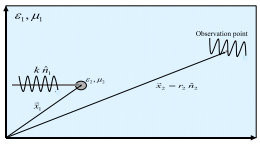

Figure 2.2: Scattering from a small dielectric sphere.

following a collection of particles (SLS). Later we will describe the DLS method in detail that is mainly used to study the dynamics of the aging colloidal gels and glasses in this thesis.

2.1.1 Single particle light scattering

Rayleigh approximation

The scattering of electromagnetic waves by systems whose dimensions are small compared to the wavelength can be described by Rayleigh scattering [75, 73, 72]. In such cases it is convenient to think of the incident radiation fields as inducing electric and magnetic multipoles that oscillate with the same frequency in definite phase relationship with the incident wave and radiate energy in all directions. If the wavelength of the radiation, λ, is long compared to the size of the scatterer R, i.e. $kR << 1$, only the lowest multipoles, usually electric and magnetic dipoles are important. Consider a plane mono-chromatic wave in an environment with refractive index n_1 and electric and magnetic permittivities ε_1 and μ_1 to be incident on a scatterer with refractive index n_2 and electric and magnetic permittivities ε_2 and μ_2 (see Fig. 2.2). If the incident direction is defined by unit vector $\hat{\mathbf{n}}_1$ and the incident polarization vector is $\hat{\epsilon}_1$, the incident electric and magnetic fields are

$$\begin{aligned} \mathbf{E_i} &= \hat{\epsilon}_1 E_0 \exp(ik\hat{\mathbf{n}}_1.\mathbf{x_1} - i\omega t) \\ \mathbf{H_i} &= \hat{\mathbf{n}}_1 \times \mathbf{E_i}/Z_1 \end{aligned} \tag{2.1}$$

where the wave vector $k = \omega/c_1$ and $Z_1 = \sqrt{\mu_1/\varepsilon_1}$. These fields induce oscillating electric, $\mathbf{p}\exp(-i\omega t)$, and magnetic, $\mathbf{m}\exp(-i\omega t)$, dipole moments in the small scatterer due to the difference between the refractive index of the scatterer and the surrounding medium. These dipoles, therefore radiate energy in all directions. In the far field at a distance r from the scatterer $k|\mathbf{x_2}-\mathbf{x_1}| = kr \gg 1$ the scattered

fields are (see Ref. [72] Sec. (9.2))

$$\begin{aligned}\mathbf{E_s} &= \frac{1}{4\pi\varepsilon_1}k^2\frac{\exp(ik(r_2-\hat{\mathbf{n_2}}.\mathbf{x_1})-i\omega t)}{r}[(\hat{\mathbf{n_2}}\times\mathbf{p})\times\hat{\mathbf{n_2}}-\hat{\mathbf{n_2}}\times\mathbf{m}/c] \quad (2.2)\\ \mathbf{H_s} &= \hat{\mathbf{n_2}}\times\mathbf{E_s}/Z_1\end{aligned}$$

where $\hat{\mathbf{n_2}}$ is a unit vector in the direction of observation and $r_2 = |\mathbf{x_2}|$.

As an example, let us look at the scattering from a small dielectric sphere of radius R with $\mu_2 = \mu_1$ and a uniform isotropic dielectric constant $\varepsilon_2(\omega)$. Then there is no induced magnetic moment and the induced electric dipole moment in the presence of uniform electric field is (see Ref. [72] Sec.(4.5))

$$\mathbf{p}_{ind} \equiv \gamma E_i = 4\pi\varepsilon_1(\frac{\varepsilon_2/\varepsilon_1-1}{\varepsilon_2/\varepsilon_1+2})R^3E_i \quad (2.3)$$

where we have introduced γ as the electric polarizability. Detectors such as photomultipliers or photodiodes respond to the intensity rather than the electric field of incident light. The instantaneous intensity that is defined as the rate of passage of energy through unit area perpendicular to the direction of propagation with certain polarization $\hat{\epsilon}$ averaged over the oscillation period, is given by

$$\begin{aligned}I_i &= \frac{1}{2Z_1}|\hat{\epsilon_1}^*.\mathbf{E}_i|^2 \quad (2.4)\\ I_s &= \frac{1}{2Z_1}|\hat{\epsilon_2}^*.\mathbf{E}_s|^2\end{aligned}$$

Therefore the ratio of scattered intensity in direction $\hat{\mathbf{n_2}}$ to the incident intensity is

$$\frac{I_s}{I_i} = \frac{k^4R^6}{r^2}(\frac{\varepsilon_2/\varepsilon_1-1}{\varepsilon_2/\varepsilon_1+2})^2|\hat{\epsilon_2}^*.\hat{\epsilon_1}|^2 = \frac{\omega^4\gamma^2}{(4\pi\epsilon_1)^2c_1^2r^2}|\hat{\epsilon_2}^*.\hat{\epsilon_1}|^2 \quad (2.5)$$

The fourth power dependence on ω was predicted by Lord Rayleigh on the basis of dimensional arguments. Note that the factor $|\hat{\epsilon_2}^*.\hat{\epsilon_1}|^2$ for the case that the polarization of incident and scattered light are in the scattering plane gives us a factor of $\cos^2\theta$ (θ is the angle between the unit vectors $\hat{\mathbf{n_1}}$ and $\hat{\mathbf{n_2}}$). While in the case that both polarizations are perpendicular to the scattering plane it is equal to 1. Therefore, there is no angular dependence for scattered intensity in the Rayleigh regime when polarization is perpendicular to scattering plane.

Scattering experiments are usually defined in terms of the Rayleigh ratio that is defined as $r^2\frac{I_s}{I_iV_s}$ in which V_s is the scattering volume. This ratio is independent of the apparatus constants and is solely determined by the properties of the scattering system.

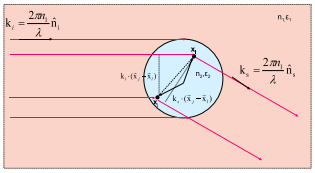

Figure 2.3: A schematic representation of scattering of light by a dielectric sphere of dielectric constant ε_2 refractive index n_2 in a medium with dielectric constant ε_1 refractive index n_1. $\mathbf{x}_l$ and $\mathbf{x}_j$ are the coordinates of two positions in the sample.

Rayleigh-Gans-Debye approximation

In the Rayleigh approximation the particles are considered as point dipoles. Further extension to dielectric objects of arbitrary size (not too large) can be achieved [75, 73] under the following conditions:

1. only a small fraction of the incident light is scattered and no multiple scattering occurs.

2. the incident light is not refracted at the interface between the surrounding medium and the particle, i.e.

$$|n_2 - n_1| \ll 1 \; . \tag{2.6}$$

3. the phase difference between the light traversing through a particle and the light passing through the surrounding medium is small, i.e.

$$2\pi|n_2 - n_1|\frac{L}{\lambda_0} \ll 1 \; ; \tag{2.7}$$

   where L is the largest dimension of the particle λ_0 is the wavelength of light in vacuum.

The particle can be considered as being composed of infinitesimally small volume elements each of them acting as a point scatterer. Fig. 2.3 shows a macromolecule with a scattering segment at position $\mathbf{x_j}$ relative to the center of mass. Collimated incident light with the wave vector $\mathbf{k_i} = \frac{2\pi n_1}{\lambda}\hat{\mathbf{n}}_\mathbf{i}$ passes through the different positions of the sample. The phase difference between the scattered light in the direction $\hat{\mathbf{n}}_\mathbf{2}$ from two different points in the sample is equal to $\frac{2\pi n_1}{\lambda}[\hat{\mathbf{n}}_\mathbf{i}.(\mathbf{x_j} - \mathbf{x_l}) - \hat{\mathbf{n}}_\mathbf{s}.(\mathbf{x_j} - \mathbf{x_l})]$ which can be rephrased as $(\mathbf{k_i} - \mathbf{k_s}).(\mathbf{x_j} - \mathbf{x_l})$.

The scattered wave vector is defined as $\mathbf{k_s} = \frac{2\pi n_1}{\lambda}\hat{\mathbf{n_s}}$. The difference between the incident wave vector and scattered wave vector is usually called the scattering wave vector denoted as $\mathbf{q} = \mathbf{k_i} - \mathbf{k_s}$ with the magnitude $|\mathbf{q}| = \frac{4\pi}{\lambda}\sin(\theta/2) = 2k\sin(\theta/2)$, where $k = 2\pi/\lambda = |\mathbf{k}_i| = |\mathbf{k}_s|$

Taking the origin at $\mathbf{x_l}$, to every position at $\mathbf{x_j}$ we can associate a phase factor as $\mathbf{q}.\mathbf{x_j}$. Accordingly, the electric field of the light scattered by the jth volume element can be written as

$$\mathbf{E_j} = b_j \exp(i\mathbf{q}.\mathbf{x_j}) E_0 \exp(-i\omega t)\hat{\epsilon}_s \tag{2.8}$$

where $\hat{\epsilon}_s$ is the polarization of the scattered light which would be the same as the polarization of incident light for the case the polarizability is isotropic and thus a scalar. From here, we assume an isotropic polarizability and that the polarization vectors of scattered and incident light are the same $\hat{\epsilon}_i = \hat{\epsilon}_s$. Therefore we skip the vector sign for the electric field. The amplitude b_j can be derived from Eq. (2.2) assuming the local polarization $p_j = \gamma_j E_0$

$$b_j = \frac{1}{4\pi\varepsilon_1} k^2 \frac{\exp(ikr)}{r}\gamma_j, \tag{2.9}$$

Here r is the distance of the center of mass of the particle from the detector. In the simple case of an isotropic material the polarizability can be estimated as $\gamma_j = (\varepsilon_j - \varepsilon_1)\delta V_s$, with V_s being the scattering volume. Therefore, the total scattered field is the sum of the electric fields scattered from different volume elements.

$$\mathbf{E}_s = E_0 \exp(-i\omega t) \sum_j b_j \exp(i\mathbf{q}.\mathbf{x_j})\hat{\epsilon}_s. \tag{2.10}$$

which can be written as an integration

$$\mathbf{E}_s = E_0 \exp(-i\omega t) \frac{1}{4\pi} k^2 \frac{\exp(ikr)}{r} \int_{V_p} d\mathbf{x}(\varepsilon_2(\mathbf{x}) - \varepsilon_1)/\varepsilon_1 \exp(i\mathbf{q}.\mathbf{x})\hat{\epsilon}_s. \tag{2.11}$$

This can be expressed in terms of refractive indices ($n = \sqrt{\frac{\varepsilon}{\varepsilon_0}}$) when ε_1 and ε_2 are not too different [75].

$$\mathbf{E}_s = E_0 \exp(-i\omega t) \frac{1}{2\pi} k^2 \frac{\exp(ikr)}{r} \int_{V_p} d\mathbf{x}(n_2(\mathbf{x}) - n_1)/n_1 \exp(i\mathbf{q}.\mathbf{x})\hat{\epsilon}_s \tag{2.12}$$

Mie scattering

For a spherical particle of arbitrary size, the angular distribution of scattered light intensity is given by the Mie theory [73, 78]. The solution is obtained by solving the problem of a plane electromagnetic wave incident on a uniform uncharged sphere of arbitrary radius and refractive index. The basic idea is to expand the incident plane wave of a fixed polarization, Eq. (2.1) in a Fourier series using the appropriate vectorial basis functions that satisfy Maxwell's equations in spherical coordinates. We then apply the suitable boundary conditions at the surface of the sphere to deduce the Fourier expansions of the scattered fields inside and outside the sphere. It can be shown that the proper basis functions are the vector spherical harmonics **M** and **N** of the form

$$\mathbf{M}_{eml} = \frac{-m}{\sin\theta}\sin(m\phi)P_l^m(\cos\theta)z_n(kr)\hat{\theta} - \cos(m\phi)\frac{dP_l^m(\cos\theta)}{d\theta}z_n(kr)\hat{\phi} \quad (2.13)$$

$$\mathbf{M}_{oml} = \frac{m}{\sin\theta}\cos(m\phi)P_l^m(\cos\theta)z_n(kr)\hat{\theta} - \sin(m\phi)\frac{dP_l^m(\cos\theta)}{d\theta}z_n(kr)\hat{\phi} \quad (2.14)$$

$$\begin{aligned}\mathbf{N}_{eml} &= \frac{z_n(kr)}{kr}\cos(m\phi)n(n+1)P_l^m(\cos\theta)\hat{\mathbf{r}} \\ &+ \cos(m\phi)\frac{dP_l^m(\cos\theta)}{d\theta}\frac{1}{kr}\frac{d}{d(kr)}[kr\, z_n(kr)]\hat{\theta} \\ &- m\sin(m\phi)\frac{P_l^m(\cos\theta)}{\sin\theta}\frac{1}{kr}\frac{d}{d(kr)}[kr\, z_n(kr)]\hat{\phi}\end{aligned} \quad (2.15)$$

$$\begin{aligned}\mathbf{N}_{oml} &= \frac{z_n(kr)}{kr}\sin(m\phi)n(n+1)P_l^m(\cos\theta)\hat{\mathbf{r}} \\ &+ \sin(m\phi)\frac{dP_l^m(\cos\theta)}{d\theta}\frac{1}{kr}\frac{d}{d(kr)}[kr\, z_n(kr)]\hat{\theta} \\ &+ m\cos(m\phi)\frac{P_l^m(\cos\theta)}{\sin\theta}\frac{1}{kr}\frac{d}{d(kr)}[kr\, z_n(kr)]\hat{\phi}\end{aligned} \quad (2.16)$$

where $z_n = \{j_l, y_l\}$ are the spherical Bessel functions of the first and second kind of order l and P_l^m are the Legendre polynomials of the first kind of degree l and order m. The subscripts o and e denote the sine and cosine functions (odd and even) for the θ dependence.

Now, we express the incoming plane wave in this basis, assuming that the electric field is polarized in the x direction and is propagating in the z direction.

$$\begin{aligned} \mathbf{E_i} &= \hat{\mathbf{x}}_1 E_0 \exp(ikr\cos\theta) \\ \hat{\mathbf{x_1}} &= \sin\theta\cos\phi\,\hat{\mathbf{r}} + \cos\theta\cos\phi\,\hat{\theta} - \sin\phi\,\hat{\phi} \end{aligned} \tag{2.17}$$

From now on, we omit the trivial time dependence of the electric field $\exp(-i\omega t)$.

Using the orthogonality of the basis functions and rejecting harmonics involving y_n (since they diverge at the origin), the infinite vector spherical harmonic expansion of the plane wave is given by:

$$\mathbf{E}_i = E_0 \sum_{l=1}^{\infty} i^l \frac{2l+1}{l(l+1)} (\mathbf{M}_{01l}^{(1)} - i\mathbf{N}_{r1l}^{(1)}) \tag{2.18}$$

where the superscript (1) denotes a radial dependence given by the spherical Bessel of the first kind. The expression for $\mathbf{H}$ follows from taking the curl of $\mathbf{E}$.

We should solve the Maxwell equations for the field inside the sphere and the scattered field, given the incident field above (Eq. 2.18). In order to do this we must impose the boundary conditions on the fields at the surface of the sphere:

$$(\mathbf{E}_i + \mathbf{E}_s - \mathbf{E}_a) \times \hat{\mathbf{r}} = (\mathbf{H}_i + \mathbf{H}_s - \mathbf{H}_a) \times \hat{\mathbf{r}} = 0 \tag{2.19}$$

where $\mathbf{E}_i$ is the incident field, $\mathbf{E}_s$ is the scattered field and $\mathbf{E}_a$ is the electric field inside the sphere, with magnetic fields similarly defined.

To determine the coefficients, we should expand the internal and scattered fields in our basis. Here, we are interested in solutions of the fields outside the sphere. The resulting scattered fields outside the sphere are:

$$\begin{aligned} \mathbf{E}_s &= E_0 \sum_{l=1}^{\infty} i^l \frac{2l+1}{l(l+1)} (ia_l \mathbf{N}_{e1l}^{(3)} - b_l \mathbf{M}_{o1l}^{(3)}) \\ \mathbf{H}_s &= \frac{k}{\omega\mu_1} \sum_{l=1}^{\infty} i^l \frac{2l+1}{l(l+1)} (ib_l \mathbf{N}_{o1l}^{(3)} + a_l \mathbf{N}_{e1l}^{(3)}) \end{aligned} \tag{2.20}$$

where the superscript (3) indicates the radial dependence given by the the first (outgoing wave) Hankel function defined as

$$h_l^1(kr) = j_l(kr) + iy_l(kr) \longrightarrow^{kr \gg l^2} \frac{(-i)^l \exp(ikr)}{ikr} \tag{2.21}$$

and the coefficients are:

$$\begin{aligned} a_l &= \frac{\mu_1 n^2 j_l(nx)[x j_l(x)]' - \mu_2 j_l(x)[nx j_l(nx)]'}{\mu_1 n^2 j_l(nx)[x h_l^{(1)}(x)]' - \mu_2 h_l^{(1)}(x)[nx j_l(nx)]'} \\ b_l &= \frac{\mu_2 j_l(nx)[x j_l(x)]' - \mu_1 j_l(x)[nx j_l(nx)]'}{\mu_2 j_l(nx)[x h_l^{(1)}(x)]' - \mu_1 h_l^{(1)}(x)[nx j_l(nx)]'} \end{aligned} \tag{2.22}$$

where the prime indicates a derivative and $x = kR$ the size parameter and $n = n_2/n_1$ is the relative refractive index.

Now that we have the expressions for the scattered field at any point in space, we can determine the coefficients to any desired accuracy by summing the well-known expressions for the Bessel functions to as many terms as necessary. The coefficients can, in turn, be multiplied by the basis functions and summed to any desired degree of accuracy in order to get the scattered field at any point in space. In practice, the detector is usually positioned at a large distance from the scattering cell, ($r \gg L$ where L is the largest dimension of the scatterer), so we are interested in the dependence of the field at fixed r . If we set $\phi = \pi/2$ and let θ vary, we get the angular dependence of the scattered field for incoming light polarized perpendicular to the scattering plane.

2.1.2 Static Light Scattering (SLS)

Form factor

In experiments the scattered intensity of light is measured rather than the electric field is measured. Now consider a dilute suspension of colloidal particles inside a solvent with dielectric properties that obey the conditions (1-3) of Sec. 2.1.1 corresponding to the Rayleigh-Gans-Debye regime. By measuring the scattered intensity from an ensemble of colloidal particles, we can obtain the information about the size and shape of the particles.

The **Form Factor**, $F(q)$, of the particles is defined as the scattered intensity observed at wave vector $\mathbf{q}$ normalized to the scattered intensity at zero wave vector [75].

$$F(q) \equiv \langle \frac{|\mathbf{E}_s(q).\hat{\epsilon}_s|^2}{|\mathbf{E}_s(q=0).\hat{\epsilon}_s|^2} \rangle_{angle} = \langle \frac{\int_{V_p} d\mathbf{x}(n_2(\mathbf{x}) - n_1)/n_1 \exp(i\mathbf{q}.\mathbf{x})}{\int_{V_p} d\mathbf{x}(n_2(\mathbf{x}) - n_1)/n_1} \rangle_{angle} \tag{2.23}$$

In the forward direction, there is no phase difference between waves scattered from different volume elements within the sample; therefore, in the limit $q \to 0$, $F(q) \to 1$.

It would be interesting at this point to apply the above formalism to find the q-dependence of the scattered intensity for uniform spheres and disks. This yields the following form factors for spheres of radius R as:

$$F(q) = \left[3 \frac{\sin(qR) - qR\cos(qR)}{(qR)^3} \right]^2 \tag{2.24}$$

In general, a platelet such as a Laponite particle can be modelled as a cylinder of radius R and thickness L. For randomly oriented monodisperse cylinders we have

$$F(q) = \int_0^{\pi/2} \left[\frac{2J_1(qR\sin\alpha)}{qR\sin\alpha} \frac{\sin(\frac{1}{2}qL\cos\alpha)}{\frac{1}{2}qL\cos\alpha)} \right]^2 \sin\alpha d\alpha \tag{2.25}$$

where $J_1(x)$ is the first order Bessel function and the integration is over the orientation of the cylinders α. For more details see [77] and references therein. In the limit of disks with infinitesimal thickness and radius R, the form factor reduces to:

$$F(q) = \frac{2}{q^2R^2} \left[1 - \frac{1}{qR} J_1(2qR) \right] \tag{2.26}$$

A nice summary of form factors for different geometries also can be found in [77].

Effect of polydispersity

In the presence of particle size polydispersity with a size distribution $P(R)$, the total intensity $I^{poly}(q)$ becomes a weighted average of intensities $dI(q;R)$ of light scattered by $P(R)dR$ monodisperse particles of radius R in the range R and $R + dR$. The definition of the form factor modifies to [75]:

$$\begin{aligned} F^{poly}(q) &\equiv \langle \frac{|E_s^{poly}(q)|^2}{|E_s^{poly}(q=0)|^2} \rangle_{angle} \\ &= \langle \frac{\int_0^{R_{max}} dRP(R) \int_{V_R} d\mathbf{x}(n_2(\mathbf{x}) - n_1)/n_1 \exp(i\mathbf{q}.\mathbf{x})}{\int_0^{R_{max}} dRP(R) \int_{V_R} d\mathbf{x}(n_2(\mathbf{x}) - n_1)/n_1} \rangle_{angle} \end{aligned} \tag{2.27}$$

Structure factor

Now that we know about the q-dependence of scattered light from a single particle, let us see how the scattered intensity will be affected by a collection of interacting particles undergoing Brownian motion. In this case the total scattered field can be written as the sum of integrals ranging over the volumes $V_p, p = 1, 2, ..., N$, occupied by the N colloidal particles in the scattering volume:

$$\mathbf{E}_s = E_0 \exp(-i\omega t)\frac{1}{2\pi}k^2\frac{\exp(ikr)}{r}\sum_{p=1}^{N}\int_{V_p} d\mathbf{x}\,(n_2(\mathbf{x})-n_1)/n_1\exp(i\mathbf{q}.\mathbf{x})\hat{\epsilon}_s \quad (2.28)$$

The integration range V_p is the volume that is occupied by the p^{th} particle. For non-spherical particles this depends on the orientation of the particles. V_p also depends on the position of the p^{th} particle for any geometrical shape. Let $\mathbf{x}_p$ denote a fixed point inside the p^{th} particle, which is referred to as its position coordinate. The position coordinate dependence of V_p can easily be accounted for explicitly by changing for each p the integration variable to $\mathbf{x}' = \mathbf{x} - \mathbf{x}_p$. The new integration range V_p^0 corresponds to the volume occupied by the particle with its position coordinate at the origin. In terms of these new integration variables Eq. (2.28) reads

$$\mathbf{E}_s = E_0 \exp(-i\omega t)\frac{1}{2\pi}k^2\frac{\exp(ikr)}{r}\sum_{p=1}^{N}\exp(i\mathbf{q}.\mathbf{x}_p)\int_{V_p^0} d\mathbf{x}'\,(n_2(\mathbf{x}')-n_1)/n_1\exp(i\mathbf{q}.\mathbf{x}')\hat{\epsilon}_s. \quad (2.29)$$

Now we can calculate the mean intensity [75] from Eq. (2.29) as

$$I_s = \frac{1}{2Z_1} < |E_s(q,t).\hat{\epsilon}_s|^2 >= \frac{I_0 V_s}{r^2}\frac{k^4}{(2\pi)^2}\bar{\rho}\times\frac{1}{N}\sum_{p,m=1}^{N} B_p(q)B_m^*(q)\langle\exp(i\mathbf{q}.(\mathbf{x}_p-\mathbf{x}_m)\rangle \quad (2.30)$$

where $B_p(q) = \int_{V_p^0} d\mathbf{x}\,(n_2(\mathbf{x})-n_1)/\varepsilon_1\exp(i\mathbf{q}.\mathbf{x}')$ and $\bar{\rho} = \frac{N}{V_s}$, with V_s the total scattering volume and $\langle ...\rangle$ denotes the ensemble average over the orientations and positions of the the Brownian particles. Experimentally, this is realized by measuring and averaging the instantaneous intensity over a time long enough for the system to explore a large number of these configurations.

Now suppose that the particles are identical. Then $B_p(q) = B(q)$ and Eq. (2.30) can be simplified to

$$I_s = \frac{I_0 V_s}{r^2}\frac{k^4}{(2\pi)^2}\bar{\rho} < |B(q)|^2 > \times\frac{1}{N}\sum_{p,m=1}^{N}\langle\exp(i\mathbf{q}.(\mathbf{x}_p-\mathbf{x}_m)\rangle \quad (2.31)$$

Comparing the value of $< |B(q)|^2 >$ with the expression for the form factor in Eq. (2.23), we see that $< |B(q)|^2 >$ is the form factor times $V_p^2|\frac{\bar{n_2}-n_1}{n_1}|^2$, with $\bar{n_2}$ being the average refractive index of the particles.

The total scattered intensity of the particles can be factorized into two parts. The first part results from the scattering of single particles and it is nothing but the form factor. The second part accounts for the interferences of the light scattered from different particles; it is a measure of the positional correlations of the particles. We call it the *structure factor* $S(q)$ and it is defined as [75]:

$$S(q) = \frac{1}{N}\sum_{p,m=1}^{N}\langle\exp(i\mathbf{q}.(\mathbf{x}_p - \mathbf{x}_m)\rangle = |\frac{1}{\sqrt{N}}\sum_{p=1}^{N}\langle\exp(i\mathbf{q}.\mathbf{x}_p)\rangle|^2 \geq 0 \tag{2.32}$$

Therefore the total scattered intensity can be rewritten as:

$$I_s = \frac{I_0 V_s}{r^2}\frac{k^4}{(2\pi)^2}\bar{\rho}\times V_p^2|\frac{\bar{n_2} - n_1}{n_1}|^2 F(q)S(q) \tag{2.33}$$

The ensemble average in the structure factor can be expressed as an integral of the probability distribution function for the positions of the particles. The pair-distribution function is defined as

$$\begin{aligned} g(\mathbf{x}) &:= \lim_{N,V\to\infty}\frac{1}{V}\langle\sum_{p\neq m}^{N}\delta[\mathbf{x} - (\mathbf{x}_p - \mathbf{x}_m)]\,\rangle/\rho^2 \qquad (2.34)\\ &= \frac{1}{V\rho^2}\frac{1}{Z_N(V,T)}\sum_{p\neq m}^{N}\int d\mathbf{x}^N \exp(-\beta V_N(\mathbf{x}^N))\delta[\mathbf{x} - (\mathbf{x}_p - \mathbf{x}_m)] \end{aligned}$$

where ρ is the average number density of the particles and we have assumed that system is homogenous. $g(\mathbf{x})$ expresses the correlation between the densities measured at any two points with separation $\mathbf{x}$. If the system is isotropic $g(\mathbf{x})$ will only depend on the distance between the particles and is usually called the radial distribution function. As can be seen from its definition, $g(\mathbf{x})$ is directly related to the interaction potential between the particles and will be equal to 1, in ideal gas limit. The general properties of $g(x)$ which readily follow from its definition Eq. (2.34)are summarized below.

$$g(\mathbf{x}) \geq 0\ , g(\mathbf{x}\to\infty) = 1 \tag{2.35}$$

$$g(\mathbf{x}) \approx 0\ for\ \beta u(\mathbf{x}) \gg 1 \tag{2.36}$$

$$g(\mathbf{x}) = \exp(-\beta u(\mathbf{x})) + O(\rho) \tag{2.37}$$

Decomposing the sum in $S(q)$ into two terms the ones with $m = p$ and the ones

with $m \neq p$, we have

$$S(q) = \frac{1}{N}\sum_{p,m=1}^{N}\langle \exp(i\mathbf{q}.(\mathbf{x}_p - \mathbf{x}_m)\rangle = 1 + \frac{1}{N}\sum_{p\neq m}^{N}\langle \exp(i\mathbf{q}.(\mathbf{x}_p - \mathbf{x}_m)\rangle \quad (2.38)$$

$$= 1 + \frac{1}{N}\langle \sum_{p\neq m}^{N}\int d\mathbf{x}\exp(i\mathbf{q}.\mathbf{x})\delta[\mathbf{x} - (\mathbf{x}_p - \mathbf{x}_m)]\,\rangle$$

The term $\frac{1}{N}\langle\sum_{p\neq m}^{N}\int d\mathbf{x}\exp(i\mathbf{q}.\mathbf{x})\delta[\mathbf{x} - (\mathbf{x}_p - \mathbf{x}_m)]\,\rangle$ is nothing but the Fourier transform of $\rho\, g(x)$. As a final result we have

$$S(\mathbf{q}) = 1 + \rho\int d\mathbf{x}\exp(i\mathbf{q}.\mathbf{x})\,(g(\mathbf{x}) - 1) \quad (2.39)$$

$S(q)$ gives us information on the spatial arrangements of the particles inside the sample. In the $q \to 0$ limit, it is directly related to the macroscopic thermodynamic quantity of isothermal compressibility.

$$\lim_{\mathbf{q}\to 0} S(q) = \rho k_B T\,\chi_T(\rho, T) \quad (2.40)$$

2.1.3 Dynamic light scattering (DLS)

The speckle pattern from a sample illuminated with light reflects the instantaneous configuration of the scattering particles (see Fig. 2.1). Thus if one places a detector of the size of a typical speckle at a particular point in the far field, the intensity measured at this point will fluctuate according to the movement of the scatterers. In dynamic light scattering experiments [74] the objective is to measure the time dependence of the fluctuating intensities resulting form the density fluctuations, in contrast to the SLS which measures the mean intensity. The simplest function characterizing the fluctuations of the intensity is the normalized intensity autocorrelation function (IACF), defined as,

$$g(q,t) = \frac{\langle I_s(q,t)I_s(q,0)\rangle}{\langle I_s(q)\rangle^2} \quad (2.41)$$

By studying the time dependence of the scattered intensity and its temporal correlations, one can extract useful information about the dynamics of the scatterers inside the sample. One expects that at sufficiently large times the intensities $I(q,0)$ and $I(q,t)$ to be totally uncorrelated,

$$\lim_{t\to\infty} = \langle I_s(q,t)I_s(q,0)\rangle = \langle I_s(q)\rangle^2. \quad (2.42)$$

As it is obvious that we are working with scattered intensities, we skip the subscript s from now on. The normalized intensity correlation function reaches the limit $g(q,t) \to 1$ for sufficiently large delay times. Defining $\delta I(q,t) = I(q,t) - < I(q) >$, the normalized IACF can be rewritten as

$$g(q,t) = 1 + \frac{\langle \delta I(q,t) \delta I(q,0) \rangle}{\langle I(q) \rangle^2} \tag{2.43}$$

This relation shows that the fluctuations of intensity (not the intensities absolute values) are relevant for the intensity correlation function. DLS experiments measure the intensity correlation function because the detector counts the number of photons. However, when light impinges on matter it is the electromagnetic field of light that induces an oscillating dipole moment that radiates a secondary electric field of light. Therefore, it is important to establish the relationship between the field and intensity correlation function. Under the condition that the electric field amplitude is a zero-mean Gaussian variable, the Siegert relation [74] connects the normalized electric field and intensity correlation functions.

$$g(q,t) = 1 + \psi \frac{\langle (\mathbf{E}_s.(q,t).\hat{\epsilon}_s)(\mathbf{E}_s^*(q,0).\hat{\epsilon}_s) \rangle}{2 Z_1 \langle I(q) \rangle} = 1 + \psi |f(q,t)|^2 \tag{2.44}$$

where ψ is a coherence factor that depends on the size of detector relative to the speckle size and in the ideal case is 1, but in experiments is somewhat smaller than 1. The normalized electric-field time-correlation $f(q,t)$ is usually called the *intermediate scattering function* and can be expressed in terms of the dynamic structure factor [74] using Eq. (2.8)

$$f(q,t) := \frac{\langle \sum_{i,j} \exp[i\mathbf{q}.(\mathbf{x}_i(t) - \mathbf{x}_j(0))] \rangle}{\langle \sum_{i,j} \exp[i\mathbf{q}.(\mathbf{x}_i(0) - \mathbf{x}_j(0))] \rangle} = \frac{S(q,t)}{S(q)} \tag{2.45}$$

Dynamic light scattering by spherical particles undergoing Brownian motion

Here, we calculate the intermediate scattering function (ISF) of a dilute suspension of spherical particles, i.e. we neglect the interactions between the particles [74]. As a result we have $\exp[i\mathbf{q}.(\mathbf{x}_i(t) - \mathbf{x}_j(0))] = \delta_{ij} \exp[i\mathbf{q}.(\mathbf{x}_i(t) - \mathbf{x}_i(0))]$.

Furthermore the static structure factor is equal to 1 for non-interacting particles, therefore ISF reduces to

$$f(q,t) = \langle \exp[i\mathbf{q}.(\mathbf{x}_i(t) - \mathbf{x}_i(0))] \rangle. \tag{2.46}$$

In order to calculate this average we need to know the probability distribution function $P(\mathbf{x}, t; \mathbf{x}_0, 0)$, which is equal to $P(\mathbf{x}_0)P(\mathbf{x}, t|\mathbf{x}_0, 0)$. For dilute suspensions $P(\mathbf{x}_0) = 1/V$ and the conditional probability distribution function, $P(\mathbf{x}, t|\mathbf{x}_0, 0)$, is the solution of the diffusion equation for a single particle with initial condition $\mathbf{x}(t = 0) = \mathbf{x}_0$:

$$\frac{\partial}{\partial t} P(\mathbf{x}, t|\mathbf{x}_0, 0) = D\nabla^2 P(\mathbf{x}, t|\mathbf{x}_0, 0) \tag{2.47}$$

Here, D is the translational diffusion coefficient of the particles. As a result the ISF is obtained from

$$\begin{aligned} f(q,t) &= \frac{1}{V} \int d\mathbf{x} d\mathbf{x}_0 P(\mathbf{x} - \mathbf{x}_0, t|0, 0) \exp[i\mathbf{q}.(\mathbf{x}(t) - \mathbf{x}(0))] \qquad (2.48) \\ &= \int d\mathbf{x}' P(\mathbf{x}', t|0, 0) \exp(i\mathbf{q}.\mathbf{x}') \end{aligned}$$

This shows that the ISF, $f(q,t)$, is actually the Fourier-transform of the solution of the diffusion equation.

Taking the Fourier transform of the diffusion equation Eq. (2.47) we can calculate $f(q,t)$, which leads to the result

$$f(q,t) = \exp(-Dq^2 t) \tag{2.49}$$

Dynamic light scattering from axially symmetric particles

The anisotropic shape of particles gives rise to an anisotropic polarizability tensor. When such particles are placed in an electric field, the components of the dipole moments induced by the field $p_\alpha = \gamma_{\alpha\beta} E_\beta$ will not necessarily be parallel to the applied field. In such a case, the scattered field will have a non-zero component in the direction perpendicular to the polarization of the incident field. DLS under such conditions can provide us some information about the rotational motion of the particles [74]. Here, we focus on particles with axial symmetry which include ellipsoids of arbitrary aspect ratios. Rods and disks can be considered as limiting cases of ellipsoids. Furthermore, our treatment is restricted to small particle sizes, $R/\lambda \ll 1$, so that we can use the Rayleigh approximation.

For such particles, the eigenvalues of the polarizability tensor correspond to the directions perpendicular, $\gamma_\perp$, and parallel, $\gamma_{||}$, to the symmetry axis.

The total electric field scattered by particles with axially symmetric optical anisotropy (when the incident electric field is linearly polarized in vertical direction) has two components. The first is the vertically *polarized* component E_{VV} with an amplitude proportional to the average polarizability ,$\gamma = (\gamma_{||} + 2\gamma_{\perp})/3$. The second one is the horizontal *depolarized* component E_{VH}. Its amplitude is proportional to the intrinsic particle anisotropy $\beta = \gamma_{||} - \gamma_{\perp}$, which is the difference between the polarizabilities parallel and perpendicular to the optical axis.

Polarized and depolarized dynamic light scattering (DLS and DDLS) experiments measure the time correlations of VV and VH scattered intensities, respectively.

Therefore, we would like to measure the following electric field correlations

$$\begin{aligned} f_{VV}(q,t) &= \frac{\langle E_{VV}(q,t)E^*_{VV}(q,0)\rangle}{< I_{VV}(q) >} \\ &= \frac{\sum_{i,j=1}^{N}\langle \gamma^i_{VV}(t)\gamma^j_{VV}(0)\exp[i\mathbf{q}.(\mathbf{r}_i(t)-\mathbf{r}_j(0))]\rangle}{\sum_{i,j=1}^{N}\langle \gamma^i_{VV}(0)\gamma^j_{VV}(0)\exp[i\mathbf{q}.(\mathbf{r}_i(0)-\mathbf{r}_j(0))]\rangle} \\ f_{VH}(q,t) &= \frac{\langle E_{VH}(q,t)E^*_{VH}(q,0)\rangle}{< I_{VH}(q) >} \\ &= \frac{\sum_{i,j=1}^{N}\langle \gamma^i_{VH}(t)\gamma^j_{VH}(0)\exp[i\mathbf{q}.(\mathbf{r}_i(t)-\mathbf{r}_j(0))]\rangle}{\sum_{i,j=1}^{N}\langle \gamma^i_{VH}(0)\gamma^j_{VH}(0)\exp[i\mathbf{q}.(\mathbf{r}_i(0)-\mathbf{r}_j(0))]\rangle} \end{aligned} \tag{2.50}$$

These expressions in general are too complicated to calculate. However, assuming that the suspension is dilute enough so that orientations and positions of different particles are uncorrelated, we can proceed further [74].

In order to calculate these averages we need to obtain the probability distribution function of position and orientation of the particles $P(\mathbf{r}, \hat{\mathbf{u}}, t)$ in which $\mathbf{r}$ and $\hat{\mathbf{u}}$ characterize the position and orientation of the particle, respectively. The probability distribution function for dilute non-interacting particles obeys the Smoluchowski equation of the form:

$$\begin{aligned} \frac{\partial}{\partial t}P(\mathbf{r},\hat{\mathbf{u}},t) &= \hat{\mathcal{L}}_s P(\mathbf{r},\hat{\mathbf{u}},t) \\ \hat{\mathcal{L}}_s &= \bar{D}_t\nabla_r^2 + D_r\hat{\mathcal{R}} + \triangle D\nabla_r\cdot[\hat{\mathbf{u}}\hat{\mathbf{u}} - \frac{1}{3}\hat{\mathbf{I}}]\cdot\nabla_r \end{aligned} \tag{2.51}$$

with the initial condition $P(\mathbf{r},\hat{\mathbf{u}},t=0) = \delta(\mathbf{r}-\mathbf{r}_0)\delta(\hat{\mathbf{u}}-\hat{\mathbf{u}}_0)$. D_r is the rotational diffusion of the particles symmetry axes, $\bar{D}_t = 1/3(D_{||} + 2D_{\perp})$ is the weighted average of the two translational diffusion coefficients, and $\triangle D = D_{||} - D_{\perp}$ represents the difference between the two. The term proportional to $\triangle D$ in Eq. (2.51)

describes the coupling between the translational and rotational diffusion and the rotation operator is defined as $\hat{\mathcal{R}} = \hat{\mathbf{u}} \times \nabla_{\hat{u}}$.

To progress further, we ignore the coupling between the translation and rotation [74]. This leads to independent equations for the translational and rotational probability distributions. Consequently, the intermediate scattering functions factorize into a product of the correlations of the orientation of the polarizations which are purely local and do not depend on q, and the q-dependent translational correlations.

$$f_{VV}(q,t) = \langle \gamma^i_{VV}(t)\gamma^i_{VV}(0)\rangle \langle \exp[i\mathbf{q}.(\mathbf{r}_i(t) - \mathbf{r}_i(0))]\rangle \tag{2.52}$$

$$f_{VH}(q,t) = \langle \gamma^i_{VH}(t)\gamma^i_{VH}(0)\rangle \langle \exp[i\mathbf{q}.(\mathbf{r}_i(t) - \mathbf{r}_i(0))]\rangle \tag{2.53}$$

In order to calculate the polarizability correlations, the laboratory-fixed components of the polarizability tensor(γ_{VV} and γ_{VH}) are first decomposed in the reference frame fixed to the particle ($\gamma_{||}$, $\gamma_{\perp}$), hence expressed as functions of the angles of orientation. [74]. This turns out to be the product of spherical harmonics, $< Y^*_{2,-1}(\hat{\mathbf{u}}(0))Y_{2,-1}(\hat{\mathbf{u}}(t)) >$, whose average can be calculated from the rotational part of the Smoluchowski equation [75]. Likewise the translational part is calculated from the diffusion equation which is the translational part of the Smoluchowski equation. The resulting correlations are:

$$f_{VV}(q,t) = \frac{[\gamma^2 + \frac{4}{45}\beta^2 \exp(-6D_r t)]F_s(q,t)}{\alpha^2 + \frac{4}{45}\beta^2} \tag{2.54}$$

$$f_{VH}(q,t) = F_s(q,t)\exp(-6D_r t) \tag{2.55}$$

where γ is the average polarizability of the particles. $F_s(q,t) =< \exp(i\vec{q}.[\mathbf{r_i}(0) - \mathbf{r_i}(t)]) >$ is the translational self-correlation function. The contribution of the rotational motion to the VV correlation, is proportional to $\frac{4}{45}\beta^2$, i.e. optical anisotropy. This is usually small, therefore the rotational contribution to f_{VV} can be neglected. Hence the dynamics of f_{VV} reflects mainly the translational diffusion of the particles, while f_{VH} is determined by both translational and rotational motion.

Now let us estimate the magnitude of the coupling $\triangle D$ between rotational and translational diffusion for Laponite particles considered as disks of radius $R =$ 15nm and thickness 1nm. The translational and rotational diffusion coefficients of disks can be obtained from the general formula for diffusion of ellipsoids with

major semi-axis b and minor semi-axis a. The aspect ratio is defined as $\rho = a/b$. The disk corresponds to $a = 0$ and $b = R$.

The rotational diffusion of ellipsoids with above specifications first calculated by Perrin [79] is given by [74]:

$$D_r = \frac{3k_BT}{16\pi\eta b^3}\frac{(2\rho^2-1)G(\rho)-\rho}{\rho^4-1} \tag{2.56}$$

where η is the shear viscosity of the solution and $G(\rho)$ is a function of aspect ratio ρ. For oblate ellipsoids $\rho < 1$,$G(\rho)$ is

$$G(\rho) = (1-\rho^2)^{-1/2}\tan^{-1}\frac{(1-\rho^2)^{1/2}}{\rho} \tag{2.57}$$

and for prolate ellipsoids $\rho > 1$, $G(\rho)$ has the form

$$G(\rho) = (\rho^2-1)^{-1/2}\ln[(\rho^2-1)^{1/2}+\rho]. \tag{2.58}$$

Similarly, the translational diffusion coefficients can be expressed in terms of the above functions [74, 80]:

$$D_{||} = \frac{k_BT}{8\pi\eta b}G(\rho) \tag{2.59}$$

$$D_{\perp} = \frac{k_BT}{16\pi\eta b}G(\rho) \tag{2.60}$$

For disks taking $a = 0$ and $b = R$, we obtain

$$D_{||} = \frac{k_BT}{16\eta R} \tag{2.61}$$

$$D_{\perp} = \frac{3k_BT}{32\eta R} \tag{2.62}$$

As said before in DLS experiments in the VV mode, we measure the average translational diffusion $D_{0t} = 1/3(D_{||} + 2D_{\perp}) = \frac{kT}{12\eta R}$ for translational diffusion. The rotational degree of freedom around the symmetry axis can not be detected by depolarized DLS (VH mode), hence we only consider the rotation of the symmetry axis for the rotational diffusion which is

$$D_{0r} = \frac{3kT}{32\eta R^3}. \tag{2.63}$$

The relative anisotropy for Laponite particles reads: $\triangle D/D_{0t} = 0.375$, which is considerable. However, for short-time diffusion the coupling terms become important only for large scattering vectors: $qR > 1$ [75].

"Heterodyne" dynamic light scattering experiments

In the heterodyne method of light scattering, a reference beam (derived directly from the laser) is mixed with the light scattered from the sample, at the detector [74]. The reference beam is obtained either by deflecting a small fraction of intensity of laser light before it reaches the sample or by scattering the incident light from a solid object in the scattering volume. In this situation the total electric field at the detector can be written as

$$E_{tot}(\mathbf{q},t) = E_s(t) + E_L \tag{2.64}$$

Assuming that the local oscillator field E_L and the scattered light E_s are statistically independent, the intensity correlation function is:

$$\begin{aligned} G(q,t) &= \langle I_{tot}(\mathbf{q},t) I_{tot}(\mathbf{q},0)\rangle \qquad (2.65)\\ &= \langle I_s(\mathbf{q},t) I_s(\mathbf{q},0)\rangle + 2I_L(\mathbf{q})\Re(\langle E_s(\mathbf{q},t)E_s^*(\mathbf{q},0)\rangle) + 2\langle I_s(\mathbf{q})\rangle I_L(\mathbf{q}) + I_L^2(\mathbf{q}) \end{aligned}$$

In the case that $I_L \gg < I_s >$, the above function simplifies to

$$G(q,t) = 2I_L(\mathbf{q})\Re(\langle E_s(\mathbf{q},t)E_s^*(\mathbf{q},0)\rangle) + I_L^2(\mathbf{q}) \tag{2.66}$$

For dilute solutions of spherical particles, the heterodyne density fluctuation Eq. (2.66) becomes

$$G(q,t) = I_L^2(\mathbf{q}) + 2I_L(\mathbf{q})\langle I_s(\mathbf{q})\rangle \exp(-Dq^2 t). \tag{2.67}$$

2.1.4 Dynamic light scattering in non-ergodic media

In an ergodic fluid-like medium, the scattering particles are able to diffuse throughout the medium and undergo Brownian motion. Given enough time, the system evolves through a representative of all possible spatial configurations. In the course of a single experiment the system can explore enough of phase space so that the time average inherent in a measurement of a quantity gives a good estimate of its ensemble average.

In non-ergodic media such as gels and glasses, the scattering elements are localized near fixed average positions and are able only to make limited Brownian motion about these fixed positions. By virtue of this localization of scatterers, one sample of a non-ergodic system will be trapped in a restricted region of the phase space, or *sub-ensemble*, whose location and extent are determined respectively by the average positions of the scatterers and the magnitudes of their displacements. Consequently, in the course of a measurement only a restricted part of phase space

is explored, so that the time average is not necessarily equivalent to the ensemble average.

A measurement on a single non-ergodic sample provides an average over only a single sub-ensemble. Therefore, the full ensemble average of a property of a non-ergodic medium can be obtained in practice by measuring many independent sub-ensembles of the medium and averaging over them. In a light scattering experiment, the illuminated region of the sample, or *scattering volume*, seen by the detector ($\sim (200\mu m)^3$) is generally much smaller than the size of the sample ($\sim 1cm^3$) itself. Thus, one experimental sample consists of many independent sub-ensembles. Then an ensemble average of the dynamic structure factor $f(q,t)$ can be obtained by moving the sample through a series of positions so that different scattering volumes within the sample are illuminated. However, this approach for constructing the ensemble average is tedious and time-consuming. Especially, it is not practical for samples with relatively fast aging. An alternative approach would be to attempt to calculate the ensemble-averaged dynamic structure factor from its time-averaged value. Of course, this requires a knowledge of the ensemble-averaged intensity. Here, we briefly review this method which is developed by Pusey and van Megen [81].

Considering a medium which contains discrete particles or scatterers, the instantaneous field amplitude of the light scattered by N particles in a scattering volume V is

$$E(\mathbf{q},t) = \sum_{j=1}^{N} b_j \exp[i\mathbf{q}.\mathbf{r}_j(t)] \tag{2.68}$$

Non-ergodicity of the medium is introduced by allowing only limited excursions $\{\mathbf{\Delta}_j(t)\}$ of the particles about their fixed average positions $\mathbf{R}_j$. In this model, a sub-ensemble corresponds to a particular set of fixed positions $\mathbf{R}_j$. As a result a time average defined as $< X >_T = \lim_{T\to\infty} \frac{1}{T}\int_0^T dtX(t)$. Thus we can write

$$\mathbf{r}_j(t) = \mathbf{R}_j + \Delta_j(t) \tag{2.69}$$

where $\mathbf{R}_j =< \mathbf{r}_j(t) >_T$.

We now assume that:

1. The number N of the particles in the scattering volume V is large;
2. The linear dimension $V^{1/3}$ is much greater than q^{-1};
3. The medium is amorphous, i.e. the range of correlation between the particles' position is, in the full ensemble, much smaller than $V^{1/3}$;

4. In any sub-ensemble the range of correlation between the displacements $\{\mathbf{\Delta}_j(t)\}$ is also much smaller than $V^{1/3}$.

Now, our aim is to calculate the time-averaged properties of light scattered by a volume V within the non-ergodic media. For a single scattering volume in a non-ergodic medium, the total scattered field Eq. (2.68) is not a zero-mean complex Gaussian variable. This is because of the spatial restriction of the scatterers that result in small fluctuations of the phase factors ($\mathbf{q}.\mathbf{r}_j(t) < 2\pi$). However, with the help of Eq. (2.69) the scattered electric field can be written as the sum of a fluctuating component E_F and a time-independent static component E_C,

$$E(\mathbf{q},t) = E_F(\mathbf{q},t) + E_C(\mathbf{q},t), \tag{2.70}$$

where

$$E_F(\mathbf{q},t) = \sum_{j=1}^{N} b_j \exp[i\mathbf{q}.\mathbf{R}_j]\{\exp[i\mathbf{q}.\mathbf{\Delta}_j(t)] - \langle\exp(i\mathbf{q}.\mathbf{\Delta}_j(t))\rangle_T\}, \tag{2.71}$$

and

$$E_C(\mathbf{q}) = \sum_{j=1}^{N} b_j \exp[i\mathbf{q}.\mathbf{R}_j]\langle\exp(i\mathbf{q}.\mathbf{\Delta}_j(t))\rangle_T. \tag{2.72}$$

Taking advantage of assumptions (1-4), it can be shown that $E(\mathbf{q},t)$ is a zero-mean complex Gaussian variable [81]. Although the total field $E(\mathbf{q},t)$ scattered by a single volume of a non-ergodic medium considered as a function of time is not a zero-mean complex Gaussian variable, it can be decomposed into the sum of such a quantity E_F, and a constant component E_C. This insight greatly simplifies the analysis of the properties of the total field, and as a result $\langle E(\mathbf{q})\rangle_T = E_C(\mathbf{q})$ and $\langle I(\mathbf{q})\rangle_T = I_C(\mathbf{q}) + \langle I_F(\mathbf{q})\rangle_T$.

The calculation of time-averaged intensity correlation function associated with Eq. (2.70) follows from recognizing that it is equivalent to usual "heterodyne" situation where a Gaussian field and a constant field are mixed. Thus,

$$\begin{aligned}\langle I(\mathbf{q},t)I(\mathbf{q},0)\rangle_T &= \langle I_F(\mathbf{q},t)I_F(\mathbf{q},0)\rangle_T + 2I_C(\mathbf{q})\langle E_F(\mathbf{q},t)E_F^*(\mathbf{q},0)\rangle_T \\ &+ 2\langle I_F(\mathbf{q})\rangle_T I_C(\mathbf{q}) + I_C^2(\mathbf{q}).\end{aligned} \tag{2.73}$$

Now, we need to determine the time correlation function of the fluctuating component of the field. This correlation is related to the ensemble averaged normalized electric field correlation $f(\mathbf{q},t) = (Nb^2)^{-1}\sum_{j=1}^{N}\sum_{k=1}^{N}\langle b_j b_k \exp[i\mathbf{q}.(\mathbf{r}_j(0) - \mathbf{r}_k(t)]\rangle_E$:

$$\langle E_F(\mathbf{q},t)E_F^*(\mathbf{q},0)\rangle_T = \langle I_C(\mathbf{q})\rangle_E[f(\mathbf{q},t) - f(\mathbf{q},\infty)] \tag{2.74}$$

where $f(\mathbf{q},\infty)$ is defined as $\lim f(\mathbf{q},t\rightarrow\infty)$ [81]. Taking the $t=0$ limit of Eq. (2.74) gives

$$\langle I_F(\mathbf{q},t)\rangle_T = \langle I(\mathbf{q})\rangle_E[1-f(\mathbf{q},\infty)]. \tag{2.75}$$

Indeed Eq. (2.75) shows that $f(\mathbf{q},\infty)$ is the fraction of frozen-in density fluctuations in the non-ergodic medium, which is known as the non-ergodicity parameter.

The Gaussian property of $E_F(\mathbf{q},t)$ allows us to determine $\langle I_F(\mathbf{q},t)I_F(\mathbf{q},0)\rangle_T$ in terms of its electric field correlation function Eq. (2.74) by employing the Siegert relation Eq. (2.43).

Finally, from Eq. (2.73), (2.74) and (2.75) we get

$$\begin{aligned} g_T(\mathbf{q},t) &= \frac{\langle I(\mathbf{q},t)I(\mathbf{q},0)\rangle_T}{\langle I(\mathbf{q})\rangle_T^2} \qquad (2.76)\\ &= 1+Y^2\{[f(\mathbf{q},t)]^2-[f(\mathbf{q},\infty)]^2\}+2Y(1-Y)[f(\mathbf{q},t)-f(\mathbf{q},\infty)] \end{aligned}$$

in which $Y\equiv\langle I(\mathbf{q})\rangle_E/I(\mathbf{q})\rangle_T$. Inversion of Eq. (2.76) will give us our desired ensemble-averaged electric field correlation $f(\mathbf{q},t)$ in terms of the time-averaged ICF for a particular position in the sample (sub-ensemble) and the ensemble-averaged intensity $I(\mathbf{q})\rangle_E$. The full ensemble-average can be obtained from rapidly rotating and/or translating the sample to average over a large number of sub-ensembles.

$$f(\mathbf{q},t) = 1+(I(\mathbf{q})\rangle_T/I(\mathbf{q})\rangle_E)\{[g_T(q,t)-g_T(q,0)+1]^{1/2}-1\} \tag{2.77}$$

The non-ergodicity parameter $f(\mathbf{q},\infty)$ is obtained from the $t=\infty$ limit of Eq. (2.77)

$$f(\mathbf{q},\infty) = 1+(I(\mathbf{q})\rangle_T/I(\mathbf{q})\rangle_E)\{[2-g_T(q,0)]^{1/2}-1\} \tag{2.78}$$

where the rigorous limit $g(\mathbf{q},\infty)=0$ has been used [81, 82].

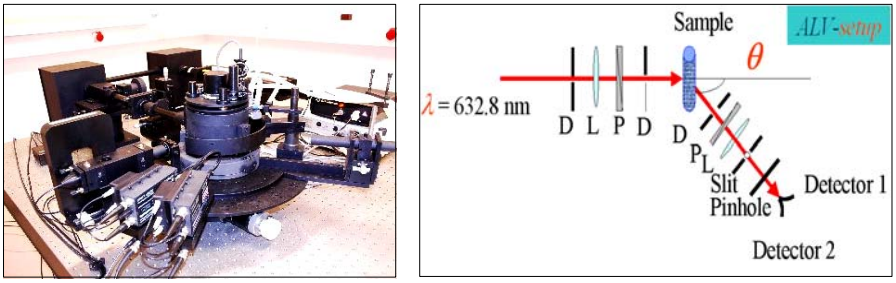

Figure 2.4: The dynamic light scattering setup used in our experiments.

Experimental setup

The dynamic light scattering setup used in our experiments is a standard one from the ALV-Laser Vertriebsgesellschaft GmbH company. The dynamic light scattering setup used in our experiments is a standard one from the ALV-Laser Vertriebsgesellschaft GmbH company. Figure 2.4 shows schematically the DLS setup. It consists of a a helium-neon laser with wavelength $\lambda = 632.8$nm . The laser light passes through a polarizer to define the polarization of incident light and several other optical elements for the purpose of alignment before it is focused on the sample. The sample tube is placed inside a quartz vat. To reduce the scattering from stray light the vat is filled with an index matched liquid (in our experiments: filtered Toluene). The scattered light from the sample traverses an analyzer which selects a given polarization direction before reaching the detectors. The detectors consist of two optical fibers coupled to avalanche photodiodes that can be used as separate channels (single mode) or together in cross correlation mode. The signal from the detectors is fed into an ALV 60X0 multiple-tau digital correlator that calculates the scattered light intensity correlation function. This correlator allows sampling times as fast as 6.5 ns. This gives us the opportunity to detect fast relaxation times of the order of a few μs. The "FAST MODE" of the ALV-60X0 correlator only works in the cross correlation mode, since the available single photon detectors do not offer good enough characteristics to allow measuring correlations at very short times. In our experiments only two special cases of the polarization for scattered light are used. The VV mode in which the polarization of the incident and scattered light are both vertical and parallel, and the VH mode in which the polarization the scattered light is horizontal and perpendicular to the polarization of incoming vertically polarized light. The setup

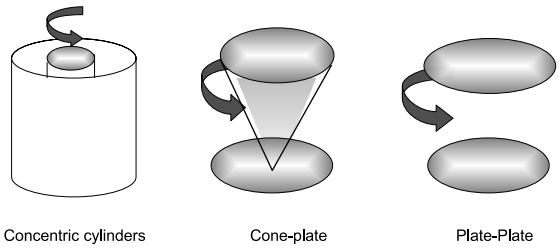

Figure 2.5: The three most common geometries used in rheometers to apply shear through drag flows

is also equipped with a cuvette rotation and translation unit. This unit allows the measurement of non ergodic samples which due to their non ergodic behavior can not be measured using a standard goniometric setup. The idea is that by using turning and up/down movement different speckles of the sample can be measured. Thus by measuring a large enough number of such independent speckles we can obtain the ensemble-averaged scattered intensity.

2.2 Rheology

Rheology is the study of the deformation and flow of a material in response to an applied stress (which can be strain imposed). Simple solids store energy and provide a spring-like elastic response, whereas simple liquids dissipate energy through viscous flow. For more complex viscoelastic materials rheological measurements reveal both the solid and fluid-like responses and generally depend on the time scale at which the sample is probed [83, 84]. One way to characterize the rheological response is to measure the shear modulus as a function of frequency. Traditionally, these measurements are performed on several milliliters of material in a mechanical rheometer by applying a small amplitude oscillatory shear strain $\gamma_0 \sin(\omega t)$ where γ_0 is the amplitude and ω is the frequency of oscillation, and measuring the resultant shear stress. Typically, commercial rheometers probe frequencies up to 10 Hz. The upper range is limited by the onset of inertial effects, when the oscillatory shear wave decays appreciably before propagating throughout the entire sample. For small shear strain amplitudes the structure is not significantly deformed and the material remains in equilibrium. In this case, the affine deformation of the material controls the measured stress. The time-dependent stress is linearly proportional to the strain, and is given by [84]:

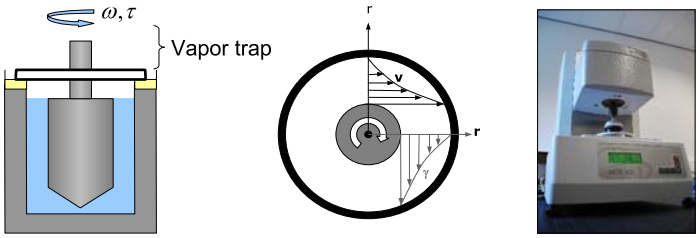

Figure 2.6: a) the schematic Couette geometry b) velocity gradient and deformation gradient in Couette geometry c) the rheometer MCR300 used in our experiments.

$$\sigma(t) = \gamma_0[G'(\omega)\sin(\omega t) + G''(\omega)\cos(\omega t)] \tag{2.79}$$

$G'(\omega)$ is the response in phase with the applied strain and is called the elastic or storage modulus, a measure of the storage of elastic energy by the sample. $G''(\omega)$ is the response out of phase with the applied strain, and in phase with the strain rate $\dot{\gamma}$, and is called the viscous or loss modulus, a measure of viscous dissipation of energy. The complex shear modulus is defined as $G^* \equiv G' + iG''$. Alternatively, it is possible to apply stress and measure strain and obtain equivalent material properties.

The most common geometries used in rheometers [83] to apply shear through simple drag flows are: sliding plates, Concentric cylinders (Couette flow), Cone-Plate and Plate-Plate disks (torsional flow), see Fig. 2.5.

Rheology measurements such as these have given valuable insight into the structural rearrangements and mechanical response of a wide range of materials. They are particularly valuable in characterizing soft materials or complex fluids, such as colloidal suspensions, polymer solutions and gels, emulsions, and surfactant mixtures [85, 83, 84].

In this thesis, we take advantage of classical rheology to study the evolution of viscoelastic properties of Laponite suspensions in the frequency range $0.01 < f < 10Hz$.

Experimental setup

The rheometer used in our experiments is a controlled shear stress rheometer (Anton Paar Physica MCR 300) with Couette geometry (CC27) (See Fig. 2.6) and occasionally cone-plate geometry. The temperature is controlled by a Peltier element (TEZ/K 150 P-C). In order to prevent evaporation during the long time

measurements, we installed a vapor trap.

2.3 Microrheology

Microrheology [86, 87, 88] is a relatively recent technique that allows us to measure the frequency-dependent response function of viscoelastic soft materials which is related to the shear moduli via the Stokes relation. It is based on the detection of small displacements, $x(t)$, of (sub)micron-sized probe particles inserted in a liquid or any other viscoelastic medium whose mechanical response, one wants to measure.

Considering the fragility of soft materials, it is promising to use a technique that can be less invasive compared to conventional rheometry. Furthermore, microrheology can probe the mechanical properties of soft materials over a wide range of frequencies ($0.1 - 10^5$Hz), while most commercial rheometers are usually restricted to frequencies of up to 10 Hz; beyond that, the inertia of the measurement geometry becomes important. The upper limit in our experiments is also set by inertial effects of the probe particle. However, since the particle is very small we can go to much higher frequencies. Moreover, conventional rheometers provide us with average bulk properties and do not allow for local measurements in inhomogeneous systems, which could in principle be the case for gels and network forming materials. This can be tested by comparing the microrheology measurements done at different positions of the sample.

There are two broad classes of microrheology (MR) techniques: those involving the active manipulation of probes by the local application of stress and those measuring the passive motions of particles due to thermal fluctuations. In either case, when the probe particles are much larger than any structural size of the material, then their fluctuating motions are a measure the macroscopic stress relaxation. Smaller particles measure the local mechanical response and also probe the effect of steric hindrances caused by local microstructure.

In the active method the response of the probe particle to an applied oscillatory stress is measured. This allows one to measure the real and imaginary parts of the response function directly as a function of the oscillation frequency. The manipulation of probe particles can be achieved by various experimental techniques such as magnetic or electric fields, optical tweezers, and atomic force microscopy techniques.

In passive microrheology experiments, when the displacement fluctuations of a probe particle (Eq. (1.15))are measured, one can obtain the imaginary part of the response function by assuming that the fluctuation-dissipation relation (FDR)

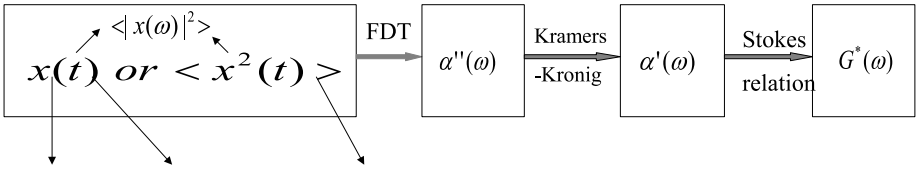

Figure 2.7: Diagrammatic summary of steps to extract the viscoelastic shear modulus in passive microrheology.

holds. The real part of the response can then be extracted from linear response theory using the Kramers-Kronig relation (Eq. (1.12)). Once both the imaginary and real parts of response function are known, we can use Stokes relation to obtain the complex shear modulus $G^* = \frac{1}{6\pi\eta R}$. In Fig. 2.7, a summary of steps to extract the viscoelastic shear moduli from the particle displacement is shown. Using the generalized Stokes-Einstein relation to obtain the macroscopic viscoelastic shear moduli of a material requires that the medium around the sphere to be treated as a continuum material. This necessitates a bead size larger than any structural length scales in the material. Therefore, one-particle microrheology is very sensitive to the local environment of the embedded bead and will not yield the macroscopic shear modulus if the material is inhomogeneous. To remedy this insufficiency, two-particle microrheology [89] has been developed. Two-particle microrheology eliminates the motion due to purely local structure and mechanics by measuring the cross-correlated motion of pairs of tracer particles within the sample. The correlated motion of the particles is not affected by the size or even shape of the tracer particles and is independent of the specific coupling between the probe and the medium. Furthermore, the length scale being probed is not the individual bead radius R but is the distance r between the tracers, which is typically 10-100 microns. This increase in length scale means that the technique is insensitive to short wavelength heterogeneities in the sample smaller than the bead separation distance and thus may probe bulk rheology even if individual particles do not.

To take full advantage of the range of frequencies and to be able to calculate the real part of the response from the Kramers-Kronig integral in passive microrheology experiments, it is necessary to use techniques that measure the mean-squared displacement (MSD) of embedded spheres with excellent temporal and spatial resolution. The MSD can be calculated from methods that directly track the particle position as a function of time or can be obtained from ensemble-averaged light

scattering experiments. Methods of particle detection vary significantly in temporal and spatial resolution. Additionally, techniques differ significantly in their ability to provide statistical accuracy over an ensemble of probes. Therefore each of these detection methods has advantages and disadvantages whose applicability depends on the type of measurements needed.

Particle tracking methods can be divided into imaging (microscopy) and non-imaging (laser detection) techniques.

The available imaging techniques are video and confocal microscopy. Techniques in image processing have been developed to automate the process of accurate particle center location to simultaneously track hundreds of embedded probes in a single field of view of the microscope with submicron precision. While video microscopy is limited to frequencies available to the camera, the strength of the technique is in its ability to obtain good statistics on ensembles of beads. Embedded spheres are imaged with a conventional light microscope using either fluorescence or bright field microscopy. Using bright field microscopy, spheres larger than a few hundred nanometers can be observed but the diffraction limited resolving power of the microscope precludes the study of smaller probes. Fluorescent labelling offers the ability to observe smaller probes up to 20 nm, which now act as point sources of light.

In a homogeneous isotropic material it is sufficient to examine the projection of the particle trajectory along a single axis. In heterogeneous materials, it may be useful to be able to obtain a two- or three-dimensional particle trajectory. In video microscopy, the motion of the particle is projected into the plane of the focus and a two dimensional trajectory is obtained for further analysis. Confocal microscopy is currently most widely used to follow the three dimensional motion of fluorescently tagged colloids [90, 91].

Non-imaging techniques are based on laser detection schemes which take advantage of optical trapping [92, 87]. In this method very low laser power is used so that the trapping force on the particle is quite low compared to the thermally driven forces of the bead ($< 5\%$). The thermally driven motion will cause the bead to move off the beams axis and deflection of the laser beam can be measured. From this deflection the displacement of the single bead is detected from which the MSD [92] or the power spectral density [87], the position correlation function in frequency space, can be calculated. This detection scheme has excellent spatiotemporal resolution such that individual particles are tracked with subnanometer precision at frequencies up to 100 kHz.

In dynamic light scattering experiments, if dilute concentrations of probe particles are used, they are statistically independent and their motion is solely due to

thermal impulses, hence one measures the self-intermediate scattering function:

$$f(q,t) = \exp[-\frac{q^2\langle\Delta r^2(t)\rangle}{6}] \times \{1 + \frac{1}{2}(\frac{q^2\langle\Delta r^2(t)\rangle}{6})^2\alpha_2(t) + \cdots\} \tag{2.80}$$

where $\alpha_2(t) = \frac{3<\Delta r^4(t)>}{5<\Delta r^2(t)>^2} - 1$ is the first non-Gaussian correction to the distribution of particle displacements. By truncating Eq. 2.80 at the second term in the curly brackets we can solve it to obtain $\langle\Delta r^2(t)\rangle$, the particle mean-squared displacement (MSD), and $\alpha_2(t)$ from measurements of $F_s(q,t)$ made at two different wave vectors [93]. Alternatively, $\langle\Delta r^2(t)\rangle$ can be extracted from the Gaussian approximation for the self-intermediate scattering function,

$$f(q,t) = \exp[-\frac{q^2\langle\Delta r^2(t)\rangle}{6}] \tag{2.81}$$

which is recovered from Eq. 2.80 when the quantity $q^2\langle\Delta r^2(t)/6$ is small.

Light scattering methods inherently average over a large ensemble of particles, and are not appropriate for samples that may exhibit local heterogeneity. However, for homogeneous samples, light scattering has the advantage of better averaging, a larger statistical accuracy, and a larger accessible frequency range than any macroscopic measurement or video-based microrheology technique.

A comprehensive review about various microrheology techniques and their applications is written by M.L. Gardel, et. al. [94]. For further information the reader can consult the concise reviews written by F. C. MacKintosh et. al. [95], M. J. Solomon [96] and A. Mukhopadhyay [97].

In this thesis, we use a microrheology technique based on optical trapping that was developed in the group of Prof. Christoph Schmidt's at the Free University of Amsterdam (VU) [98, 99]. In the following, I review the basics of optical trapping, detection and data analysis for active and passive microrheology.

2.3.1 Principles of Laser trapping

Laser trapping is a micromechanical technique that is broadly used in soft condensed matter. An optical trap employs a highly focused beam of light [100, 101, 102] to capture and manipulate small dielectric particles. Optical trapping of particles uses the momentum transfer of light scattered or diffracted by a dielectric object near the focus of light. The resulting optical force has traditionally been decomposed into two components: [94]

1. The scattering force or radiation pressure which acts along the direction of the propagating beam.

2. The gradient force which arises from induced dipole interactions with the electric field gradient and tends to pull the particles toward the focus.

In the Rayleigh regime ($d \ll \lambda$) the trapped particles are treated as point dipoles, since the electromagnetic force is a constant on the scale of the particle. The scattering force is given by

$$\mathbf{F}_s = n_s \frac{\langle \mathbf{S} \rangle \sigma}{c} \tag{2.82}$$

where $\langle \mathbf{S} \rangle$ is the time-averaged Poynting vector of the electromagnetic field and σ is the scattering cross section of a Rayleigh particle of diameter d immersed in a solvent of refractive index n_1.

The gradient force is the *Lorentz force* acting on the dipole by the electromagnetic wave:

$$\mathbf{F}_g = \frac{\gamma}{2} \nabla \langle \mathbf{E}^2 \rangle. \tag{2.83}$$

$\mathbf{E}$ is the electric field and γ is the polarizability as defined in Eq. 2.3. For stable trapping in all three dimensions, the axial gradient component of the force pulling the particles toward the focal region must exceed the scattering component of the force pushing it away from that region. This condition necessitates a very steep gradient in the light. Steep electric field gradients can be achieved using a high numerical aperture objective lens to focus the laser beam onto the sample; this allows the gradient force to dominate and form a stable three dimensional trap. As a result of this balance between gradient force and scattering force, the axial equilibrium position of the trapped particle (trap center) is located slightly above the focal plane. At the trap center the potential energy is given by

$$U = -\frac{3V_p n_2}{c} \frac{n_2^2 - n_1^2}{n_2^2 + 2n_1^2} I_0 \exp(-r^2/L^2) \tag{2.84}$$

where V_p is the volume of dielectric particle, n_2 its refractive index, and I_0 is the intensity of the laser light. Here r is the radial distance from the center of trap and L is the width of the Gaussian laser profile at the trap. The force on the particle as it moves away from the trap center is given by

$$\mathbf{F} = -\nabla U = -k_t r \exp(-r^2/L^2) \hat{\mathbf{r}} \tag{2.85}$$

in which k_t named as trap stiffness, is

$$k_t = \frac{6V_p n_2}{cL^2} \frac{n_2^2 - n_1^2}{n_2^2 + 2n_1^2} I_0. \tag{2.86}$$

Hence, for small displacements the force is approximated by Hook's law with an effective spring constant. From above expression, one can see that for stable trapping $n_2 > n_1$ is required. It suggests that the larger the difference in refractive indices of probe particle and surrounding medium, the more stable the trap will be. But this is not completely true. The above discussion is based on the scattering in the Rayleigh regime, while in the real experimental condition, the particle sizes are about one micrometer and the the typical laser wavelength is 1064 nm. Consequently the scattering from these particles lies in the Mie regime. Thus, the Rayliegh approach is only good for a qualitative understanding of the general features of the optical trapping. Calculations of trapping force on the basis of a more complicated Mie scattering [103] show that if the $n_2 - n_1 > 0.2$ the trapping is not stable and the particle will be propelled along the optical axis [104].

Furthermore, increasing the laser power or probe size gives rise to an enhanced trap restoring force. However, the laser power can be increased only up to a certain limit, above which more laser light would lead to heating or photo-damage of the optics or the examined system.

2.3.2 Position detection

As we said before, optical trapping can be used for non-imaging detection of nanometer-scale displacements. The basic principle behind this detection method (developed by Gittes and Schmidt) [105] is the far-field interference of the outgoing laser light with the scattered light from the trapped particle.

One can achieve trapping in an ordinary light microscope by focusing the laser in the specimen plane with a high numerical aperture lens (in practice a microscope objective). One convenient way to detect the particle motion uses a quadrant diode; a light sensitive diode which is divided into four equal segments being able to detect the changes in the intensity distribution. It is placed in the back focal plane of the condenser lens that collimates the outgoing laser light and the light scattered from the trapped particle (See Fig. 2.8). The intensity of the interference pattern in the back focal plane does not depend on the position of the focus and one can reposition the trapped bead in the specimen plane without changing the photodiode signal. The pattern in the back focal plane represents the angular-intensity distribution of light that has passed through the focus, and the back-focal plane detection is equivalent to performing an angular scattering experiment.

The distribution is only affected by the motion of the trapped object with respect to the trap center. That is why this plane is imaged onto a quadrant photodiode. This method of displacement detection of the trapped particle is

2.3. .

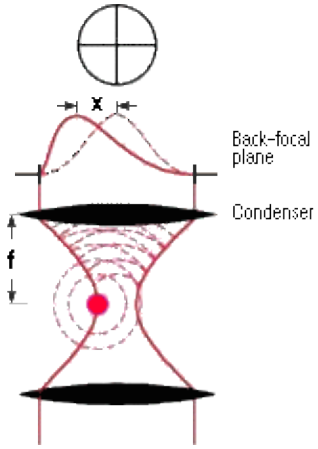

Figure 2.8: The non-imaging detection technique is based on the interference between outgoing incident laser light with the scattered light from the trapped particle, known as back-focal plane interferometry.

called *back-focal plane interferometry.*

The intensity profile in the back-focal plane as a function of lateral displacement of the bead diameter d is [105]

$$\frac{\delta I(x)}{I_0} \cong \frac{2k^4\gamma}{\pi r^2} x \exp(-x^2/L^2)\theta\cos(\phi)\exp(-k^2L^2\theta^2/4). \tag{2.87}$$

The above equation describes the angular-interference pattern caused by a particle displacement of magnitude x, from the optical axis in the focal plane, observed in the direction (θ, ϕ). As said before the quadrant photodiode is oriented for detection along the $\pm x$ and $\pm y$ axes; intensity changes on the $(+)$ and $(-)$ halves are equal and opposite. Integrating Eq. 2.87 over angles θ and ϕ with $-\pi/2 < \phi < \pi/2$ and $\sin\theta \approx 0$ gives the absolute response of the detector.

$$\frac{\delta I_+(x)}{I_0} = \frac{I_+ - I_-}{I_+ + I_-} \approx \frac{16}{\sqrt{\pi}}\frac{k\gamma}{L^2}G(x/L) \tag{2.88}$$
$$G(u) = \exp(-2u^2)\int_0^u \exp(y^2)dy$$

For $x \ll L$, the response is proportional to d^3/L^3; showing a sensitive dependence on particle and focus size.

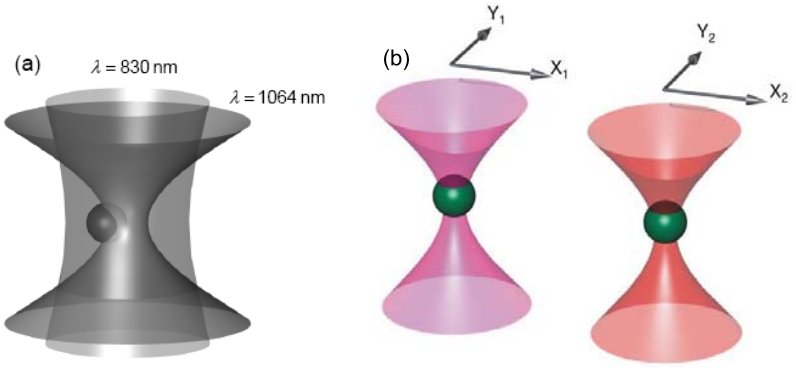

Figure 2.9: Two laser traps a) in overlapping condition b) at different positions

It should be noticed that the expression in Eq. 2.88 is derived in the Rayleigh approximation, but has been found to quantitatively agree with observed response for particle sizes in the Mie regime [105].

2.3.3 Experimental setup

Passive microrheology

The setup consists [98, 106] of two independent linearly-polarized lasers $\lambda_1 = 1064$ nm (Nd:YVO4, Compass, Coherent, Santa Clara, CA, USA) and $\lambda_2 = 830$ nm (diode laser, CW, IQ1C140, Laser 2000) which form two independent optical traps. The two lasers can be used for trapping two beads at different positions or in an overlapping condition (see Fig. 2.9). The lasers are protected against back reflections by means of optical isolators (37 dB isolation, Optics for Research, Caldwell, NJ) in front of them to enhance their stability.

In order to have maximum stability, we run the lasers at their highest power. As a result, we control the laser powers via a combination of a rotatable half-wave plate and a polarizer. The wave plate rotates the linear input polarization while only a fixed polarization passes through the polarizer. Hence the output laser power can be tuned from 0 to 100 % by rotating the half-wave plate. Furthermore, two shutters S1 and S2 were placed in the optical path to facilitate switching the traps on and off independently.

Fig. 2.10 shows a schematic of the experimental setup used in two-particle microrheology experiments.

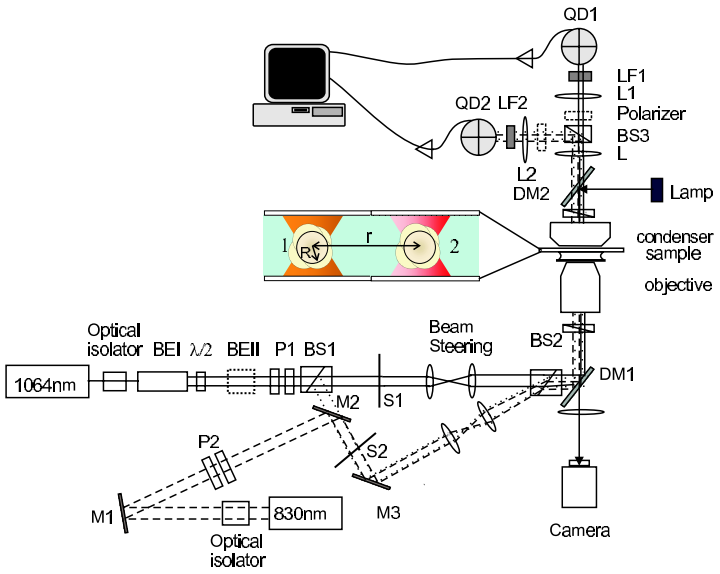

Figure 2.10: The schematic of experimental setup used in passive microrheology experiments, reproduced from [106].

The 1064 nm laser is first expanded by a 3 × beam expander (BE1) to extend the Rayleigh range. After passing through the half-wave plate, the beam is further expanded by a second 3 × Beam expander (BE2) to ≈ 101 mm in width. A polarization beam splitter (BS1) splits the light into two perpendicularly polarized beams. Like this, part of the beam is deflected and the direct beam (not deflected) passes through a second beam splitter (BS2). The 830 nm laser beam is guided into the path of the deflected 1064 nm beam by Mirror M2. The direct and indirect beams are recombined by the second beam splitter BM2 and then are coupled into the microscope via a dichroic mirror (DM1). Stable trapping is achieved using a high numerical aperture objective lens which is part of a custom-built inverted microscope. For each of the lasers, two lenses (f=80 mm) in telescope configuration allow the control of the beam foci positions in the plane perpendicular to the beam directions. The two beams are focused into the sample chamber through a high numerical objective of the microscope (100× , NA 1.3, Neofluor, Zeiss). A CCD camera takes an image of the trapped particles for calibration purposes. After passing through the sample the laser light

was collected by an oil immersion condenser (1.4NA, Zeiss) and passed through a second dichroic mirror (DM2) towards the detectors. The lights scattered from the two traps are separated by a third beam splitter (BS3). Another lens L(f= 50 mm) was placed before the polarizing BS3 to collimate the divergent beams. The light intensity distribution in the condensers back-focal plane is projected by lenses L1 and L2 onto the quadrant photodiodes (QPD1 and QPD2) for each of the traps, yielding a spatial resolution of about 0.1 nm for the particle position. In order to remove the cross-talk between the two lasers with different wavelengths, a laser line filter is placed in front of each quantum photodiode. The 1064 nm laser is imaged onto a PN photodiode with reverse bias voltage of 100 V, while the 830 nm light is detected with a standard silicon-type PN operated quantum photodiode with a reverse bias voltage of 15 V.

As explained before (Sec. 2.3.2), we use back-focal plane interferometry to detect the position fluctuations of the trapped bead away from the trap center [105]. The interference signals of the laser beams detected by the quadrant photodiodes are converted to voltages and amplified by low-noise amplifiers. A customized Labview data acquisition program is used to acquire a time series of the particle position from the quantum photodiode for a minimum time of 45s. Eventually an A/D converter digitizes the data at 195 kHz frequency.

In order to measure the spontaneous Brownian motion of the probe particles, we minimized the trap power of the two lasers. During our measurements the typical power of each laser was less than 10 mW.

For imaging the samples, we used the microscope in differential interference contrast (DIC) mode, with Köhler illumination using a fiber-coupled mercury arc lamp (100 W, 546 nm line). The illumination light was coupled into the condenser lens via DM2, which transmits the laser light but reflects the illumination light. Images were recorded by an Ultricon tube camera (Model VT100, Dage-MTI). Focusing in the sample was controlled by a DC motor which moves both objective and the condenser with respect to the fixed sample. The sample is mounted on a 3-axis piezo stage with 0.7 nm precision.

Active microrheology

The experimental arrangement [99] shown in Fig. 2.11 similar to the two-particle passive microrheology setup consists of two optical traps formed by two independent polarized laser beams whose centers are overlapping. The difference with the passive MR arrangement is that now the stronger laser (λ = 1064 nm) is used to drive the oscillations of the trapped particle (drive laser), and the weaker stationary trap (λ = 830 nm) to detect the position of the particle (probe laser).

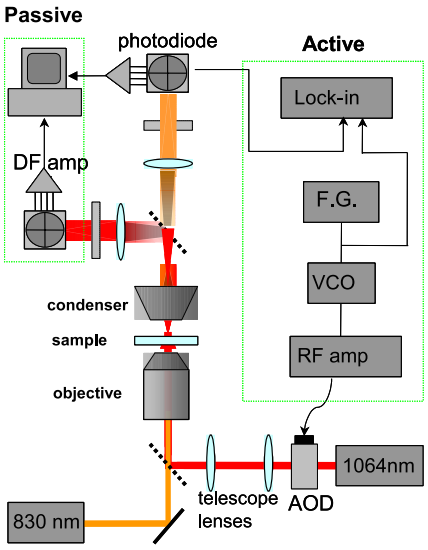

Figure 2.11: The schematic of experimental setup used in active microrheology experiments

The drive laser oscillates the trapped particle with an Acousto-Optical Deflector (AOD). The AOD consists of a transparent TeO2 crystal inside which an optical diffraction grating is generated by density changes associated with a travelling ultrasound acoustic wave. A piezo-electric transducer which is driven by a voltage-controlled oscillator (VCO) generates the acoustic wave which deflects the incident light beam to the direction of Bragg reflection. In this way VCO implements the oscillatory motion of laser beam. By sinusoidally modulating the output frequency of VCO, the Bragg-reflection angle (thus laser beam focus at the sample plane) is oscillated. The output signal from quantum photodiode that detects the probe laser is fed into a lock-in amplifier (model SR830, Stanford research systems). The lock-in amplifier sensitively measures the amplitude and phase delay of output-signal compared to internally generated reference signal, which is supplied to the VCO.

2.3.4 Data analysis: Passive microrheology

Passive microrheology (MR) can be performed in two ways: one-particle and two-particle. In this subsection we discuss the theory and data analysis method for

either of them.

One-particle Microrheology

In one-particle MR, we extract the complex compliance from the position fluctuations of one particle. The time-series data of the bead displacement measured by the quantum photodiode is Fourier transformed to calculate the power spectrum of displacement fluctuations in the frequency domain $\langle|x(\omega)|^2\rangle$ for each of the x and y directions. The power spectrum of the thermal fluctuations of the probe is related to the imaginary part of the complex compliance $\alpha(\omega) = \alpha'(\omega) - \imath\alpha''(\omega)$ via the FDT (Sec. 1.3.1).

$$\alpha''(\omega) = \frac{\omega\langle|x(\omega)|^2\rangle}{2k_BT} \tag{2.89}$$

Provided that $\alpha''(\omega)$ is known over a large range of frequency, one can recover the real part of the response function from the Kramers-Kronig relation Eq. (1.12): $\alpha'(\omega) = \frac{2}{\pi}P\int_0^\infty \frac{\omega'\alpha''(\omega')}{\omega'^2-\omega^2}d\omega'$. Before calculating the shear modulus, we should calibrate the setup and correct for the trap stiffness that shows up at low frequencies. The particle displacement $x(t)$ and the applied trapping force change linearly with the output voltage of the quantum photodiode. In order to obtain the calibration factor Calf $= x(t)/V(t)$ and the trap stiffness, we measure the power spectra of several beads in pure solvent, all from the same batch used in the experiments. Subsequently, we average over these to get good statistics at low frequencies. The power spectra in the solvent are measured under exactly the same conditions (optical alignment and laser power) as those used in measurements of other samples. The trap can be considered as a harmonic potential in which the bead executes Brownian motion, leading to its Langevin equation of motion:

$$k_t x + \xi\dot{x} = \zeta(t), \tag{2.90}$$

where we have ignored the inertia of the bead. Here k_t denotes the effective trap stiffness, ξ the friction coefficient and $\zeta(t)$ represents a Gaussian white noise with zero time average and constant power spectrum $\langle|\zeta(\omega)|^2\rangle = 2\xi k_BT$. Calculating the Fourier transform of the Langevin equation, Eq. (2.90), the power spectrum of displacement fluctuations is found to have a Lorentzian shape.

$$S_x(\omega) = \langle|x(\omega)|^2\rangle = \frac{2k_BT}{\xi(\omega_c^2+\omega^2)} = (\text{Calf})^2\langle|V(\omega)|^2\rangle \tag{2.91}$$

where $\omega_c = \frac{k_t}{\xi}$ is introduced as the characteristic frequency of the trap. Fig. 2.12 shows a typical power spectrum measured for silica beads in water. As can be

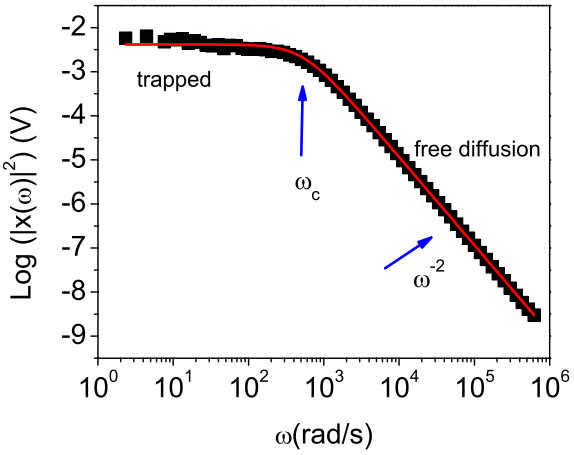

Figure 2.12: The measured power spectrum (averaged over several beads) of 0.5 micrometer silica particles in water trapped by a 1064 nm laser.

seen it is well described by the Lorentzian form of Eq. (2.91). At high frequencies $\omega >> \omega_c$ the quantity $S_\infty^V = \omega^2 S_x(\omega)$ is almost constant, and must be equal to $2k_BT/\xi$. The calibration factor can then be obtained from using the Stokes formula, $\xi = 6\pi\eta R$, if one knows the bead diameter, the solvent viscosity, and the temperature.

$$\text{Calf[m/V]} = [\frac{2k_BT}{\xi S_\infty^V}]^{\frac{1}{2}}. \tag{2.92}$$

The trap stiffness can be found by fitting the Lorentzian form of Eq. (2.91) to the power spectrum of the output voltage measured in the solvent. The true complex compliance α is obtained from the apparent complex compliance χ that is directly calculated from the power spectrum, through the relation [98]

$$\alpha = \frac{\chi}{1 - k_t\chi}. \tag{2.93}$$

Finally, the complex shear modulus $G^*(\omega) = G'(\omega) + G''(\omega)$ can be obtained from the corrected complex compliance through the Stokes relation

$$G^*(\omega) = \frac{1}{6\pi R\alpha(\omega)}, \tag{2.94}$$

where R is the radius of probe bead.

Two-particle microrheology

In two-particle MR, we calculate the correlated fluctuations of two probe beads inside the material. In general, when we have a certain number of particles, the displacement of particle m in direction i is related to the force applied to particle n in direction j via the complex response tensor $u_i^{(m)}(\omega) = \alpha_{ij}^{(m,n)}(\omega) F_j^{(n)}(\omega)$.

In the case of two particles, the response tensors $\alpha_{ij}^{(1,1)}$ and $\alpha_{ij}^{(2,2)}$ describe how each of the particles number 1 and 2 respond to the forces applied to the same particle, while $\alpha_{ij}^{(1,2)}$ describes how particle 1 responds to the forces on particle 2.

In thermal equilibrium and in the absence of external forces, FDT relates the imaginary part of response tensor to the spectrum of displacement fluctuations of the particles.

$$\alpha_{ij}^{(m,n)}(\omega) = \frac{\omega}{2k_B T} S_{ij}^{(m,n)}(\omega), \tag{2.95}$$

where the spectra of thermal fluctuations $S_{ij}^{(m,n)}$ are defined as

$$S_{ij}^{(m,n)}(\omega) = \int_0^\infty \langle u_i^{(m)}(t) u_j^{(n)}(0) \rangle e^{i\omega t} dt. \tag{2.96}$$

The problem of two hydrodynamically correlated particles in a viscoelastic medium is the analogue of two conducting spheres surrounded by a dielectric medium. In [107] this analogy was used to work out the relation between the response tensor and the rheological properties of the medium.

The cross component part of the response tensor $\alpha_{ij}^{(1,2)}$ can be decomposed into two parts $\alpha_{||}$ parallel to the vector $\mathbf{r}$ separating the two beads and $\alpha_\perp$ perpendicular to $\mathbf{r}$: $\alpha_{ij}^{(1,2)} = \alpha_{||} \hat{r}_i \hat{r}_j + \alpha_\perp (\delta_{ij} - \hat{r}_i \hat{r}_j)$. For incompressible fluids each of the components are related to the complex shear modulus as

$$\alpha_{||}(\omega) = 2\alpha_\perp(\omega) = \frac{1}{4\pi r G^*(\omega)}. \tag{2.97}$$

Due to the presence of the traps, again we measure an apparent response χ function. Therefore, the measured response function must be corrected for the trap stiffness. The relation between the apparent and true response can be obtained similarly to the one-particle method, as has been explained in detail in reference [98].

2.3.5 Data analysis: Active microrheology

In this method, developed by D. Mizuno et. al. [99], we actively exert an external sinusoidal perturbation on the trapped particle in the y direction and measure

phase and displacement amplitude of the particle in response to the applied force. In our experiments we oscillate the drive laser with frequency $f = \frac{\omega}{2\pi}$ and the oscillation amplitude L. Consequently, this exerts an oscillatory force of magnitude $\Re\{k_1[L\exp(\imath\omega t) - x(t)]\}$ on the bead. The equation of motion of the bead excited by an oscillatory force, ignoring its inertia (low Reynolds number), is described as

$$\int_{-\infty}^{t} \xi(t-t')\dot{x}(t')dt' + k_2 x(t) = k_1[L\exp(\imath\omega t) - x(t)] + \zeta(t) \tag{2.98}$$

where k_1, k_2 refer to the trap stiffness of drive and probe lasers, respectively. $\xi(t-t')$ is a time-domain friction coefficient that reflects the memory effects in viscoelastic materials. $\zeta(t)$ is the random force arising from the medium. In the active scheme, $\zeta(t)$ can be set to zero, since it averages out. Here, $f_0 = k_1 L\exp(\imath\omega t)$ can be interpreted as the apparent oscillatory force exerted by the drive laser. The particle displacement caused by the apparent oscillatory force is denoted as $x_\omega(t)$. The apparent response to the sinusoidal force is defined as

$$< x_\omega(t) >= \alpha^*(\omega) f_0 \exp(\imath\omega t) \tag{2.99}$$

In practice, lock-in amplifier measures the particle displacements at the oscillation frequency, $< x_\omega(t) >= x_0^*(\omega)\exp(\imath\omega t)$, with $x_0^*(\omega) = A(\omega)\exp(\imath\varphi(\omega))$. Laplace transforming Eq. (2.98), with the Laplace transform defined as $f(s) = \int_0^\infty f(t)e^{-st}dt$, and taking the limit $(s \to \imath\omega)$, the apparent complex compliance, according to Eq. (2.99), is

$$\alpha_{app} = \frac{x_0^*(\omega)}{f_0} = \frac{1}{(k_1+k_2) + \imath\omega\xi}. \tag{2.100}$$

The true response of the system is $\frac{1}{\imath\omega\xi}$, therefore the apparent complex compliance must be corrected similar to the passive section from equation (2.93) with effective trap stiffness $k_t = k_1 + k_2$.

As it is clear from the above formalism, analyzing the data in the active method requires knowing the trap stiffness and calibration of measured amplitude of response as well as a correction to the measured amplitude and phase of the response. The trap stiffness and the calibration factor for the output voltage in the case of the drive laser and overlapping of the probe and the drive lasers can be found in the same way as explained for passive measurements. To determine the amplitude of laser oscillations L we record oscillatory motion of a bead trapped by the drive laser for different input voltage values, using video microscopy. Fig. 2.13a shows the position of an oscillating particle as a function of time for $V_{input} = 4mV$. By fitting it with a sine wave we can determine the amplitude of the oscillation.

Plotting the amplitude versus voltage gives us the calibration factor and from there the laser amplitude corresponding to the applied voltage in the measurements (L(nm)= calf $\times$ V_{input} (V)).

All instruments have their own characteristic response, which has to be corrected from the direct output of the lock-in amplifier. In order to correct the phase and amplitude of the response, we measure the acousto-optical deflector (AOD) response.

To acquire the AOD response we measure the interference signal from a large probe particle stuck to the cover slip while oscillating the drive laser. Since the particle does not move in response to the oscillations of the drive laser, the output voltage of the quantum photodiode that detects the probe laser does not give any response, however the probe particle diffracts the drive laser beam. Hence, the change in the interference pattern detected in the back- focal plane of the condenser lens is not due to bead motion but due to the presence of AOD. The output of the quantum photodiode that detects the drive laser is fed into the lock-in amplifier and gives us the AOD response.

Fig. 2.13c and Fig. 2.13d show the response function of our experimental system (amplitude and phase delay). We can see that the amplitude of the lock-in amplifier output decreases at frequencies lower than 1 Hz. This is due to the AC coupling to the input signal channel. Therefore, a significant phase delay also occurs in this region which has to be corrected. The phase delay is due to the finite propagating time of the acoustic wave in the AOD. Since the piezo-electric transducer is placed at the edge of the crystal in the AOD, it takes some time for the generated ultrasonic wave to reach the position where the incident laser is crossed (and diffracted). The phase delay changes linearly with the oscillation frequency in the high frequency region.

Since the drive laser is strong, there is a danger that it heats up the sample. This can lead to refractive index gradient that can act as an optical lens causing the deflection of the probe laser. This phenomenon is called photothermal lens effect. This effect should be taken into account if its impact is large. We tested this by measuring the AOD response in an aged sample without presence of the beads. No significant effect was observed.

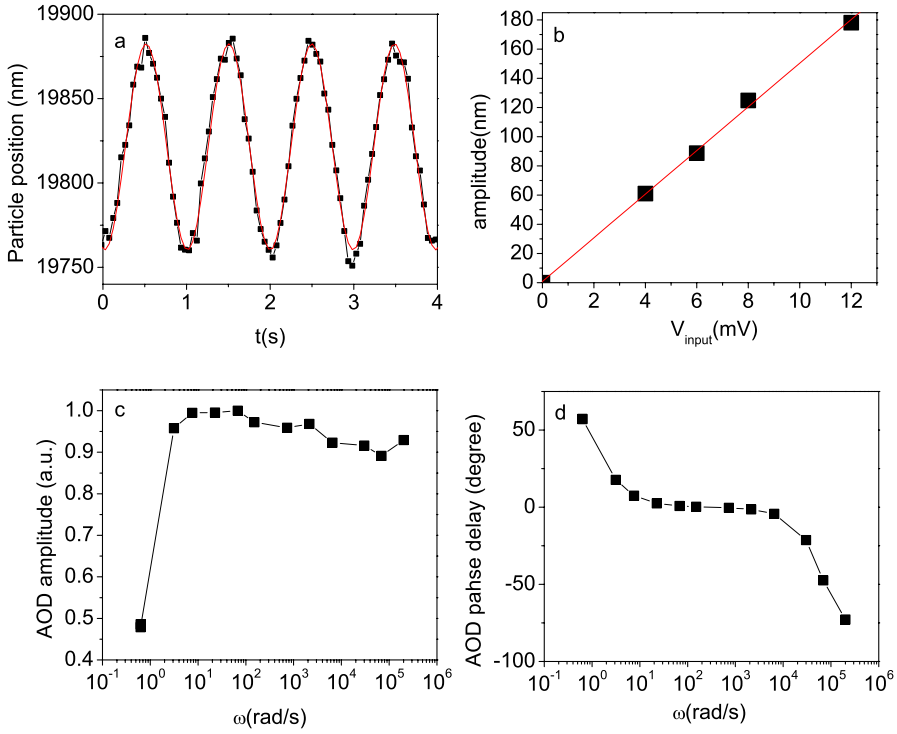

Figure 2.13: a) The position of trapped particle (silica d=0.5 μm) in water obtained by analyzing video images b) changing the oscillation amplitude, linear relation between quantum photodiode output and particle displacement was obtained. c) Amplitude and d) phase delay of the system response obtained for a typical optical alignment. The oscillating drive laser is diffracted by the colloidal particle stuck to the glass surface and the resultant response in quantum photodiode is detected.

3.

Distinct Pathways for Aging of Laponite Suspensions

3.1 Introduction

The main issue in the study of glasses is that from the point of view of their molecular structure, they closely resemble liquids. On the other hand, their mechanical properties are much closer to those of solids: ordinary window glass, for instance, does not flow on human timescales [108, 109]. To explain the extremely high viscosity of glassy systems, it is commonly accepted that the motion of molecules or particles that constitute the glass are blocked by the neighboring molecules, who in turn are blocked also by their neighbors and so on, making it impossible for the system to flow.

Translated in terms of the free energy of the system, the paradigm for glasses is that of a complicated free energy landscape, with many local minima of the free energy. Therefore after a quench into a glassy state, the system falls into a local minimum of the free energy. As the system ages, both the mechanical properties and the diffusion coefficient change in time. The interpretation of this time evolution is that at early times after the quench, the system is able to access at least part of the phase space, and can get out of local minima by thermal activation. However, as time goes on, the system finds deeper and deeper minima of free energy, that are more difficult to escape from. Consequently the evolution becomes slower. Because of this, the system cannot reach thermodynamic equilibrium: it becomes non-ergodic. During the aging, the viscosity increases and the diffusion

coefficient of the particles decreases, emphasizing the link between the blocking of the particle motion and trapping of the system in deeper and deeper valleys of the free-energy landscape.

However, although this provides an appealing intuitive picture of glassy dynamics, to our knowledge there is no direct experimental evidence for the existence of such a complicated free-energy landscape with many local minima [110, 111]. Here, we are able to provide such evidence by showing that for a soft glassy material, multiple paths can be taken through the free energy landscape, that can even lead to different 'final' non-ergodic states at the late stages of aging.

3.2 Gels and glasses in the Laponite system

The system we consider is a suspension of anisotropic and charged colloidal particles suspended in water: Laponite, a synthetic clay [49, 64, 50, 52, 14, 67, 112]. When dissolved in water, Laponite spontaneously evolves from an initially ergodic liquid-like state to a non-ergodic solid-like state. During this process the relevant physical observables of the system change with waiting time. This is called aging, meaning that there is a significant time dependence of measurable quantities such as diffusion coefficient and viscosity. To be more precise, in aging systems correlations and response functions become waiting-time (t_w) dependent, and a significant part of the relaxation takes place on a time scale which grows with this waiting time. In Laponite the aging speed (the rate of change of e.g. relaxation time or viscosity) depends on the concentration of Laponite. The higher the Laponite concentration, the faster it evolves. For example for a sample of Laponite 3.5 wt%, within an hour the relaxation time of system grows by more than an order of magnitude, while for a sample of 0.2 wt%, only a small change in the relaxation function is observed within a month (see Fig. 3.1).

The study of colloids has allowed for a significant contribution to elucidating the basic physics of glass transition [42, 46]. In colloidal systems, as the particle volume fraction is increased, the particles become increasingly slower and for even higher volume fractions the glass transition is encountered. On the other hand, colloidal gels are known to form at extremely low volume fractions $\approx 10^{-4} - 10^{-2}$ in the presence of strong attractions [113]. Gelation and the glass transition have important similarities. Both are ergodic to non-ergodic transitions that are kinetic, rather than thermodynamic in origin, and distinguishing between these two types of non-ergodic states experimentally is a longstanding controversy [65, 66, 64, 67, 50]. The experiments reported below provide direct criteria for distinguishing gels from glasses. This allows us to show that for a

range of Laponite concentrations, two distinctly different non-ergodic states can result (at late times of aging): either the glass or the gel forms with roughly equal probability. There is no way to tell beforehand which of the two options will be taken by the sample, suggesting that there are at least two metastable minima in the system. In addition, our results show that the free energy landscape is indeed complicated, since a number of samples are observed to hesitate between the two options for a long time and an initial evolution in one of the two directions can lead to a final state that is the other one.

We subsequently show that if salt is added to the system, thereby screening the electrostatic repulsion between the particles, even a third option appears to exist for the system. At high salt concentrations, the system ends up having some characteristic features of the glass, whereas other features are those of the gel. We propose that this happens because a glass is formed from small gel-like clusters of particles; this state is dubbed attractive glass.

3.3 Experimental details

Since Laponite can absorb water up to 20% of its weight, it was first dried in an oven at 100^oC for one week and was subsequently stored in a desiccator.

We prepare a number of Laponite samples in a wide range of concentrations and salt contents. Laponite solutions without added salt are prepared in ultra pure Millipore water ($18.2M\Omega cm^{-1}$) and are stirred vigorously by a magnet between 1 and 2 hours to make sure that the Laponite particles are fully dispersed. The dispersions are filtered using Millipore Millex AA $0.8\mu m$ filter units to obtain a reproducible initial state [50]. This instant defines the zero of waiting time, $t_w = 0$.

The Laponite solutions with pH=10 are prepared in pH=10 solution, obtained from mixing 10^{-4} mole of NaOH in Millipore water. The samples with non-zero salt content are prepared by diluting the Laponite suspensions in pure water with a more concentrated salt solution [114]. For instance, a sample of 0.8 wt %, 6mM NaCl is prepared by mixing equal volumes of 1.6 wt% Laponite solution in pure water with 12mM salt solution.

A standard dynamic light scattering ($\lambda = 632.8nm$) measures the time-averaged intensity correlation functions (Eq. (3.1)) in VV mode, i.e. when polarization of incident light and scattered light are both perpendicular (vertical) relative to the scattering plane.

$$g_{\mathrm{t}}(q,t) = \frac{< I(q,t)I(q,0) >_t}{< I(q,0) >_t^2} \tag{3.1}$$

where $\langle\rangle_t$ stands for the time average. This is related to the intermediate scattering function $f(q,t)$ in the ergodic regime through Siegert relation Eq. (2.44) and in the non-ergodic regime this correlation together with the ensemble-averaged scattered intensify can be used to calculate $f(q,t)$ (see Sec. 2.1.4 for details).

The measurements are performed at scattering wave vector $q = \frac{4\pi n}{\lambda}\sin(\frac{\theta}{2})$, in which $\theta = 90^o$ is the scattering angle. The correlation functions are measured at a rate depending on the speed of aging of different Laponite suspensions. For experimental details of light scattering experiments and the DLS setup, see Sec. 2.1.

3.4 Experimental evidence for an intricate free-energy landscape

Measuring the intensity correlations of scattered light from numerous Laponite dispersions, one observes two regimes of aging in the evolution of the intensity correlations: In the first regime the system is ergodic, whereas the second regime corresponds to a non-ergodic (arrested) state. This suggests that in the non-ergodic regime the dynamics is slower. The cross-over from the former to the latter is visible in the experiments: the time-averaged normalized correlation function no longer varies between one and zero, i.e. a part of the degrees of freedom is frozen in on the time scale of the measurement. The waiting time for which the time-averaged correlation functions are not equal to their ensemble-averaged values, i.e. their values change from one position to another in the sample. This defines the *ergodicity-breaking time* t_{eb}. Figure (3.1) shows the evolution of intermediate scattering functions $f(q,t)$ for two different samples. In both cases, the correlation functions evolve from an ergodic state to a non-ergodic state, as the system ages. However, the low- and high-concentration samples are observed to behave in a distinctly different manner.

In the ergodic regime, as depicted in Fig. 3.1 for both low and high concentration samples, the intermediate scattering functions $f(q,t)$ decay in two steps, and mainly two relaxations can be observed. The first one, observed for short delay times t, is relatively fast and appears to be independent of waiting time for the high concentration samples (example: Lap 3.5 wt % in panel a), while it increases considerably for the low concentration samples (example: Lap 0.2 wt % in panel b). The second relaxation, observed for longer delay times, depends strongly on the waiting time for both types of samples.

At this point it is worth emphasizing that the range of delay times which are

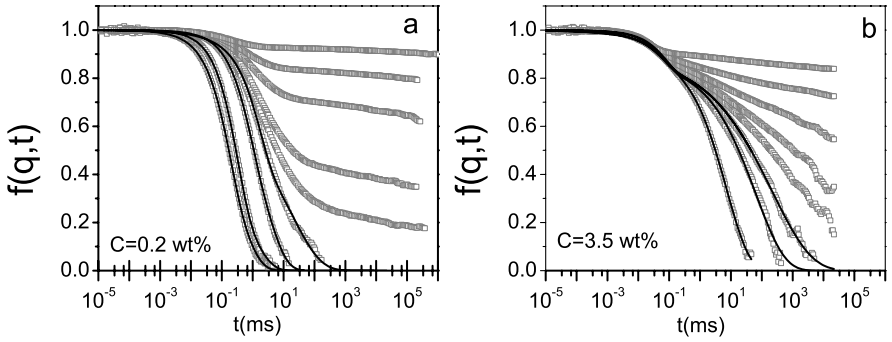

Figure 3.1: Evolution of intermediate scattering function for two Laponite concentrations, at scattering angle 90^o. The unit of the delay time is millisecond. The symbols present the measured correlation functions at increasing waiting times (from left to right) that are ($t_w = 1, 49, 71, 80, 85, 89, 99, 112, 141$ days) for $C = 0.2$ wt% and ($t_w = 7, 40, 54, 71, 86, 113, 260, 1356$ min) for $C = 3.5$ wt%. In both panels, the lines on the curves that decay to zero (ergodic stage) show the fits with $A\exp(-t/\tau_1) + (1-A)\exp(-(t/\tau_2)^\beta)$.

measured in our experiments are of the order the microscopic time scale for the Brownian motion $\frac{(2R)^2}{D_0} \approx 10^{-5}$ s and this time scale can be very different from t_w, which can vary from minutes to days depending on the situation. Therefore in our data in the ergodic regime there is a clear time separation between the waiting times and relaxation times. In the non-ergodic regime the relaxation time can be comparable to the waiting time. However with the standard dynamic light scattering technique we can not measure delay times longer than 10^4 s.

Before ergodicity breaking $t_w < t_{eb}$, as can be observed from the fits shown in Fig. (3.1), both the low-and the high concentration samples can be described by a sum of a single exponential and a stretched exponential [49, 115, 52]:

$$f(q,t) = A\exp(-t/\tau_1) + (1-A)\exp(-(t/\tau_2)^\beta) \tag{3.2}$$

Here τ_1 is related to the inverse of the short-time diffusion $\tau_1 = 1/(D_s q^2)$. τ_2 can be used as a measure for the growth of slow relaxation time, although it is not the mean relaxation time, since β which characterizes the width of distribution of relaxation times also evolves with waiting time. However, assuming that the resulting stretched exponential is a weighted average of single exponentials with different relaxations $\int_0^\infty f(\tau)\exp(-t/\tau) = \exp(-(t/\tau_2)^\beta)$, it can be shown that

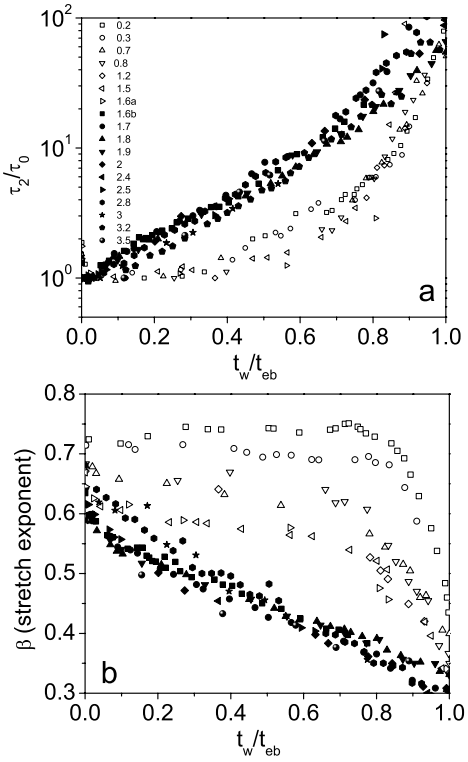

Figure 3.2: The evolution of a) the slow relaxation time normalized to its initial value τ_2/τ_0 and b) the stretching exponent β versus scaled waiting time t_w/t_{eb} for different Laponite samples. The colloid concentrations are shown in the legend. The samples can be divided into two groups according to the evolution of slow relaxation times. In both figures (and the following ones), the open symbols correspond to gels, and the filled symbols to glasses.

the mean relaxation time is $\tau_m = \tau_2 \frac{1}{\beta}\Gamma(\frac{1}{\beta})$ [52, 116], where Γ is the Euler Gamma function. Ruzicka et. al. have shown that the growth of τ_2 and τ_m are similar and occur at the same rate [52]. Thus, here we plot τ_2 as a function of waiting time, which directly comes out of the fitting. τ_2 is found to grow dramatically with waiting time and its evolution is well described for all the samples by the general form:

$$\tau_2(t_w) = \tau_0 \exp(B\frac{t_w}{t_w^\infty - t_w}) \tag{3.3}$$

in agreement with earlier observations [52, 115]. Here $\tau_0 = \tau_2(t_w \approx 0)$ results from fitting of the correlation function at $t_w \approx 0$. B and t_w^∞ are left as free fitting parameters in Eq. (3.3) to be determined. Through our analysis, it turned out that for lower concentrations $t_{eb} \approx t_w^\infty$ and for higher concentrations $t_{eb} \approx 0.6t_w^\infty$. Therefore, t_w^∞ can be interpreted as the time characterizing the transition from fluid-like to solid-like state. The B values are found to be ≈ 0.7 for low concentration samples and ≈ 6 for high concentration samples.

Interestingly, if we plot the quantities τ_2/τ_0 and β as a function of scaled waiting time t_w/t_{eb} , the data of all the different concentrations split up into two branches as shown in Fig. 3.2 (remember that t_{eb} characterizes the time that system becomes non-ergodic). All the data for both the τ_2/τ_0 collapse on a single curve and so does the data for β parameters of lower concentrations while the data at higher clay concentrations fall on another master curve. We already observed from the direct comparison of Fig. 3.1(a) with Fig. 3.1(b) that the aging process is qualitatively different for the low- and high concentration samples. Ruzicka et. al. [52] found similar results, scaling the waiting time with the fitting parameter t_w^∞. Here, we use the ergodicity-breaking time t_{eb} as the parameter to scale the data, since it is directly extracted from the measurements, so it is a physically accessible time that characterizes the transition from ergodic to non-ergodic state.

Now, we turn to the non-ergodic regime of aging. The evolution of non-ergodic states in our system is followed in time again using light scattering. For waiting times $t_w > t_{eb}$, we calculate the ensemble-averaged electric field correlation function i.e. intermediate scattering function $f(q, t, t_w)$ from the time-averaged intensity correlation function $g_t(q, t, t_w)$ and ensemble-averaged intensity I_E measured by rotating the sample at different heights [49, 81, 42](see Sec. 2.1.4)

$$f(q, t, t_w) = 1 + (I_t/I_E)\{[g_t(q, t, t_w) - g_t(q, 0) + 1]^{1/2} - 1\} \tag{3.4}$$

In the non-ergodic regime, the aging rate of the system can be quantified by measuring the time evolution of the non-ergodicity parameter $f(q, \infty, t_w) = limf(q, t \to \infty, t_w)$ (for more details see Sec. 2.1.4). Note that the long time limit $t \to \infty$ is taken with respect to the Brownian time scale $\tau_B = \frac{(2R)^2}{6D_0} \approx 10^{-5}$ s, i.e $t \gg \tau_B$. Note that our definition of non-ergodicity parameter here is different from what is usually used in glass community in which the limit of both $t \to \infty$ and $t_w \to \infty$ are taken.

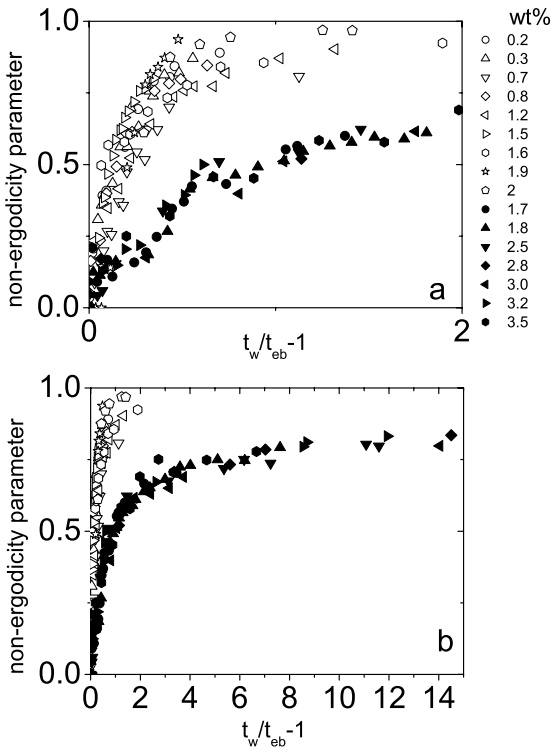

Figure 3.3: a) The evolution of the non-ergodicity parameter $f(q, \infty, t_w)$ versus reduced waiting time $t_w/t_{eb} - 1$ for different Laponite samples. The colloid concentrations are shown in the legend. The samples can be divided into two groups according to the evolution of non-ergodicity parameters. In both figures, the open symbols correspond to gels, the filled symbols to the glass. b) the evolution of non-ergodicity parameter of glass samples at very large waiting times. As can be seen, the non-ergodicity parameter does not go beyond 0.85.

The non-ergodicity parameter, (which quantifies the fraction of frozen-in fluctuations [82, 81]), of all the samples with different Laponite concentrations collapses also onto two distinct master curves when plotted as a function of reduced waiting time $(t_w/t_{eb} - 1)$ (Fig. 3.3)(the -1 shift is because for $t_w/t_{eb} < 1$ the non-ergodicity parameter is identical to 0). This shows that two possible routes towards non-ergodicity exist. In the first group of samples (low concentrations)

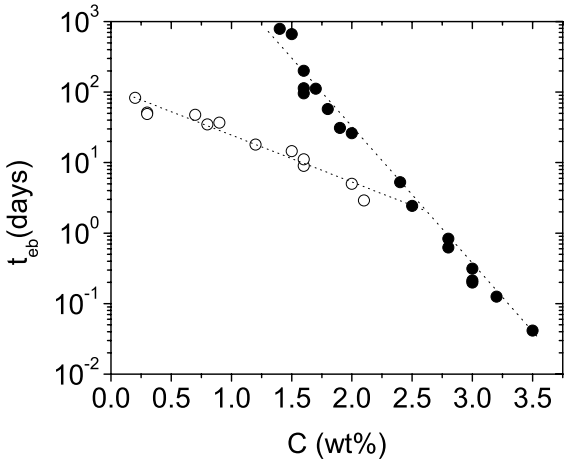

Figure 3.4: The ergodicity-breaking time as a function of concentration of Laponite particles.

the non-ergodicity parameter almost reaches unity: the colloidal particles are completely blocked, suggesting that they are rigidly held in place, as they would be in a gel-like structure. In the second group (high concentrations), the non-ergodicity parameter evolves at a slower rate and goes to ≈ 0.8 at late times, indicating that there is still some freedom for the particles to move: the hindrance of the particles is only sterical, as it would be in a glass. In fact measuring the non-ergodicity parameter for a couple of (glassy) samples until $t_w/t_{eb} = 15$ (Fig. 3.3b), we found that $f(q, \infty)$ did not exceed 0.835.

Perhaps the most striking observation is that for the intermediate concentrations $1.3 < C < 2.3wt\%$, samples of identical concentrations may evolve at very different rates, thus having a very different ergodicity-breaking point. In Fig. (3.4), we have plotted the ergodicity-breaking time of the ensemble of the samples we have measured as a function of concentration. The samples fall into two separate groups, and the samples in the intermediate concentration region fall in either of the two. This suggests that the intermediate concentration samples have two options, either following the same trend as the samples of high concentration or behaving similarly to the samples of low concentrations.

The difference between the two states becomes clear if we look at the rest of the data. As is shown in fig. 3.5, the short time diffusion coefficient is almost con-

stant for the samples of high concentration ($C > 2.3\,wt\%$); this corresponds to the 'rattling in the cage' motion reported earlier for colloidal glasses [115]. However, D_s decreases significantly with waiting time for low concentrations ($C < 1.4\,wt\%$) which is again related to the incorporation of the colloidal particles in a gel network [52]. In addition, the slow relaxation time τ_2, is found to grow exponentially with waiting time for high concentrations, in agreement with earlier observations for the glassy state [52, 115]. However, for the gel phase, the relaxation time increases faster than exponentially (Fig. 3.2a); this is likely to be related to the formation of small clusters in the beginning that subsequently aggregate to form a macroscopic structure (with a large relaxation time) [117], a situation similar to diffusion-limited cluster aggregation (DLCA).

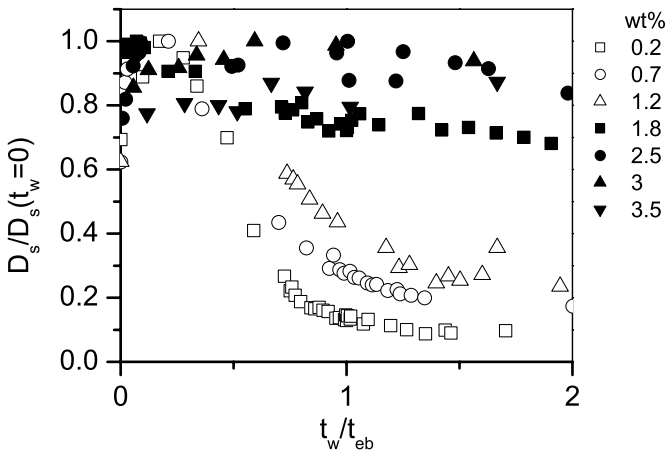

Figure 3.5: The evolution of short-time translational diffusion normalized to its initial value ($t_w \approx 0$) as a function of t_w/t_{eb}.

The measured static structure factor proportional to the intensity of scattered light (Fig. 3.6) provides two further pieces of evidence for structure formation. First, for all the low-concentration samples, the scattered intensity at a fixed scattering angle of 90^o consistently increases with waiting time, while for the high concentration ones it does not evolve much (Fig. 3.6a). The increase of scattered light intensity is usually attributed to formation a network or clusters of particles [113, 118, 117, 119]. Second, although the range of wave vectors is rather limited, measurement of the static structure factor $S(q)$ for the different samples, a power law behavior for $S(q)$ appears to be observed for the lowest concentration

samples with an exponent 1.1 ± 0.2. This exponent is indeed lower than the fractal dimension characterizing DLCA $d_f \approx 1.8$, [113, 118, 119] indicating that less compact string like clusters are formed for such low volume fractions. To the contrary, an almost flat structure factor is found for the highest concentrations, suggesting homogeneity (Fig. 3.6b), very characteristic of a glass [50]. The noise at low q for these measurements is probably due to imperfections of the measurement cell that scatter light at small angles.

Combining all these data, we identify the low-concentration samples as colloidal gels and the high-concentration ones as colloidal glasses.

Intermediate concentrations can be either gels or glasses at late times, with no way of telling beforehand how the sample is going to evolve. That the path towards these non-ergodic states is indeed complicated follows from the observation that samples may 'hesitate' for a long time between the two states, and may evolve in one direction to end up in the other. In Fig. 3.7, some of the 'hesitating' samples are indicated by triangles. It clearly shows how a few samples in the intermediate concentration region that behaved consistently like glassy samples before the ergodicity breaking point, end up as gels at late times. Perhaps even more surprisingly, Fig. 3.7b shows that even if one looks at a single observable such as the non-ergodicity parameter, a crossover between the two behaviors can be observed; this is most evident in the data for $1.9wt\%$. The data shown in the figure are mere examples; approximately 20% of the samples in the intermediate concentration region behaved in an ambiguous way in the sense that they seemed to have a hard time to 'decide' whether they were glasses or gels.

In conclusion of this section, the nature of the non-ergodic state in Laponite suspensions has been the subject of considerable controversy: both colloidal gel [67, 64] and colloidal glass formation [50, 112] have been invoked and were thought to be mutually exclusive [67, 50, 120]. We have shown here that gel and glassy states of Laponite (in pure water) both exist and are well-defined in the limit of low and high concentrations. Besides, our data here provide a clear experimental evidence for the distinction between gel and glassy states.

In gels the main cause of aging is the building up of a network. The evidence for aggregation comes from the time evolution of scattered intensity of light. For the high concentrations we see a slight decrease of intensity (suggesting that no aggregation occurs during aging), while for the lowest concentrations we see a dramatic increase of intensity (Fig. 3.6a) suggesting aggregation or formation of a network. Slowing down of particle motion will happen when the particles are trapped in the network, which may be formed already for very low particle concentrations.

On the other hand the caging effects become relevant when the particles are

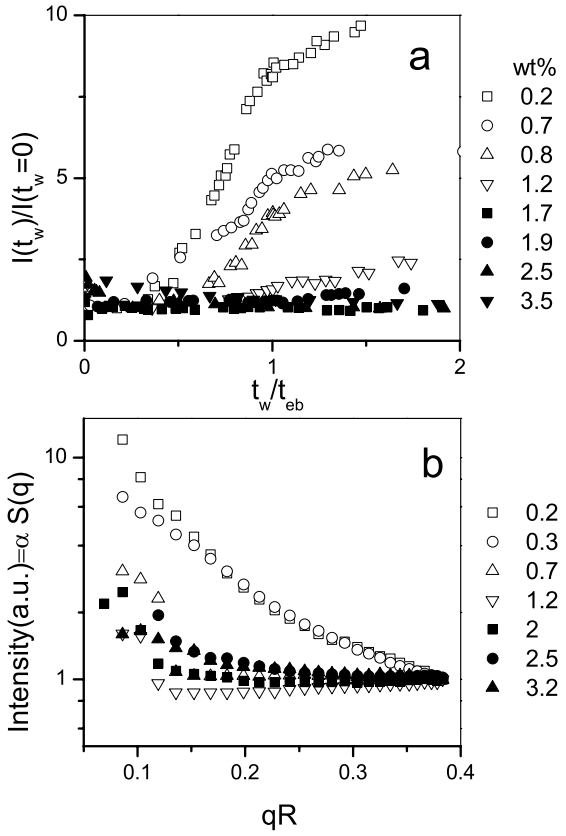

Figure 3.6: a) Scattered intensity at scattering angle 90^o as a function of reduced waiting time. So as to focus on the effect of aging, we have normalized the intensity to its value at the beginning of aging. b) The scattered intensity as a function of the dimensionless scattering wave vector qR for several Laponite concentrations. To compare the q-dependence of different samples, we have normalized the data to their value at highest measured $qR = 0.38$.

close enough to make topological constraints for the motion of neighboring particles. For the lowest concentrations the interparticle distance is several times the particles diameter, and so this is not relevant. Therefore glasses are usually formed in samples of higher concentrations and the slowing down of motion

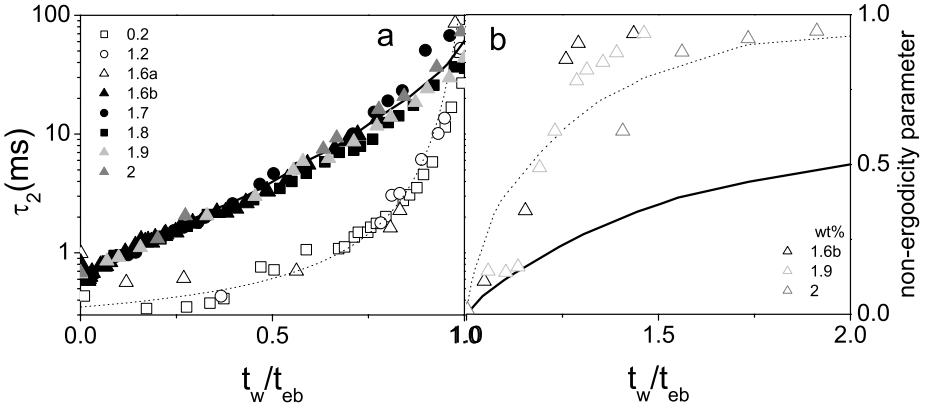

Figure 3.7: a) Slow relaxation time τ_2 as a function of scaled waiting time b) non-ergodicity parameter as a function of scaled waiting time. These samples behave like a glass at the early stages of aging and after $t_w/t_{eb} \approx 1.2$ they evolve according to the gel line. The filled lines show the glass and dotted lines show the gel line, obtained by smoothed averaging over all the samples measured.

in glasses is due to topological constraints [42, 121] that hinder the motion of particles.

Distinction of gels and glasses allows for the observation that in the intermediate concentrations the transition to non-ergodicity can occur in either direction (gel or glass), and may be accompanied by 'hesitations' between the two directions. A qualitative explanation for this behavior is provided by the free energy landscape picture of slow dynamics. Here, one attributes the slow structural relaxation to the complex pathways that connect the configurational states on the multidimensional free-energy surface. For Laponite, our data suggest that there are at least two global minima in the free energy corresponding to gel and glass states, and that different pathways towards these non-equilibrium states exist, providing the first evidence for the existence of such a complicated free-energy landscape.

3.5 Emergence of an attractive glass in Laponite suspensions

At least part of the confusion about glassy or ge-like behavior of Laponite suspensions finds its origin in the fact that some groups added salt to the suspensions [117, 51, 120], whereas others did not [63, 14]. We therefore now consider the effect of salt (NaCl) addition on aging behavior of Laponite suspensions.

We present here similar data as those described above, but with different amounts of added salt to three different samples: 0.8, 1.5 and 2.5 % of Laponite. The effect of salt in charged (spherical) colloidal systems is well-known and understood by now [122]: the salt screens the repulsive electrostatic interactions, and at sufficiently high salt the van der Waals attraction may prevail over the repulsion: the particles stick together and a gel may form. One would expect added salt in the Laponite system to have a similar effect, and thus maybe help the particles to 'decide' that they want to be gels in the intermediate region rather than glasses. It turns out that the experimental reality is quite different, and that the hesitation of the system only becomes more pronounced.

We find, first, that adding salt to a sample of a given concentration of Laponite accelerates the aging, however, the trend of evolution of the correlation function is qualitatively similar, and we observe a transition from an ergodic to a non-ergodic state(see Fig. 3.8).

Fig. 3.9 shows the ergodicity-breaking time for the three samples as a function of salt concentration. The effect is tremendous: by adding a few mM of salt, t_{eb} can decrease by 4 orders of magnitude, with a roughly exponential dependence of the ergodicity breaking time on salt concentration.

Fig. 3.10 shows that in spite of the accelerated aging, the evolution of non-ergodicity parameter $f(q, \infty)$, versus scaled waiting time t_w/t_{eb} still falls onto one of the two branches observed before for samples without salt. These branches were interpreted above as belonging to a colloidal gel or colloidal glass state. However, from Fig. 3.10b, it is evident that the samples with salt deviate from the glass line obtained from the data without adding salt for longer waiting times. These samples seem to evolve faster than glass. Measurements performed on these samples at very long waiting times (a year later) showed that the non-ergodicity parameter of these samples eventually reach the value 1.

Hence, it turns out that in the presence of salt, the story is more complicated than the scenario sketched above without salt. If we look, for instance, at the scattered intensity as a function of the wave-vector (Fig. 3.11), we find that with increasing salt the intensity increases, and for the low concentration samples the wave-vector dependence of $I(q)$ increases as well (Fig. 3.11a). Both increase

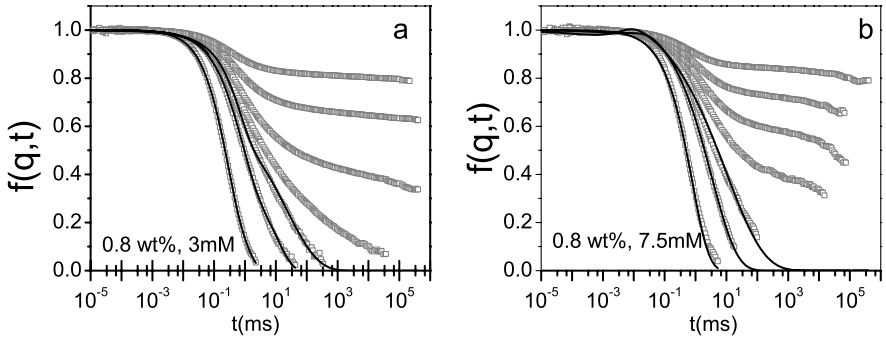

Figure 3.8: Evolution of intermediate scattering function for Laponite 0.8 wt%, with two different salt concentrations, at scattering angle 90^o. The symbols present the measured correlation functions at increasing waiting times (from left to right) that are (t_w = 0.075, 5.7, 7.3, 8.8, 9.7, 11.9, 15, 19 days) for 3 mM and (t_w =9, 44, 66, 90, 119, 164, 311 min) for 7.5 mM salt. In both panels, the lines, on the curves that decay to zero (ergodic stage), show the fits with $A\exp(-t/\tau_1) + (1-A)\exp(-(t/\tau_2)^\beta)$.

of intensity and decrease of short-time diffusion are in principle indicative of the building up of structure, and thus suggest that a gel forms. Comparing, however, with the data for the non-ergodicity parameter, we find that the high-salt concentration samples (Lap 0.8 wt% with 5 and 7.5 mM) are rather on the glass branch, whereas the low-salt concentration samples are on the gel branch. Fig. 3.12b shows again a measurement of the scattered intensity as a function of time. All of the 0.8 wt% Laponite samples (even the ones on the glassy branch of the non-ergodicity parameter) show an increase in intensity as a function of time, as if a structure was building up. All of the 1.5 wt% Laponite samples should be glassy also, according to the non-ergodicity parameter criterion; at least for the 1.5 wt%, 7.5 mM sample also a clear increase in intensity is observed. If we look at the dynamics (Fig. 3.8), similar discrepancies occur for the other samples notably at high salt.

Fig. 3.13a shows the slow relaxation time normalized to its initial value τ_0 as a function of the scaled waiting time. Again, we see that the slow relaxation of a sample of Laponite 0.8 wt%, 7.5 mM salt shows the faster-than-exponential growth that is characteristic of gels (see above). The stretching exponent associated with the relaxation times of a considerable fraction of samples also follows the behavior of gels (Fig. 3.13b). However, comparing again with the 'master

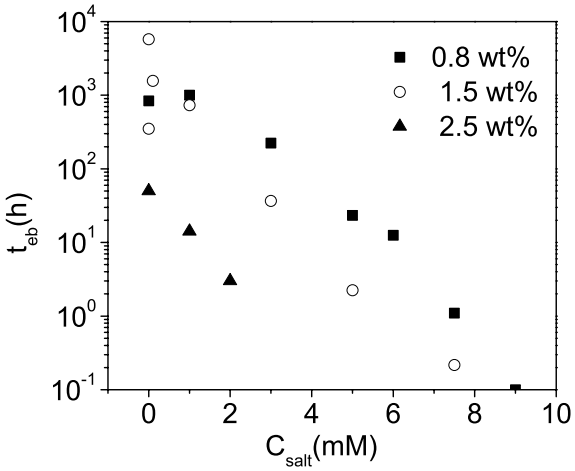

Figure 3.9: The ergodicity-breaking time t_{eb} as a function of the salt content for a few Laponite concentrations. The dependence of t_{eb} on the salt concentration is roughly an exponential decay.

curves' for the non-ergodicity parameter, the high-salt concentration samples (5, 6 and 7.5 mM) behave like glasses, so that again there seems to be an internal contradiction.

Very similarly, the short-time diffusion coefficients of these sample behave like that of a gel, so that there seems to be a problem here too (Fig. 3.12a).

It should be noted here that this behavior is very different from the one reported above without addition of salt. We see no 'hesitations' of the samples between two states in the sense that a sample that starts evolving in one direction ends up in the other one. Rather, all individually measured quantities consistently show an evolution in one direction. However, comparing between different quantities, an inconsistency appears, which is always the same one. Looking at the non-ergodicity parameter, all the samples at high salt always behave like glasses: there is no hesitation here. However, all other measured quantities: slow relaxation time and stretching exponent, scattered intensity and short-time diffusion consistently behave as if the sample were a gel. This situation is indeed quite different from the one without salt.

The data therefore suggest that although the sample has some definite characteristics of a glass, the other characteristics are those of a gel. One possible

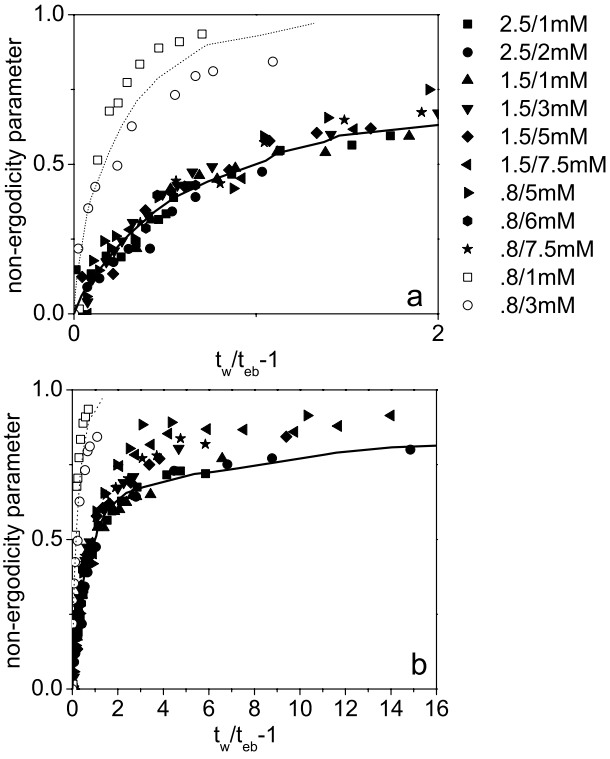

Figure 3.10: a) The evolution of the non-ergodicity parameter $f(q, \infty, t_w)$ versus reduced waiting time $t_w/t_{eb} - 1$, for different Laponite samples with salt. The colloid concentrations and salt contents are shown in the legend. The samples can be divided into two groups according to the evolution of non-ergodicity parameters. The open symbols correspond to gels, the filled symbols to the glass. The dotted line shows the gel line and the solid line the glass line. b) The evolution of the non-ergodicity parameter for long waiting times. As can be seen, for most of the samples with salt (attractive glass) the non-ergodicity parameter deviates from glass line.

way of realizing such a state is that clusters start to form, but that subsequently the clusters of particles can no longer move with respect to each other and form a glass of which the elementary building block is a cluster. The fact that clusters of particles start to form in our system is evident from the increase in scattered intensity. Then from the fact that we nonetheless and simultaneously retain some

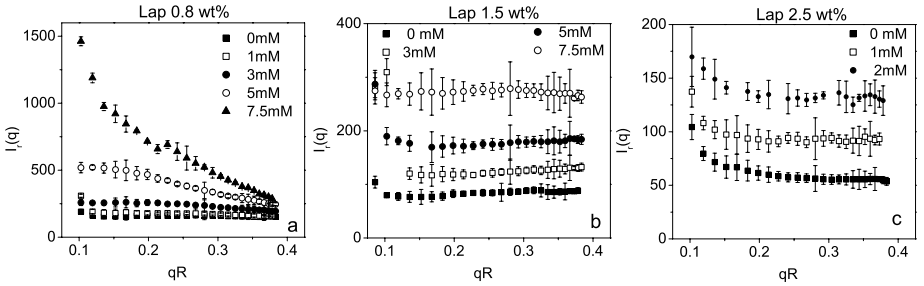

Figure 3.11: The scattered intensity relative to the toluene intensity as a function of dimensionless scattering vector qR for different amounts of added salt (NaCl) at 3 different Laponite concentrations, as shown in the legends. These data are taken a long time after the sample has become fully non-ergodic.

of the characteristics of the glassy state, we infer that subsequently the clusters are dynamically arrested by each other, as particles in a glass. Following Tanaka et al. [65], we dub this new state for the Laponite system an 'attractive glass'. Existence of attractive glass requires the presence of attractive interactions. At this moment the nature of attractive interactions between Laponite particles is unclear. Possible sources are the van der Waals interactions and the attractions between the positive charge on the rim and the negative charge on the surface of Laponite particles. Indeed, recent experiments [123] have shown evidence for a short-range attractive potential in the effective interaction potential.

Hence, to summarize, the addition of salt introduces new patterns in the aging behavior in the sense that there are samples which share some of the properties of the gel and some of the features of the glass. This behavior resembles to that of an attractive glass [46, 47]. Therefore, we suggest to call these samples attractive glasses.

At this point it is worth to compare the aging features of our attractive glass with the attractive glass formed in hard spheres with short-ranged attractions and to see if there are similarities or differences.

In hard sphere systems attractive glass is formed at moderately high volume fractions and strong enough attractions. It can be achieved in experiments by adding polymers that cause a depletion interaction [46, 47]. It is called attractive glass in the sense that in this state the particles are tightly bound in a narrow attraction well. Light scattering studies have revealed differences between attractive and repulsive glass. The distinction between attractive and repulsive glass

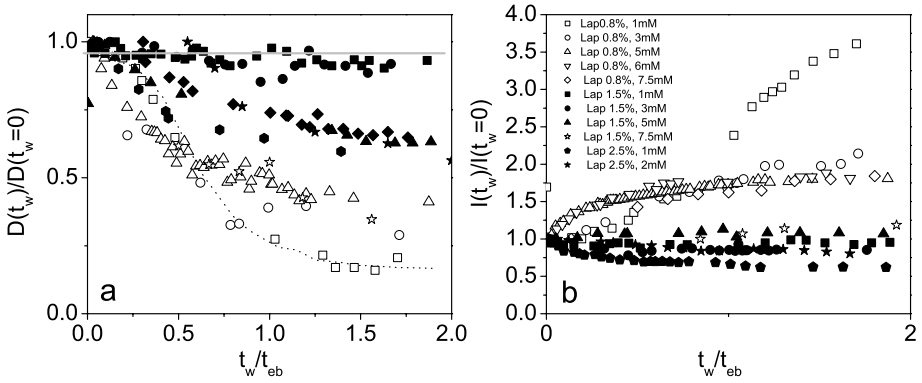

Figure 3.12: a) The evolution of short-time translational diffusion normalized to its initial value ($t_w \approx 0$) as a function of t_w/t_{eb}. The solid and dashed lines show the glass and gel line, respectively, according to the data of Laponite in pure water. b) Scatted intensity at scattering angle 90^o as a function reduced waiting time. So as to focus on the effect of aging, we have normalized the intensity to its value at the beginning of aging.

appears in both their static and dynamic properties, as described below.

Pham et. al. [46] show that upon increasing the attraction strength and entering the attractive glass region (for a fixed volume fraction of colloids), the peak position of the structure factor shifts to a higher q-value and its height slightly decreases. The increase in the q-value of the peak position shows that a significant fraction of neighboring particles get trapped in each others' narrow potential well, when the attractive glass is formed. This leads to clustering of particles and implies that the average number of nearest neighbors should decrease (leading to the decrease in peak height), and 'holes' are opened up to render the structure more heterogenous on the spatial scale of a few particles. The increased heterogeneity is reflected in a rise in the structure factor at low q values. A similar trend in our data is observed upon increasing the salt concentration that screens the repulsions, thus this is equivalent to the increase of attractions (see Fig. 3.11). Note that here we have only measured the structure factor at low q values. The increase of attraction strength leads to a rise in the value static structure factor at low q-values and a more heterogenous structure is reflected in the stronger q-dependence of structure factor at high salt concentrations.

The differences in dynamics of attractive and repulsive glasses is evident in

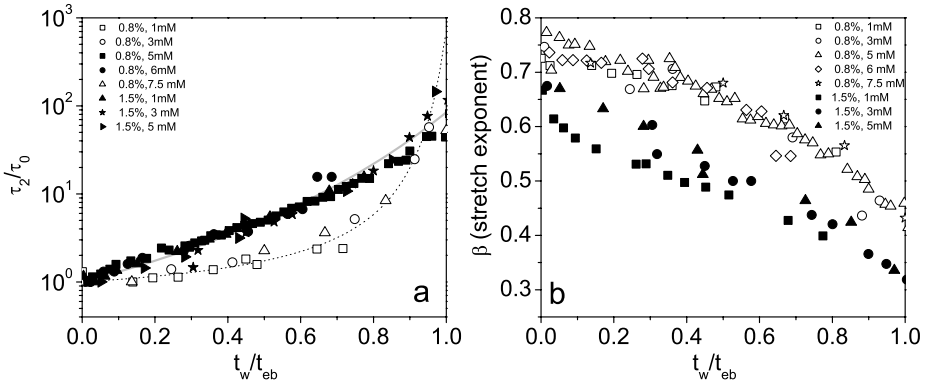

Figure 3.13: a)The evolution of slow relaxation time as a function of the scaled waiting time t_w/t_{eb}. The solid and dashed lines show the glass and gel line, respectively, obtained from smoothed averaging over the data of Laponite in pure water. b) The stretching exponent β versus t_w/t_{eb}.

both the short- and long-time relaxations [46]. The short-time dynamics of particles progressively depart from free diffusion upon increasing attraction. In fact, for the attractive glasses the particles are confined so tightly by attractive potential wells that short-time diffusion drops dramatically compared to the repulsive glass at the same particle concentration [46]. This is consistent with our attractive glass samples for which a dramatic decrease of the short-time diffusion is observed (Fig. 3.12). The evolution of the non-ergodicity parameter in attractive and repulsive glasses of hard sphere system is also different. The intermediate scattering function of a pure hard sphere glass shows a plateau at a value ≈ 0.7 for $qR \approx 3$(corresponding to particles getting stuck in their nearest-neighbor cages) and a very slow aging [46]. On the other hand, the non-ergodicity parameter of an attractive glass has a higher value ≈ 0.9 at a equal waiting time (half a day) and shows a much faster evolution with waiting time. Looking at Fig. 3.10, this strengthens the resemblance of the attractive glass observed in our system and the one in hard sphere system. Although at early times after the ergodicity-breaking the non-ergodicity parameter in attractive glass follows the same dynamics as for the repulsive glass, at later stages of aging $t_w/t_{eb} > 3$, the non-ergodicity parameter in the attractive glass evolves at a faster rate and asymptotically reaches 1 at very long waiting times, as we measured the samples a year after their preparation.

3.6 The Concluding phase diagram

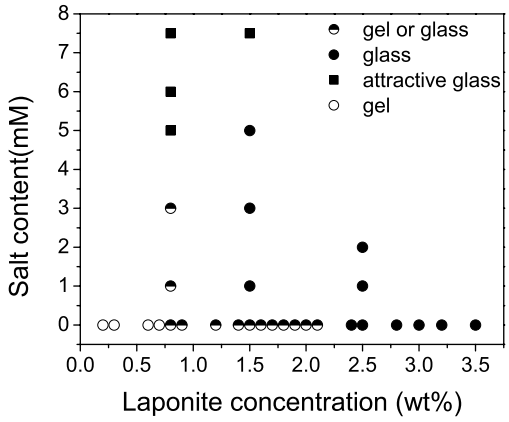

Figure 3.14: The non-equilibrium phase diagram of charged colloidal disks

In Sec. 3.4, we showed that gel and glassy states of Laponite both exist and are well-defined in the limit of low and high concentrations of Laponite without adding salt. These conclusions are reinforced by the study of Laponite with addition of salt. Upon adding a sufficient amount of salt, we even uncover a new state for Laponite, an 'attractive glass' which has some of the characteristics of the glass, and others of the gel. We tentatively propose that the glass is made up of aggregates of clustered Laponite particles that sterically hinder each other, thus arresting the motion even further. This again shows how closely glassy and gel states are connected to each other.

Our findings are summarized in Fig. 3.14 where we have plotted the phase diagram of the Laponite system in the Laponite concentration/added salt content plane as follows from the ensemble of the measurements presented above. Without salt, we observe the region between gels (low concentration) and glasses (high concentration) where the samples may 'hesitate', but always ends up being either a gel or a glass. Upon adding salt, for salinities higher than 5mM we observe the 'attractive glass' region, where the non-ergodicity parameter behaves like those for glasses, but the other measured quantities resemble closely to what would be expected for a gel.

The phenomena described here should be general for colloidal systems with effectively attractive interactions between the particles; indeed the recent discovery

of "attractive glasses" for spherical colloids [46] also suggests that gels and glasses are not necessarily clearly distinct states of matter, but rather metastable minima in an otherwise complicated free-energy landscape, resulting from both steric and attractive interactions, as suggested by some simulations [124] and experiments [125].

3.7 Discussion and conclusion

The non-equilibrium behavior of Laponite suspensions has been an active subject of research in the last decade with the aim of getting a deeper insight into the general features of aging and glassy dynamics. Several independent groups have studied different aspects of non-ergodic Laponite suspensions in different regions of phase diagram. Perhaps the earliest systematic studies come from Mourchid et. al. [48, 126, 127], Willenbacher [128] and Kroon et. al. [49, 63, 50]. Willenbacher and Mourchid et. al. focused on the rheological properties. Mourchid et. al. varied both particle concentration and ionic strength. They performed oscillatory shear measurements on samples a week after their preparation and defined a sol-gel transition line where the zero frequency elastic shear modulus increases remarkably. They further modified their phase diagram following the suggestion of Bonn et. al. [63] for the existence of a repulsive glass at very low ionic strengths ($I < 10^{-4}$ M) as shown in Fig. 1.4. Their phase diagram gives a general overview, but their method is flawed as the measurements were done after some arbitrary waiting time t_w and viscoelastic properties depend on t_w.

Willenbacher mainly studied the phenomenon of thixotropy in Laponite suspensions and was the first to observe aging of Laponite suspensions. He found that after cessation of steady shear, the magnitude of viscosity $|\eta^*|$ increased monotonically with time and even after 16 days no equilibrium viscosity value was reached. A single power law $|\eta^*| \sim t_w^n$ described the data within the time regime from 10 to $10^6 s$. The exponent $n = 0.13$ turned out to be independent of clay concentration and mechanical pre-treatment of the material.

On the other hand, Kroon et. al. [49] studied the aging of Laponite using dynamic light scattering experiments. They measured a range of sample concentrations between 2.2 and 3.5 wt%. They found that all the samples show a similar aging behavior and evolve from an initially ergodic state to a non-ergodic state around a certain time (ergodicity-breaking point) that decreases exponentially with concentration. For a sample of Laponite 3wt%, they reported growth of non-ergodicity parameter from almost zero to approximately 0.8 at $t_w = 3t_{eb}$. Bonn et. al. [63] measured the q-dependence of the intermediate scattering function for

a sample of 3.5 wt % in the non-ergodic regime and showed that the relaxation time associated with short delay times is independent of waiting time and has a q^{-2} dependence. They found similar results as Kroon et. al for the evolution of non-ergodicity parameter and an exponential decay of the form $\exp(-Aq^2)$ for its q-dependence. Furthermore, they suggested aging in this sample is due to strong electrostatic repulsions, leading to formation of a low volume fraction Wigner glass. They described the dynamics by cage-diffusion process. In a further study, Abou et. al. [14] measured the intermediate scattering functions of a couple of samples (2.5 and 2.8 wt%) in the ergodic regime of aging and showed that the correlation functions can be described by sum of a single exponential and a stretched exponential. The relaxation time of the first mode turned out to be independent of waiting time, while the relaxation time of slow mode grows exponentially with t_w. The fast mode corresponds to a rapid diffusion of particles in a cage formed by neighboring particles. The slow mode corresponds to the escape from the cages. Besides, they measured the q-dependence of intermediate scattering function and showed both fast and slow relaxation scale as $\tau_1 \sim q^{-2}$ and $\tau_2 \sim q^{-2}$.

The Munch group have also studied the aging dynamics of Laponite solutions in the high concentration region $2.5 < C < 3.5$ wt% [129, 112, 53]. In [129], Knaebel et. al. have studied the aging behavior of Laponite suspensions by multi-speckle diffusive wave spectroscopy (DWS) measurements of tracer particles of 500 nm diameter (Latex particles) in the non-ergodic regime of aging [129]. The advantage of multi-speckle DWS is that long delay times can be measured in non-ergodic samples. They observed that relaxation time of the slow mode grows with waiting time as $\tau_2 \sim t_w^{1.05\pm0.05}$. This behavior has been observed in other glassy systems and is not in contradiction with our measurements or prior measurements of other groups in which an exponential growth of relaxation time is reported. This is because the latter measurements are performed in the ergodic regime, while the former ones in the non-ergodic regime of aging. The exponential rate of aging should disappear in the non-ergodic regime, because τ_2 can never exceed t_w

The same group later performed multi-speckle dynamic light scattering experiments on Laponite suspensions [112]. They observed two regimes of aging. In the first regime the decay time of the slow mode grows exponentially with waiting time and in the second regime, called full aging regime, decay time grows linearly with waiting time. However, in the second regime they found that the relaxation function is described by a compressed exponential $\exp(-(t/\tau_2)^\beta)$, with $\beta = 1.35 \pm 0.15$ i.e a hyperdiffusive relaxation. In addition, the spatial dependence of this relaxation time scales as $\tau_2 \sim q^{-1.3}$ which is in contrast with the q-dependence observed for the non-ergodicity parameter [63]. This is in disagree-

ment with our measurements, since in the time scale they observe a decay of correlation function, our correlation functions show a plateau. The reason for this discrepancy remains unclear at this stage.

Multispeckle x-ray photon correlation spectroscopy measurements performed on Laponite samples [130] led to similar results as [112], however the range of q measured in their experiments corresponds to smaller length scales of the order of interparticle distance. A compressed exponential with the stretching exponent $\beta \approx 1.5$ and the characteristic relaxation time has the q-dependence of the form $\tau_2 \sim q^{-1}$. A convincing generic mechanism for such a hyperdiffusive behavior has not been developed. Hence, the origin of such behavior remains to be clarified.

Nicolai and Cocard [117, 51] have studied the aging of Laponite suspensions at low concentrations with added salt (1 wt%, 5mM). They observe that the mean relaxation time grows with waiting time. More importantly in agreement with our data, the scattered intensity increases with waiting time. The increase of intensity is concomitant with the evolution of q-dependence of the structure: the intensity at lower q-values increase at a faster rate, so that a strong q-dependence characteristic of fractal structures (power law behavior) and aggregation appears.

The nature of the non-ergodic state in Laponite suspensions has been the subject of considerable controversy: both colloidal gel [51, 117, 67, 64] and colloidal glass formation [50, 112] have been invoked and were thought to be mutually exclusive [67, 50]. Our data on whether Laponite is a glass or gel are in agreement with results in the literature. In our view, the controversy about the nature of non-ergodic states of Laponite suspension is due to lack of comprehensive studies on aging behavior of Laponite suspensions. Each group has only studied a specific range of concentrations or salt content. Furthermore, most of the studies have been performed in the ergodic regime of aging. Perhaps, the most complete study is the recent one of the Ruocco group [52, 68, 116], spanning both low and high concentrations region and varying the salt concentration. However, their studies are restricted only to the ergodic regime of aging and they do not present any results in the intermediate range of concentrations $1.5 < C < 2.2$. Their important finding is the existence of two different routes of evolution in the ergodic regime [52], in agreement with our measurements.

At this point it is useful also to compare our experimental results with present simulations on Laponite. Unfortunately, there are not so many simulations works on Laponite and especially its aging behavior. Most of simulation studies have focused on understanding the static properties of structures resulting from charged disks [131, 132]. Furthermore the effective interactions between the two disks are not incorporated in the right way to mimic the real situation and the range of concentrations and ionic strengths in the simulations do not match the range of

experiments. In the simulation of Dijkstra et. al. the Laponite particle and its associated double layer of coions and counterions is replaced by an effective disk which is neutral but carries a fixed quadrupole moment [131]. Their model gives rise to a sol-gel transition in which the resulting gel structure resembles more that of house of cards structure, with no long range order. In the simulations of Kutter et. al. the platelets carry discrete charged sites interacting via screened Coulomb potential. In their molecular dynamic simulations for a few concentrations and Debye lengths they obtain, gel and crystal phases. Mossa et. al. [133] used the model of Kutter et. al. to simulate the aging of Laponite suspensions with Brownian dynamics. Again they simulated a concentration higher than usual experimental conditions. However their results qualitatively agree with aging dynamics observed in the glassy region of phase diagram.

There are no simulation studies of aging during the gel formation. However, there exist simulations based on simple models which show the evolution of structure factor during the aggregation in a similar trend observed for Laponite gels. In one simple toy model, trajectories of particles undergoing Brownian motion in a solvent are computed using a Molecular Dynamics algorithm at constant temperature. When two or more particles touch each other, they stick definitively. Then the mean acceleration and velocity resulting from all independent accelerations and velocities of the particles inside the cluster are computed. And, in order to conserve the relative positions of the particles inside the cluster, the mean acceleration and velocity are used for all particles of the corresponding cluster. Thus in this method no attractive potential between particles is used for computing time reasons and the sticking is an irreversible process. The aging of resulting structure factors from this simulation are comparable to the experiments reported in [134] and Laponite experiments [117](see Fig. 3.15), thus confirming that aging in systems denoted as gel and attractive glass is due to aggregation.

Another simulation reporting gel formation is a Brownian dynamics simulation of aggregating Lennard-Jones particles, in which both cluster growth and cluster reorganization occur simultaneously [135]. The well depth in the Lennard-Jones interaction potential is chosen in such a way that it corresponds to the unstable region of phase diagram and therefore leads to irreversible aggregation. The results of their simulations show at low volume fractions there is a competition between cluster growth and cluster reorganization. At very low volume fractions loose clusters are formed. In moderately low volume fractions and a deep attraction well cluster-cluster aggregation wins. At volume fractions $\phi > 0.07$ percolating networks appear which seem to be formed by reorganization of large aggregates, during which branched strands are formed with voids in between.

Also a recent simulation has studied the aging in attractive colloidal glasses

[136]. Puertas have shown that aging of attractive glasses is broadly analogous to the aging of repulsion driven glasses, albeit with some specifications arising from interaction potential in either case: bond formation for the former, steric hindrance for the latter [136]. Specific differences appear, for instance, for the value of the non-ergodicity parameter and the aging of static structure factor in accordance with our results and earlier observations in attractive glasses [46, 47].

To summarize, we have shown Laponite suspensions can form different types of non-ergodic states (repulsive glass, gel and attractive glass) upon changing concentration and salt content. All these different types of non-ergodic states show similar features which is the aging of their dynamic structure factor. The distinction between them can be made from details of the behavior of static structure factor and translational diffusion with waiting time. While the static structure factor and short-time rotational diffusion of a glass are independent of waiting time, the same quantities are a strong function of waiting time for a gel. Besides the evolution of the non-ergodicity parameter is different in gels and glasses, providing a distinctive measure for distinguishing gels and glasses. Attractive glasses are formed in the intermediate Laponite concentrations and high salt content, their features resembling those seen in hard sphere systems to which an attractive potential is added.

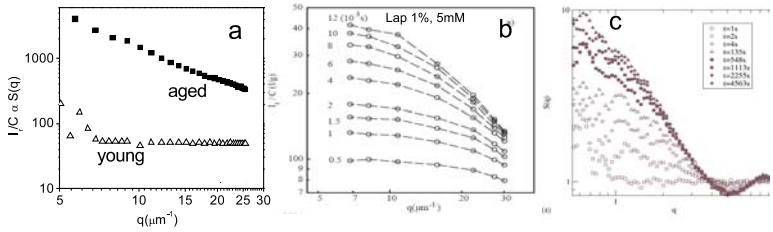

Figure 3.15: Comparison of aging of structure factor in Laponite suspensions in the gel and attractive glass phase with a simple simulation model explained in the text. a) The structure factor at initial and late stage of aging for Laponite 0.2 wt% in pure water (gel) b) The evolution of structure factor as a function of waiting time for Laponite 1 wt%, 5mM salt (attractive glass) taken from [117] c) The aging of structure factor in a simulation model of [134].

4.

Rotational Dynamics in Colloidal Gels and Glasses

4.1 Introduction

In chapter 3, we studied the translational diffusion aging dynamics of suspensions made of charge-stabilized anisotropic Laponite particles. As it was shown, the translational motion of the particles slows down as the material becomes more viscous and solid-like. Measuring the intermediate scattering function during the evolution from an ergodic to a non-ergodic state of such samples revealed that there are two pathways towards the non-ergodic state leading to glasses and gels. In the first pathway, the slowing down of motion occurs due to the topological constraints imposed by cages of neighboring particles. This mechanism is responsible for the aging of high concentration samples. The second path of evolution is characterized by the formation of clusters or networks of particles. This pathway is responsible for the aging of low concentration samples. The first group of samples can be identified as glasses and the second one as gels. These two types of non-ergodic states are distinguishable by different aging behavior of fast and slow relaxations of translational motion as well as the structure factor.

Since Laponite particles are disk-shaped, their anisotropy could in principle affect the aging. Despite various studies of the aging dynamics of translational diffusion [49, 14, 112, 53] and the viscoelastic response [115] of this system, no information is available as yet on the aging dynamics of the particles' rotational degree of freedom. Therefore, the questions that arise are:

- What is the aging behavior of the rotational motion of anisotropic particles in colloidal gels and glasses?

- Is the aging behavior of rotational diffusion different between colloidal gels and glasses and does this provide an extra criterion for distinguishing gels and glasses?

This allows us to study whether translational-rotational decoupling can be observed in colloidal glasses. Such decoupling is characteristic of supercooled liquids with dynamic heterogeneity [5, 11, 30, 31]. Recent studies on (hard-sphere) colloidal glasses reveal the presence of such dynamical heterogeneities [28]; it would be interesting to see whether this has repercussions for the rotational dynamics.

The aging dynamics of the rotational motion of the particles can be investigated using depolarized dynamic light scattering (See Sec. 2.1.3). Here we describe for the first time, the evolution of the rotational diffusion during the aging of colloidal gels and glasses. We find that together with the slowing down of the translational motion, the rotational motion of the particles slows down as well both in gels and glasses. Furthermore, we find that the evolution of both short- and long-time rotational diffusion is distinctly different for the systems that evolve into gel and glass non-ergodic states. Thus, this provides another criterion for discerning them from each other.

4.2 Results

In depolarized dynamic light scattering (DDLS), one measures the correlation functions of the scattered light intensity whose polarization (horizontal) is perpendicular to the polarization of incident light (vertical), i.e. the VH mode, as opposed to the VV mode for which the polarization of scattered and incident light are both vertical. Similar to VV intensity correlations, one observes two regimes of aging in the evolution of the VH intensity correlations: the ergodic and non-ergodic regimes. Here, we focus only on the aging of VH correlations in the ergodic regime. We found that for a wide range of concentrations show that VH correlations become non-ergodic at nearly the same time as VV correlations, or at most $t_w = 0.9t_{eb}$, within the uncertainties in determining the ergodicity-breaking point.

Figures 4.1 shows the evolution of VV and VH intermediate scattering functions for one gel and one glass sample measured at a fixed scattering angle $\theta = 90^o$ corresponding to $q = 1.87 \times 10^7$ m^{-1}. In both cases, the relaxation times of the correlation functions grow with time, as the system ages. This figure shows that

not only the VV correlation functions behave differently between gels and glasses as discussed previously (chapter 3), but also their VH correlations show a distinctly different behavior.

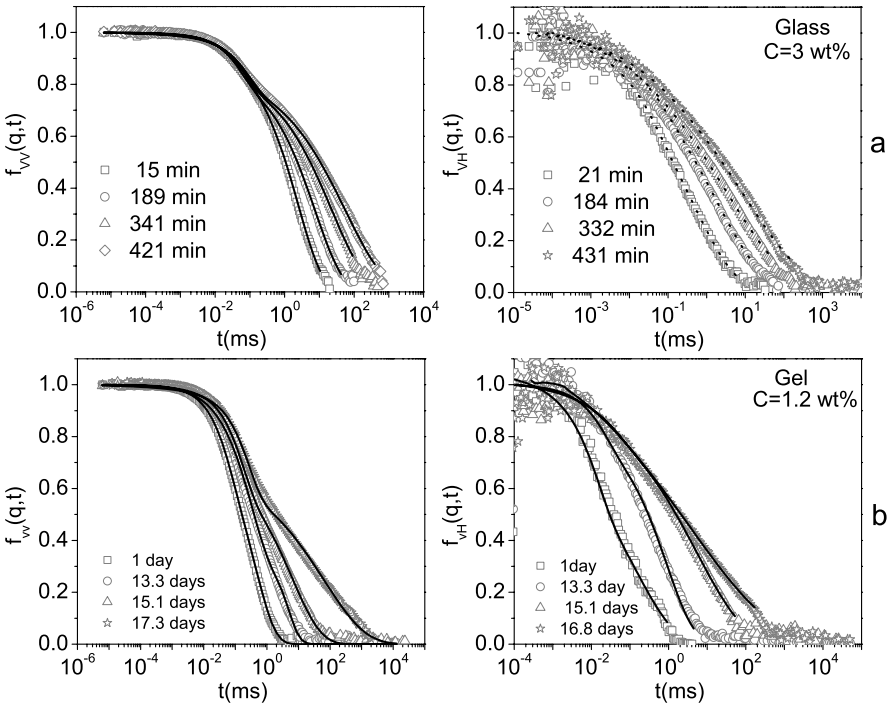

Figure 4.1: Evolution of polarized (VV) and depolarized (VH) intensity correlation functions (symbols) and their corresponding fits (solid lines) to Eq. (4.1) a) for a glass (Laponite 3 wt%, pure water) and b) for a gel (Laponite 1.2 wt%, pure water) measured at a scattering angle of 90^o. The waiting times are shown in the legends. Note that here only the correlations in the ergodic regime of aging are shown.

The VV and VH correlations become non-ergodic at nearly the same time (t_{eb} = 450 min for Laponite 3wt% and t_{eb} = 18 days for Laponite 1.2wt%). For the VH measurements, similarly to what has already been found for the VV correlation functions [115] a two-step relaxation can be observed [137].

In order to consistently describe these two processes quantitatively, we fit the normalized correlation functions, both VV and VH, by the sum of an exponential and a stretched exponential as:

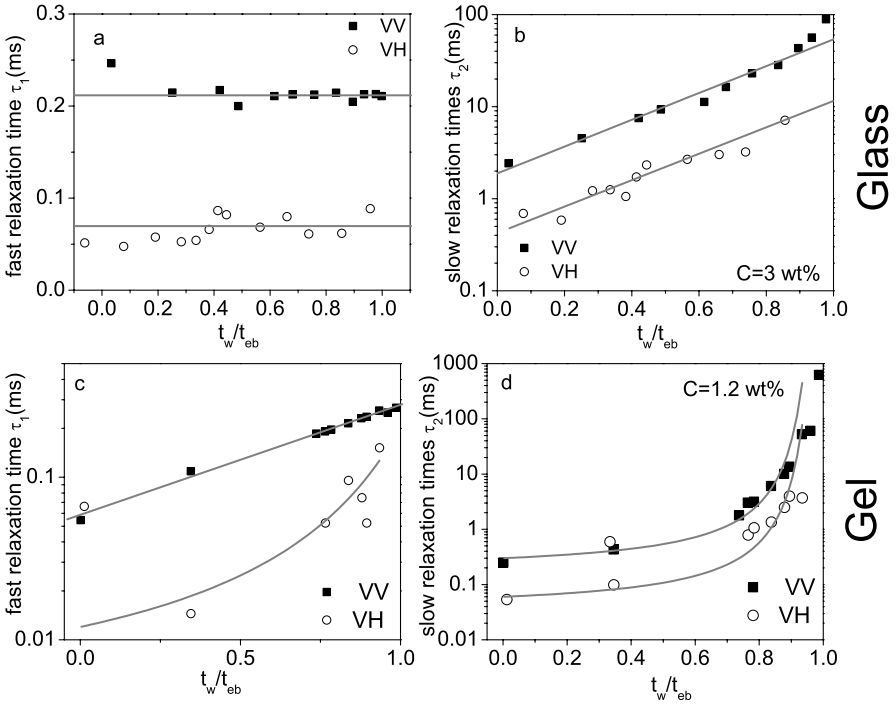

Figure 4.2: Evolution of fast τ_1 and slow τ_2 relaxation times of VV and VH correlation functions plotted versus scaled waiting time t_w/t_{eb} for a glass (Laponite 3 wt%, pure water) and a gel (Laponite 1.2 wt%, pure water). The lines show the fits of relaxation times with the general form $\tau_i(t_w) = \tau_0 \exp(B\frac{t_w}{t_w^\infty - t_w})$.

$$f(q,t) - 1 = A\exp(-t/\tau_1) + (1-A)\exp(-(t/\tau_2)^\beta) \tag{4.1}$$

The stretched exponential is used since it has been found empirically that it provides a good description of the slow relaxation processes encountered in glassy systems [138, 115]. To ensure the accuracy of the extracted value for short-time diffusion and constrain the fitting procedure, we first determined τ_1 independently, using a linear fit for $\ln(f_{VH}(q,t)-1)$ for short times ($t < 0.005$ ms), corresponding to the short-time diffusion. We find that the behavior of the fast and slow relaxation times in the VH mode (related to the rotational motion of the particles) is qualitatively similar to what is seen in the VV mode for a glass.

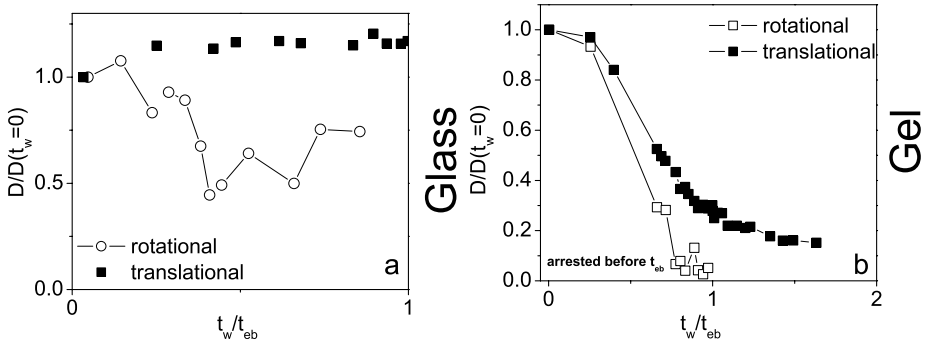

Figure 4.3: Short-time translational and rotational diffusion coefficients normalized to their values at $t_w \approx 0$ as a function of scaled aging time t_w/t_{eb} a) in a glass of Laponite C=3.2 wt% b) in a gel of Laponite C= 1.2 wt%

The relaxation times of VH correlations evolve in parallel with the relaxation times of VV correlations.

For the glass sample above the fast relaxation time is roughly constant with waiting time, while it grows remarkably in the gel sample, as demonstrated in Fig. 4.2c. This figure also suggests that the short-time rotational diffusion decreases at a faster rate than translational diffusion. To investigate this, we have plotted in Fig. 4.3, the short-time rotational and translational diffusion coefficients normalized to their initial values for a glass and a gel sample as a function of scaled waiting time. This clearly confirms that the rotational diffusion in the gel becomes restricted at a faster rate than the translational degree of freedom. In contrast for the glass both short-time and translational diffusion are almost constant as a function of waiting time.

The slow relaxation times of both translational and rotational diffusion grow exponentially in the glass sample, while in the gel phase they grow faster than exponentially. This means that the average relaxation time (the time that it takes for the particles to forget their initial orientation) increases exponentially with waiting time in the glass and faster than exponential in the gel. This is likely to be related to the formation of small clusters at early stages of aging that subsequently aggregate to form a macroscopic structure (with a large relaxation time)[117, 52], therefore restricting both translational and rotational motion of particles.

The evolution of slow relaxation times in both gel and glass and the short

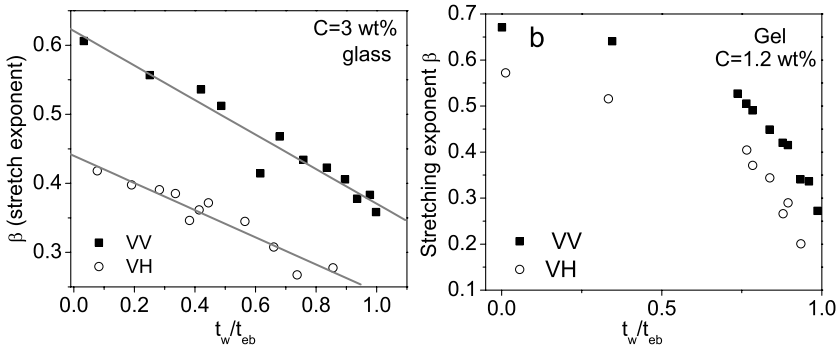

Figure 4.4: The stretching exponents β for VV and VH correlations functions plotted versus scaled waiting time t_w/t_{eb} in a glass (Laponite 3 wt%, pure water) and in a gel (Laponite 1.2 wt%, pure water)

time relaxations in the gel can be described with the general function $\tau_i(t_w) = \tau_0 \exp(B\frac{t_w}{t_w^\infty - t_w})$ (see Fig. 4.2) [52]. Indeed this function is a generalization of exponential growth that is used to describe the evolution of slow relaxation times in the glassy state [14].

Also it is observed that the stretching exponent β decreases with waiting time in both gel and glass, in parallel and at almost the same rate as the corresponding ones from VV correlation, as depicted in Fig. 4.4.

The strong resemblance between the evolution of correlation functions for the translational and rotational degrees of freedom in the gels, suggests that the evolution of rotational diffusion in all of the gel samples should be of the same character and different from the glassy samples.

In Fig. 4.5a, we have plotted short-time rotational diffusion coefficients D_r^{short}, normalized to the rotational diffusion of hard disks in the infinite dilution limit $D_{0r} = k_B T/32\eta R^3$, versus scaled waiting time t_w/t_{eb}. For hard disks of radius $R = 15$nm the translational and rotational diffusion coefficients are $D_{0t} = 2.59 \times 10^{-11}$ m^{2}s^{-1} and $D_{0r} = 1.1 \times 10^5$ s^{-1}, respectively. We see only a moderate decrease of D_r^{short} for the glass samples, while the short time rotational diffusion decreases enormously in the gels. The fact that both the short-time rotational and translational diffusion decrease significantly during the gel formation is plausible and can be caused by particles building up some type of structure. The different behavior of short-time rotational diffusion for a gel and a glass provides another criterion for their distinction. The enormous decrease of short-time rotational

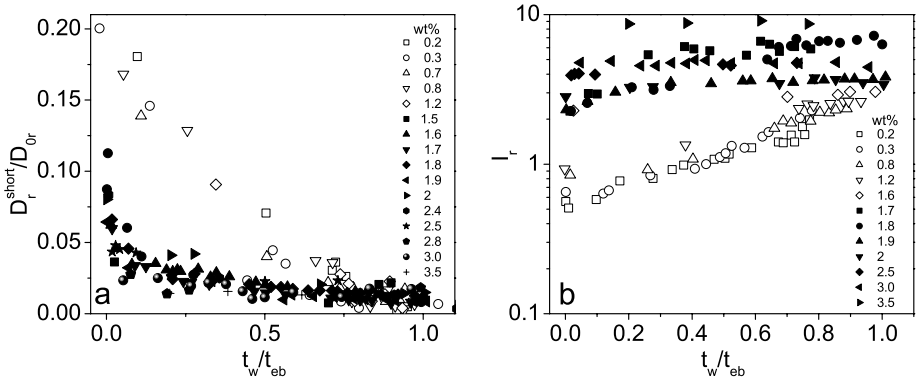

Figure 4.5: a) The short time rotational diffusion coefficients normalized to those of infinitely diluted hard disks of radius $R = 15$ nm: D_{0r} b) The VH scattered intensity relative to Toluene intensity I_r; both plots as a function of scaled waiting time t_w/t_{eb}.

diffusion in a gel also accounts for the stronger increase of its non-ergodicity parameter relative to that of glasses; for the latter, there will always remain a "rattling in the cage" motion that assures the non-ergodicity parameter does not reach unity for long times.

An issue which deserves attention at this point is that the rotational motion of particles in the final non-ergodic states of both gels and glasses is hindered, as can be deduced from Fig. 4.5a. The rotational motion of particles in glass is constrained from the very beginning due to crowding of particles at high concentrations (glass), while in the gel the rotational motion of particles is obstructed as they become part of the network or clusters. To get an idea of the difference in evolution of rotational and translational motion in gel and glass, we have plotted the short-time translational and rotational diffusion coefficients as a function of concentration at the initial and final stages of aging in Fig. 4.6. Both rotational and translational diffusion are normalized to their corresponding values for hard disks at the infinite dilution limit. As can be observed the translational diffusion decreases with time only at low concentrations (gel) while the rotational diffusion decreases in time over a wider range of concentrations and it is almost concentration-independent in the non-ergodic state.

The distinction between gels and glasses was further investigated by looking at the scattered intensity in the VH mode, as presented in Fig. 4.5b. As can be seen the scattered intensity in the VH mode behaves in a distinctly different manner for gels and glasses. The VH scattered intensity is the product of orientational

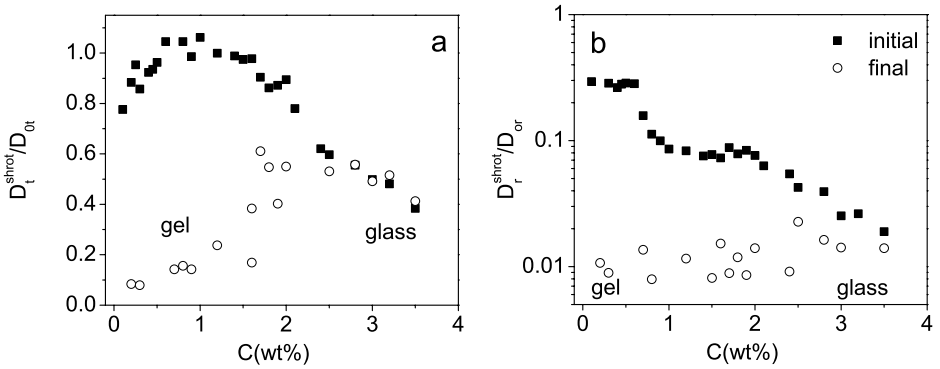

Figure 4.6: Short-time a) translational b) rotational diffusion coefficients normalized to diffusion coefficient of hard disks at infinite dilution as a function of concentration at two stages of aging: immediately after preparation and at $t_w \approx t_{eb}$.

correlations and the structure factor. Since both gel and glass states are disordered with no long-range orientational order, the increase of VH intensity can be attributed purely to growth of the gel structure, as we saw before in the increase of VV intensity.

In addition, if we plot the quantities τ_2 and β for VH correlations as a function of scaled waiting time t_w/t_{eb} , the data from all concentrations again collapse onto two master curves identified as gel and glass phases, as shown in Fig. 4.7. This is in agreement with the classification based on the aging of the translational degree of freedom in chapter 3.

To summarize, we find that both fast and slow relaxation times behave in a qualitatively similar manner in VV and VH modes. We conclude from this that both the translational and the rotational dynamics slow down as the system ages.

The fact that the VH correlation functions are well described by a stretched exponential (Fig. 4.1) suggests that rotational degrees of freedom for different particles relax with different rates. Furthermore, the decrease of the stretching exponent with waiting time expresses the fact that the distribution of these relaxation times becomes wider as the system ages, again in line with earlier observations for the translational dynamics [14].

One should keep in mind that the VV mode reflects mainly the aging of translational degree of freedom, whereas both translational and rotational degrees of freedom contribute to the VH correlations. In order to gain more insight into the rotational dynamics, we extract the orientational correlation function defined as

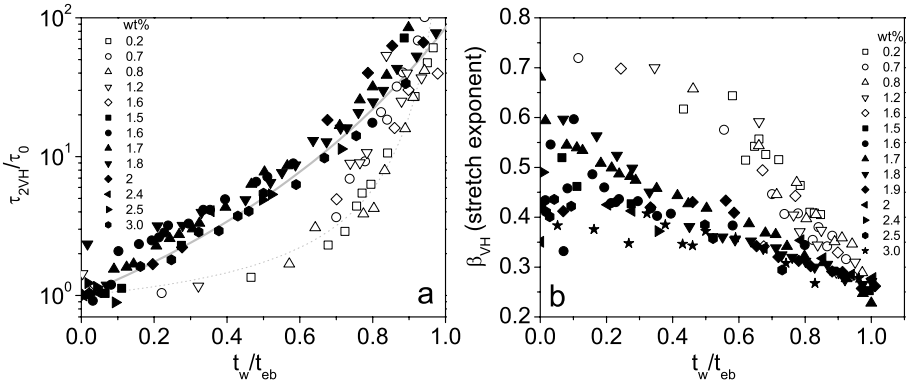

Figure 4.7: The evolution of a) the slow relaxation time normalized to its initial value τ_2/τ_0 b) the stretching exponent β of VH correlations versus scaled waiting time t_w/t_{eb} for different Laponite samples. The colloid concentrations are shown in the legend. Similarly to the translational degree of freedom, the samples can be divided into two groups according to the evolution of the slow relaxation times of VH correlations. In both figures the open symbols correspond to gels, the filled symbols to the glass. In panel a) the solid and dashed line correspond to the glass and gel lines obtained from growth of relaxation time of translational diffusion.

the ratio $f_{or} = \frac{f_{VH}}{f_{VV}}$, assuming that to a first approximation the rotational and translational motions are uncorrelated. The obtained orientational correlations for a gel and a glass are depicted in Fig. 4.8 for different waiting times. The orientational correlations of the gel and the glass clearly behave in a different manner and again can be fitted with the form of Eq. (4.1). The slow relaxation times extracted from these fits are plotted in the inset in comparison with the relaxation times from the translational degree. This confirms what we concluded before, that in both gel and glass the slow relaxation time of the orientational degree of freedom grows faster than the corresponding one for the translational degree.

4.3 Discussion and conclusions

We have measured both the translational and rotational dynamics in aging colloidal gels and glasses. The dynamics are qualitatively similar between the two degrees of freedom.

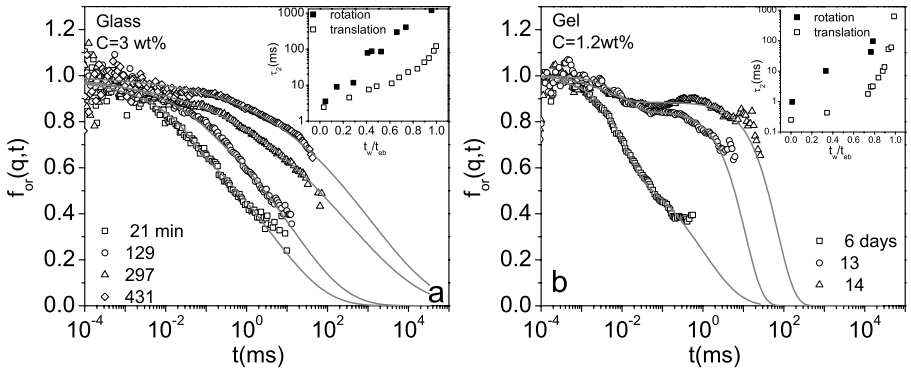

Figure 4.8: The orientational correlation functions defined as f_{VH}/f_{VV} at different waiting times in a glass (Laponite 3 wt%, pure water) and a gel (Laponite 1.2 wt%, pure water). The lines show the fits with the sum of single and stretched exponential as in Eq. (4.1). The insets show the slow relaxation times extracted from orientational correlations compared with the ones from translational diffusion

In the glass, the short-time diffusion is independent of the time elapsed since the sample preparation. The intermediate- and long time diffusion, on the other hand, slows down over several orders of magnitude during the aging. The slowing down of the rotational diffusion is much faster than that of the translational diffusion. It was suggested previously [50, 14] that the translational diffusion dynamics in this (and many other glassy systems) can be described by a cage-diffusion process: for short times or small displacements 'normal' Brownian motion is observed; however for larger times or excursions, the particles are confined in effective cages formed by their neighbors. The slow mode then corresponds to the escape of the particles from their respective cages, which becomes more and more difficult as the system ages. This shows up in the experiments as an increase of the slow relaxation time. The rotational degree of freedom that we look at here is the rotation of the disk around an axis parallel to the faces of the disk; our measurements thus indicate that this motion, too, is hindered, and more readily than the translational motion. Our results [137] are in qualitative agreement with measurements of rotational diffusion in colloidal glass of Laponite using the NMR relaxometry technique [139] which showed a strong slowing-down of rotational motion.

The short-time rotational diffusion decreases dramatically during gel-formation at a rate faster than the short-time translational diffusion. The slow relaxation

time also grows with a much faster rate compared to translational one in the gel. This can be understood from the constraints present for particles in a gel network.

An issue that deserves to be discussed is decoupling between rotational and translational diffusion and its relation to the non-exponential relaxation dynamics. The different behavior of the slow relaxation between translational and rotational diffusion in both gels and glasses (see insets of Fig. 4.8) points to the decoupling of translational and rotational diffusion.

The combination of Stokes-Einstein relation for translational diffusion and the Debye-Stokes-Einstein relation for rotational diffusion predicts that the product of translational diffusion D_t and rotational relaxation time τ_{2rot} will be a constant, even if the macroscopic viscosity increases by orders of magnitude when approaching the glass transition (by decreasing the temperature of glass forming liquids) [11, 140, 31]. However, such a relation is observed to break down in supercooled liquids approaching the glass transition [11]. This is known as the decoupling of translational and rotational diffusion. Recently it has been shown in a model system (mixture of ellipsoids and Lennard-Jones spheres) that decoupling of translational and rotational diffusion is correlated with manner of exploration of the free energy landscape [141]. Chakrabarti et. al. have shown that the decoupling between rotational and translational diffusion is signaled by an increase in the rate of fall of the average inherent structure energy [141]. Furthermore, it is found that the onset of non-exponential relaxation in the supercooled regime corresponds to the temperature below which the dynamics of the system is influenced by its energy landscape [18].

The non-exponential behavior of both translational and orientational correlations and their description by a stretched rather than a simple exponential points to a broad distribution of relaxation times for both degrees of freedom. It seems likely that this distribution of relaxation times is at least partially due to spatially heterogeneous dynamics, i.e., rotational and translational motions of particles are faster in some parts of the sample than in other parts and particles in the slow domains are responsible for the long tail of correlations. It is discussed in the literature that the dynamic heterogeneity plays a central role in the decoupling between rotational and translational diffusion [22, 142]. The diversity of the depth of meta-basins and of their connecting pathways in configuration space are expected to result in the broad spectrum of relaxation times underlying dynamic heterogeneity.

In summary, our data provide further evidence for the decoupling of translational and rotational diffusion and its correlation with dynamic heterogeneity in both gel and glassy non-ergodic states. Our data also suggest that the decoupling is stronger in heterogenous samples (gels) than the homogeneous ones (glasses),

as the the difference in the aging behavior of rotational and translational degrees of freedom is more pronounced in gels.

Finally, we would like again to emphasize that the rotational degree of freedom evolves differently in the gel and glass as the material ages. Therefore, the aging of the rotational degree of freedom provides us further indicators to distinguish between gels and glasses of Laponite suspensions.

5.

FDR in Colloidal Glasses and Gels

5.1 Introduction

Developing a statistical mechanical description of non-equilibrium systems such as glasses and gels still remains an important challenge in physics. One of the most interesting recent developments along these lines is the proposal to generalize the fluctuation dissipation relation (FDR) to non-equilibrium situations [3], as was explained in section 1.3.2. The FDR relates the response of a system to a weak external perturbation to the relaxation of the spontaneous fluctuations in equilibrium. The response function is proportional to the power spectral density of the thermal fluctuations, with a prefactor given by the temperature. This suggests a generalization for systems out of equilibrium, in which the (non-equilibrium) fluctuations are related to the response via a time-scale-dependent *effective temperature* (Eq. (1.22) or Eq. (1.24)). Deviations from fluctuation-dissipation relations (FDR) have been studied extensively in theoretical methods and simulations for various model systems such as structural glasses [143, 38], spin glasses [3, 36, 144, 13, 37], non-equilibrium ferromagnetic systems [145, 146, 147, 148], trap model [149, 150, 151] and driven systems such as a fluid under shear [152, 153, 154, 155, 156, 157, 158] aging critical systems [159, 160] and some other solvable theoretical models [161, 162, 163, 164, 165, 166]. In all simulations [143, 38] and theoretical investigations [3, 36, 144, 13, 37], where violations are found they occur when the characteristic observation time t is of the

same order or greater than the age of the system, i.e., when $t \geq t_w$ or $\omega t_w \leq 1$, where $\omega \sim 1/t$ is a measurement frequency and t_w is the waiting time.

However, the experimental support for a meaningful effective temperature is unclear. There have been few experiments on a structural glass [39], a spin glass [167], granular matter [168, 169, 170], hard sphere colloidal glasses [71, 41] and the colloidal glass of Laponite [40, 171, 25, 70], with sometimes contradictory results.

Perhaps the most convincing experiments supporting deviations from FDR are the measurements on a spin glass of Hérisson and Ocio [167]. They measured the deviations from FDR of the slope of the magnetic susceptibility together with magnetization fluctuations, in a spin glass with a quench temperature of $T = 0.8T_g = 13.3K$. They observed deviations from FDR when the delay time is larger than the waiting time. These deviations are an increasing function of the delay time for a fixed waiting time and decrease as the spin glass ages. The mean slope of FDR data corresponds to an effective temperature of about 30K, which is 2.25 times higher than the bath temperature.

Grigera and Israeloff quenched glycerol below its glass transition temperature to a temperature of 179.8 K. They determined the effective temperature of this structural glass by coupling it to a capacitor which acts as a harmonic oscillator and measured the ratio of voltage fluctuations to the frequency dependent impedance (see the Nyquist formula Eq. (1.20)). They report a weak deviation from FDR which is at most 5 degrees higher than bath temperature at the resonance frequency $f = 7.7Hz$ of their setup [39].

Bonn and Kegel have determined the effective temperature of a supercooled hard sphere colloidal fluid from the ratio of the frequency-dependent mean square displacements (MSD) derived from light scattering experiments to the viscoelastic response function measured by rheology [71]. Their results, suggest effective temperatures which are decreasing functions of frequency and 60 times larger than the bath temperature at the lowest frequency reported. However, these are not direct comparisons, since the MSD and mechanical response were measured for different samples.

Song et. al. measured the effective temperature in a hard sphere colloidal glass [41]. They determined the effective temperature from the long-time limit of MSD and the mobility of tracer particles (by applying a constant magnetic force). According to their findings, the MSD and mobility scale with the ageing time as a power law. Nevertheless, according to their analysis the glassy system thermalizes at a constant temperature independent of the age and twice the bath temperature.

For the Laponite system, especially, contradictory results have been reported for deviations of the FDR. Bellon et. al. [40, 25] measured the effective temper-

ature resulting from the Nyquist formula Eq. (1.20) which relates the voltage fluctuations to the impedance. They reported an effective temperature which is a decreasing function of waiting time and frequency and can be 1000 times larger than the bath temperature at lowest measured frequency of 1Hz. While electrical measurements report strong violation of FDR in the frequency range 1-40 Hz, the same group does not see deviations in their mechanical measurements in the frequency range 1-20 Hz [171]. These measurements by the same group seem contradictory. However one does probe different degrees of freedom in these two sets of measurements.

On the other hand, Abou et. al. report a non-monotonous behavior for the effective temperature of Laponite samples as a function of waiting time determined from the application of the Einstein relation [70, 172]. According to their measurements there is a frequency-dependent effective temperature of the form $T_{\rm eff} = f(b, \beta, t_w)(\omega/\omega_0)^{2-b-\beta}$, in which the values of both β and b evolve with waiting time; at the beginning of aging $\beta(t_w) = 0,\ \ b(t_w = 0) = 2$ and at late stages of aging $\beta(t_w) = 1,\ \ b(t_w) = 1$. The above form leads to an effective temperature which is an increasing function of frequency. Therefore, their $T_{\rm eff}$ is equal to the bath temperature T for a young sample; it subsequently increases up to maximum value at an intermediate age and then decreases when the sample further ages towards the bath temperature again. In this study the frequency-dependent effective temperature was derived by measuring the diffusion and mobility of micrometric beads embedded in the glass.

The usefulness of the extension of the FDR to non-equilibrium situations is still therefore a matter of controversy and deserves further investigation. It is important to identify the time-scales at which FDR is violated, since this has practical consequences. For instance, the passive microrheology technique (see Sec. 2.3) which is a useful tool to determine viscoelastic properties of complex fluids is based on FDR and has been used in non-ergodic systems [173].

In microrheology tracer particles are used to probe the dynamics of the fluid. Taking advantage of a combination of both *active* and *passive* microrheology techniques, we are then able to examine the validity of FDR in the form of the Einstein relation Eq. (1.15) in a wide range of frequencies (1-100k HZ) for two different glassy systems.

In passive microrheology, one measures the displacement fluctuations of the probe particles $x(t)$. While in the active method, one directly measures the mechanical response of the probe particle to an applied oscillatory force $\alpha(\omega)$. Consequently, by comparing the power spectrum of thermal fluctuations $\langle|x(\omega)|^2\rangle$ with the imaginary part of the response function $\alpha''(\omega)$, we can obtain the frequency-dependent effective temperature (See Sec. 1.3.2 and 2.3).

$$\frac{T_{\rm eff}}{T_{\rm bath}} = \frac{\omega\langle|x(\omega)|^2\rangle_{\rm passive}}{2k_BT_{\rm bath}\alpha''_{\rm active}(\omega)} = \frac{\alpha''_{\rm passive}(\omega)}{\alpha''_{\rm active}(\omega)} \tag{5.1}$$

If $T_{\rm eff} = T_{\rm bath}$, then the fluctuation-dissipation relation is valid. Microrheology technique provides a way to *directly* test the applicability of the Einstein relation in non-equilibrium systems.

Here, we examine the validity of the Einstein relation as an example of FDR (see Sec.1.3.1) in aging Laponite suspensions during the evolution from a liquid-like state to a non-ergodic gel or glass state. We also investigate the validity of FDR for a hard sphere glass.

5.2 Einstein relation in aging colloidal gels and glasses of Laponite

As was demonstrated in chapter 3 depending on Laponite concentration and salt content, different mechanisms are responsible for the evolution of system into a non-ergodic state. Laponite suspensions can form either gel-like or glassy structures. Here, we study the validity of the Einstein relation in one sample which is known to be a glass and a few gel-forming samples.

Experimental procedure

Laponite samples immediately after their preparation (see Sec. 3.3), are mixed with a small fraction ($< 10^{-4}$ vol%) of silica probe beads. The solution is then introduced into a sample chamber of about 50 μl volume, consisting of a coverslip and a microscope slide separated by a spacer of thickness 70 μm. This is sealed with vacuum grease to avoid evaporation of the sample. We then optically trap a single silica bead and perform active and passive microrheology experiments. The size of silica particles used in these experiments was either 1.16 or 0.5 micrometers in diameter. Note that the bracket <> in Eq. (5.1) refers to ensemble-averaging, while in our measurements we use time-averaging. Since the system evolves toward a non-ergodic state, one might worry that the time average may not be equal to ensemble average for the measured displacement power spectral densities (PSD). To investigate this, we confirmed that our results do not depend on the time interval used to compute the time average. Thus, we conclude that, after all, we can use the time-averaged PSD without further ensemble-averaging.

5.2.1 FDR in the Colloidal glass of Laponite

We chose a concentration of 2.8 wt% of Laponite in water (see chapter 3). The rate of aging at this concentration is slow enough, on the one hand, that no significant structural and dynamic changes occur during each individual active and passive microrheology measurement lasting at most 2 min. On the other hand, the system evolves fast enough to allow us to follow the evolution from 'liquid' to 'solid' (the sample no longer flows when the sample cell is tilted) within about 8 hours. In these experiments, we used silica particles of 1.16 μm diameter as probe particles.

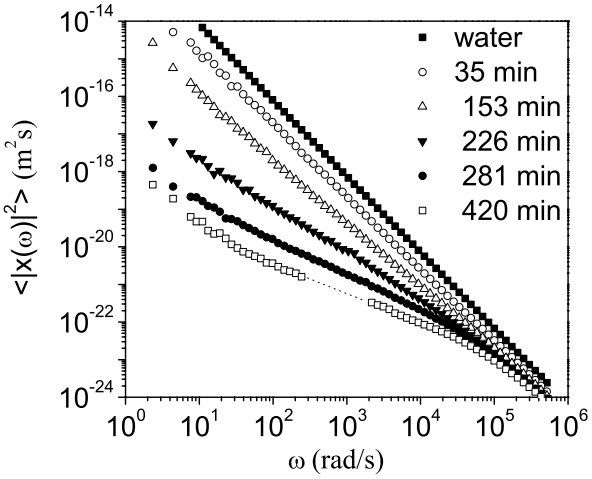

Figure 5.1: The displacement power spectral densities (PSD) of 1.16 μm silica probe particles as a function of frequency in a 2.8% Laponite solution in water with increasing age (after preparing the sample). Fluctuations were recorded for 45 seconds with the 830 nm laser focus and results averaged in x-y directions for 1 bead several times. Aging times are given in the legend. The filled squares show the PSD of a bead in pure water for comparison. An acoustic noise signal around $f \approx 200$Hz is cut out from the curve at the latest stage of aging where the displacement signal was the lowest. All experiments were done at 21^oC.

Figure 5.1 shows the displacement PSD of a single bead measured with the passive method for different aging times measured at a fixed position in the sam-

ple. It is evident that the particle motion progressively slows down with increasing waiting time, reflecting the increase in viscosity of the system. Qualitatively two regimes of aging are seen: for $t_w < 200$ min the PSD can be described by a single power law. At longer aging times two distinct slopes appear in the log-log plot (Fig. 5.1).

We also measure the (active) response of the same bead used in passive measurements, as a function of waiting time and for oscillation frequencies of f =1.2, 10.8, 116, 1035 and 12000 Hz.

Figure 5.2 depicts the amplitude and phase of the response function versus waiting time for several frequencies. We have normalized the amplitude to its value at the beginning of the measurement, $t_w \approx 45$ min. Fig. 5.2b shows the frequency dependence of the response amplitude in the early stages of aging. It is a linear function of frequency with slope 1 leading to a constant mobility, similarly to what happens for water. With time, both the amplitude and the phase of the response function decrease. Again the the frequency behavior of the phase at early stages of aging resembles that of water (phase = $\pi/2$, independently of ω). Subsequently the phase decreases and becomes frequency-dependent. As is apparent, the lowest frequency has the fastest evolution. In the latest stages of aging the frequency-behavior of the phase in the low frequency region (1-100 Hz) is similar to that of a purely elastic solid as shown in Fig. 5.2d; at higher frequencies the material behaves more like a viscoelastic fluid.

To directly compare the (passive) fluctuations with the (active) response, we express our fluctuation PSDs normalized in such a way as to permit a direct comparison with the measured $\alpha = \alpha' + i\alpha''$ in the form of Eq. (5.1). Thus, we first calculate the measured PSD multiplied by $\omega/(2k_BT)$, which we define to be called the imaginary part of passive response $\alpha''_{\text{passive}}$. We obtain the real part using a Kramers-Kroning (principal-value) integral Eq. (1.12): $\alpha'_{\text{passive}}(\omega) = \frac{2}{\pi} P \int_0^\infty \frac{\xi \alpha''_{\text{passive}}(\xi)}{\xi^2 - \omega^2} d\xi$. The cutoff error due to a finite range of frequencies sets an upper limit to $\alpha'_{\text{passive}}(\omega)$ about a decade lower than that of $\alpha''_{\text{passive}}(\omega)$. Fig. 5.3 depicts the real and imaginary parts obtained from the active and passive methods at different stages of aging. We see that the results for α''_{active} and $\alpha''_{passive}$ are identical to within the experimental errors, showing that there are no deviations from the FDR in this system over the range of frequencies and aging times probed in our experiments. Note that the small deviations between the respective $\alpha'(\omega)$ values at high frequencies are likely due to cut-off errors in the Kramers-Kronig integrals. The values of α' calculated from the extrapolated power spectrum of α'', obtained through fitting, show a significantly better agreement, as depicted by solid lines in the Fig. 5.3.

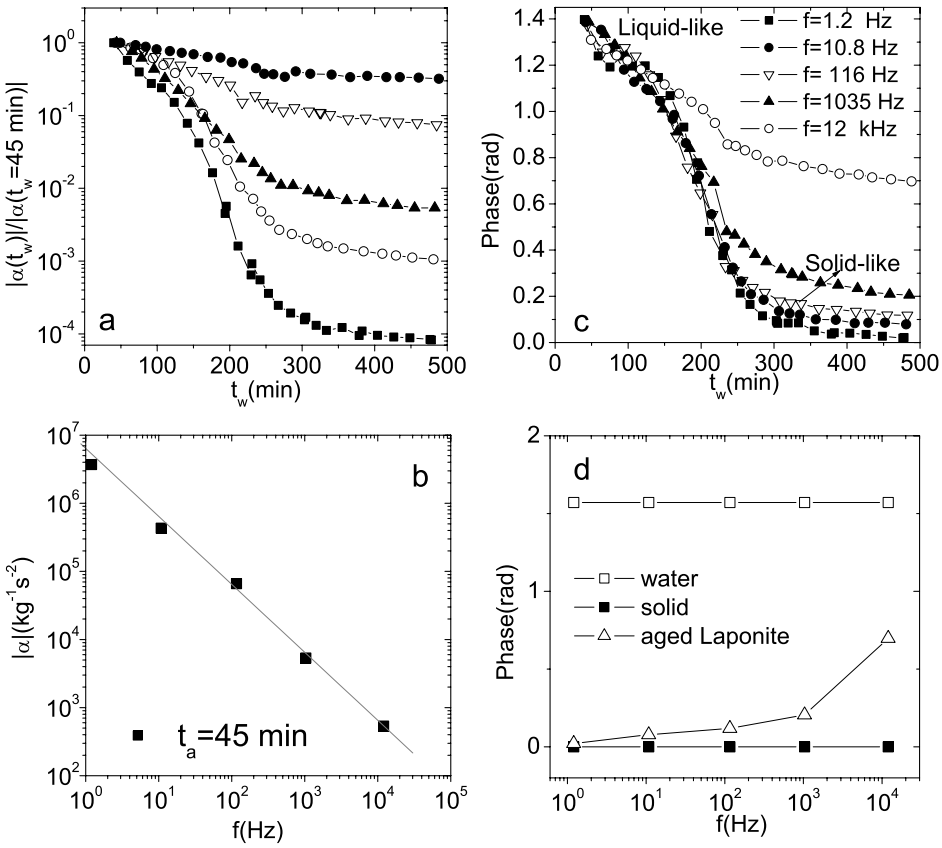

Figure 5.2: The time evolution of a) amplitude normalized to its value at $t_w = 45$ min, b) the frequency dependence of response amplitude at $t_w = 45$ min c) phase of complex compliance obtained from active microrheology measurements for 1.16 μm silica beads at frequencies (f=1.2, 10.8, 116, 1035 and 12k Hz). d) the frequency behavior of response phase in pure water, aged Laponite and a purely elastic solid. The amplitude of oscillation for the active experiments was 77 nm. Note that after 200 min, we increased the trap power from 1.47×10^{-5} to 1.21×10^{-4}, since a larger force amplitude was needed to oscillate the bead in stiffened material.

The fitting is based on assuming a simple addition of two power law contributions to the complex shear modulus (only a single power-law contribution at the

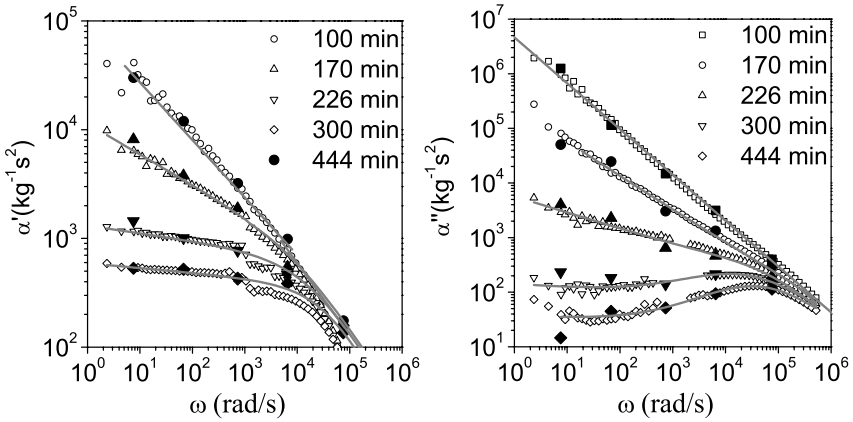

Figure 5.3: Comparison of active and passive microrheology results: Real α' and imaginary α'' parts of the frequency-dependent response functions at different stages of aging obtained from active (solid symbols) and passive (open symbols) microrheology using the same 1.16 μm diameter silica beads in the same aging sample. Imaginary parts of the response functions are obtained directly and real parts are calculated with a Kramers-Kronig integral from the PSDs for the passive experiments. Both parts were measured directly in the active experiments. An acoustic noise signal around $f = 200$Hz is cut out from the passive data at the latest stage of aging where the displacement signal was the lowest. Both parts were measured directly in the active experiments. The lines show the fits of the response function to Eq. (5.2). At early stages of aging the data can be described with one power law, while at later stages, a superposition of two power laws is needed to describe the whole frequency range.

early stages of aging) which is inversely proportional to the response function:

$$\alpha(\omega) = \frac{1}{6\pi R G^*(\omega)} = \frac{1}{C_1(\imath\omega)^a + C_2(\imath\omega)^b} \tag{5.2}$$

The above form has been chosen since a similar description in terms of a network in a more fluid-like background has been suggested before for polymeric gels [174, 175]. The interpretation of the model is that it results from an elastic structure, in addition to the more viscous response that is always present. As can be seen the agreement between the data and suggested form of the fits is excellent for both the imaginary and the real parts of response function. Despite the model being usually employed for network-like structures [174, 175], our sample is com-

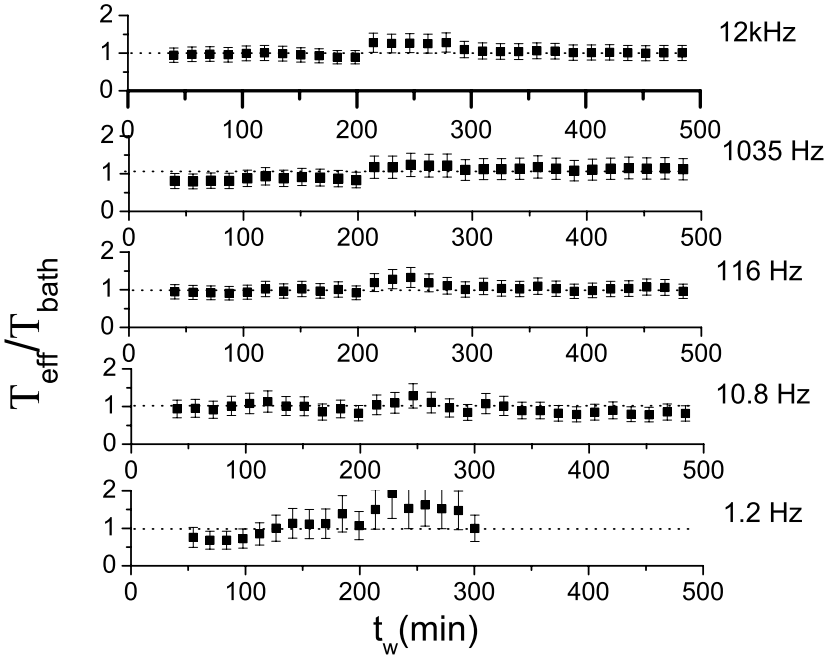

Figure 5.4: The ratio of (apparent) response derived from fluctuations via FDT and actively measured response $T_{\rm eff}/T_{\rm bath}$ as a function of waiting time for different frequencies ($f = 12000, 1035, 116, 10.8$ and 1.2 Hz from top to bottom) in Laponite colloidal glass of 2.8 wt% concentration. Note that the apparent increase after 200 min, is due to calibration errors, caused by changing the trap power to apply the oscillatory force.

pletely homogenous. In Fig. 5.4, we plot the resulting $T_{\rm eff}/T_{\rm bath} = \alpha''_{\rm passive}/\alpha''_{\rm active}$ as a function of waiting time for several different frequencies. This figure confirms again that to within experimental uncertainty the FDR holds: the measured effective temperature does not differ from bath temperature. The errors for the lowest frequency (1.2 Hz) are relatively large and the data for aging times greater than 5 h are not reliable anymore, because at long waiting times the material becomes stiff and the signal to noise ratio decreases. Consequently, $1/f$ noise from laser pointing fluctuations becomes dominant at low frequencies. This is directly visible in the passive data at low frequencies: when the fluctuations become small the error becomes large. In addition, for the active measurements the uncertainty

in determining the phase of the response becomes large at low frequencies when the elastic modulus of the material becomes dominant (See Fig. 5.2).

We conclude that these measurements show that the FDR in the form of the *Einstein relation* is valid for all the frequencies investigated here, and can be used for all the stages of aging in this system.

Since we have directly compared both the real and imaginary parts of the response functions, this represents a stronger test of the FDR than the previous measurements of Abou et. al. [70] and much more convincingly demonstrates that the FDR is valid in the measured range of frequencies for this non-equilibrium system.

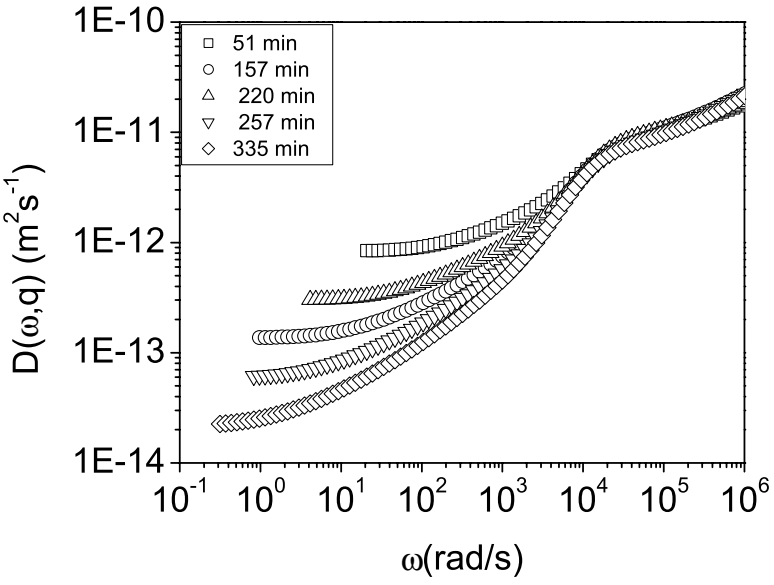

Figure 5.5: The frequency-dependent diffusion coefficient at a scattering vector corresponding to $qR = 0.3$ for different stages of aging of a colloidal glass of Laponite 3.2 wt %. The waiting times are shown in the legend.

A relevant issue here is at what time scales we might expect to find deviations from FDR. By theoretical predictions, the deviations from FDR are expected when $\omega t_w \gg 1$ [3]. However this condition makes sense for glassy systems in which the relaxation times are comparable to the waiting times. In our system, the relaxation times can be several orders of magnitude smaller than the waiting

times. The more reasonable criterion is to expect the deviations from FDR at the time scales that we see the structural relaxations and not the in-cage dynamics. To have a better idea of what is going on, we have obtained the frequency-dependent diffusion of Laponite particles from DLS measurements and compared it with the frequency-dependent diffusion coefficient of tracer particles used in our MR experiments. The DLS and MR measurements were performed simultaneously on the same sample of Laponite 3.2 wt%, in pure water. As we showed in chapter 3, the correlation functions of Laponite suspensions can be well described by a sum of a single exponential and a stretched exponential (Eq. (3.2)), in the ergodic regime of aging (see Fig. 3.1). Fortunately, the Laplace transform of a stretched exponential though difficult, can be calculated analytically. We used Mathematica to do it analytically. By knowing the form of the intermediate scattering function ($f(q,t)$) in the frequency domain ($S(q,\omega)$), we can calculate the frequency dependent diffusion coefficient [176].

$$S(q,\omega) = \int_0^\infty f(q,t)\exp(i\omega t) = \frac{1}{-i\omega + D(q,\omega)q^2} \tag{5.3}$$

Fig. 5.5 shows the frequency-dependent diffusion coefficient at a scattering vector corresponding to $qR = 0.3$ for different stages of aging.

The frequency-dependent diffusion coefficient in MR can be obtained from the power spectrum of displacements as $D(\omega) = \frac{1}{2}\omega^2|x(\omega)|^2$. In order to compare the diffusion coefficients from MR and DLS experiments, we have scaled their values with the factors $6\pi R$ and $12R$, respectively to remove the trivial dependence of diffusion coefficient to particle size. In Fig. 5.6, we have depicted the frequency-dependent diffusion of Laponite particles and the tracer particle at two different waiting times. At early stages of aging the two diffusion coefficients agree at high frequencies, while the diffusion of Laponite particles is significantly lower at low frequencies. However, as the sample ages, the two diffusions do not agree at any frequency and surprisingly the diffusion of the larger tracer particle has evolved with a faster rate than the Laponite particles. This comparison clearly shows us that in addition to the short-time dynamics, we are probing the structural relaxations. The difference in the speed of aging for diffusion of Laponite particles and tracer particle is most likely due to the different length scales that we are looking at. This suggestion agrees with the experiments of Strachan et. al. who investigated the diffusion of trace particles of different size [177] as a function of waiting time. Measuring the diffusion of tracer particles of 50, 100 and 200 nm particles in aging Laponite particles, they found that the particles relaxations are identical at the beginning of aging, however as the time proceeds, the correlation functions of the larger tracer particles evolve at a faster rate.

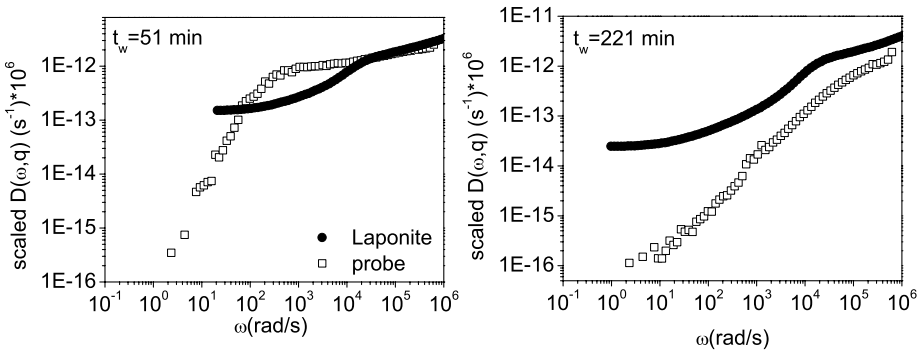

Figure 5.6: The frequency-dependent diffusion coefficient of Laponite particles at a scattering vector corresponding to $qR = 0.3$ compared to the diffusion of a probe particle of diameter 1.16 μm at two different stages of aging in a colloidal glass of Laponite 3.2 wt %. The waiting times are shown in the legend. Note the diffusion of probe and Laponite particles are scaled with their radii to be comparable.

5.2.2 FDR in colloidal gels of Laponite

Colloidal gels and attractive glasses are another class of non-equilibrium systems (See chapter 3). In such systems, similarly to what happens in glasses, correlation and response functions can be a function of time elapsed since their preparation and their relaxation times grow in time, despite the fact that the origin of aging in these samples is different: the time evolution of the gel is a result of formation of network-like clusters or aggregates. Despite a number of studies on the validity of FDR in colloidal glasses, as far as we know there has as yet been no study investigating the FDR in evolving non-equilibrium gels. In some range of Laponite concentrations and salt content, the particles form a soft colloidal gel and attractive glass which is evolving from an initially liquid-like state to a viscoelastic solid-like state.

We performed the experiments on two samples: Laponite 0.8 wt % with 6 mM salt (attractive glass) and 0.8 wt % with 3mM salt (gel). In chapter 3, we showed that the final structure factor of these samples shows a q-dependence, suggesting a heterogenous structure. Therefore, we examined the heterogeneity of these samples by measuring displacement PSD of several beads at different positions of the samples at different stages of aging. At intermediate stages of aging, the PSDs of beads measured at almost the same time but different positions were not

equal (Fig. 5.7), hence demonstrating the heterogeneity of the samples at length scales of a few micrometers, as the light scattering experiments did indeed suggest. Furthermore, at some positions in the sample we observed some anisotropy, i.e. displacement PSDs measured at x and y directions were not equal. The details of these experiments and how heterogeneity develops with time will be discussed in the next chapter. Here, we choose a few beads at different positions in the sample and investigate the validity of the Einstein relation by performing both active and passive microrheology on each bead at in the sample.

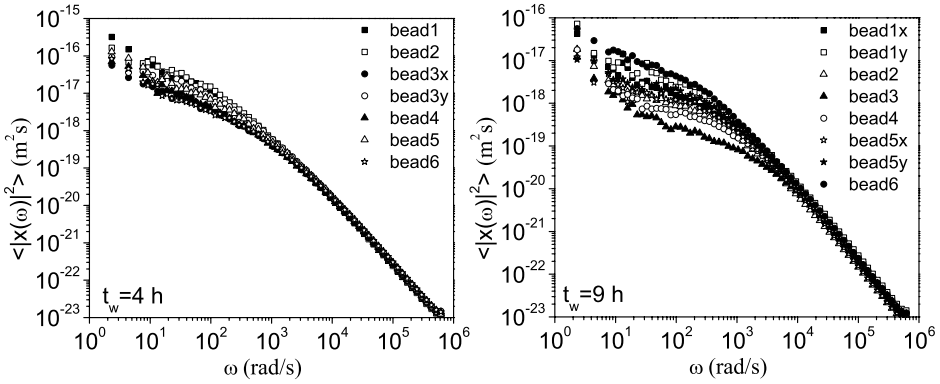

Figure 5.7: The PSDs of several silica 0.5 μm beads measured at nearly the same time at different positions of an attractive glass of Laponite 0.8 wt %, 6mM NaCl, after 4 h and 9 h.

Fig. 5.8 shows the imaginary part of response function obtained from active and passive microrheology measured at different positions of Laponite 0.8 wt%, 6mM and different stages of aging. Similar to the glass, here we also observe a good agreement, verifying the validity of FDR in the measured range of frequencies.

Fig. 5.9 shows the response function obtained from active and passive microrheology measured at 3 different positions of Laponite 0.8 wt%, 3mM. The rate of aging for this sample is slow enough, that there is no significant evolution during the one series of measurements. These data are measured 5 days after sample preparation. To inhibit sedimentation of beads, the sample chambers were rotated slowly during the aging. As can be seen, for beads (a) and (c) the measured PSDs are not equal in the x and y directions. Nevertheless the apparent response from passive microrheology in the y direction agrees well with active response obtained by exerting an oscillatory force in the y direction. Measurements

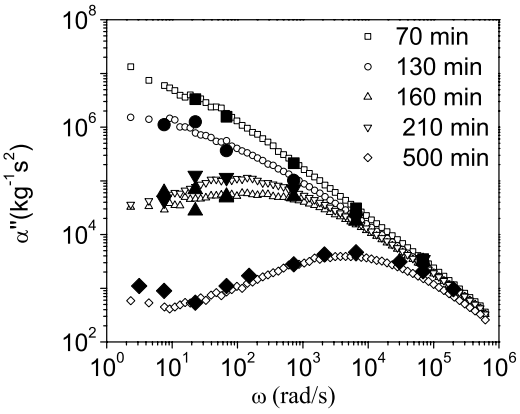

Figure 5.8: Imaginary parts α'' of the frequency-dependent response functions from active (solid symbols) and passive (open symbols) microrheology using 0.5 μm diameter silica beads at different positions of the Laponite 0.8 wt%,6mM NaCl sample measured at different stages of aging. The aging times are shown in the legend.

without rotation of the sample chamber show identical results.

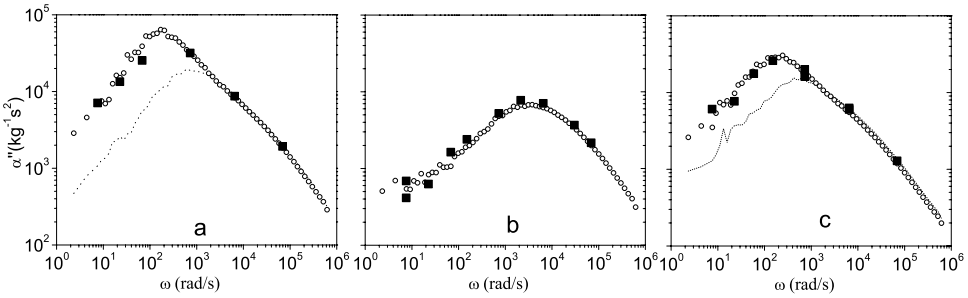

Figure 5.9: Imaginary parts α'' of the frequency-dependent response functions in the y direction from active (solid symbols) and passive (open symbols) microrheology using 0.5 μm diameter silica beads at 3 different positions of the Laponite 0.8 wt%, 3mM NaCl sample. The dotted lines in panel (a) and (c) show the α'' in the x direction which is different from its value at y direction at these positions of the sample. The data are measured 5 days after sample preparation.

The most important conclusion from this section is that despite the presence of heterogeneity in the gels, FDR in the form of the Einstein relation is valid locally at each point of the sample just as it was for the glassy system (see Fig. 5.10).

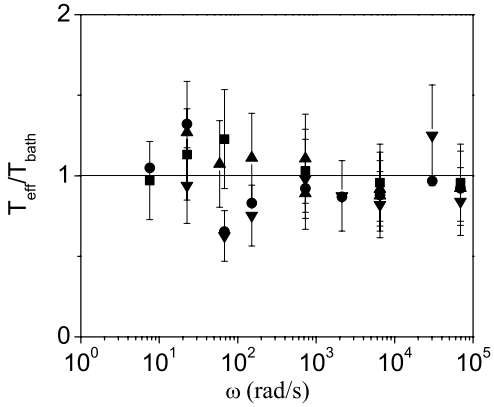

Figure 5.10: The ratio of (apparent) response derived from fluctuations via FDT and actively measured response $T_{\rm eff}/T_{\rm bath}$ as a function of frequency, obtained from 0.5 μm diameter silica beads at 4 different positions (shown by different symbols) of the Laponite 0.8 wt%, 3mM NaCl sample. The data are measured 5 days after sample preparation.

The validity of Einstein relation for a wide range of frequencies ($1 - 10^5$ Hz) allows us to obtain the viscoelastic properties of aging Laponite suspensions over a very wide frequency range from passive microrheology; classical (macroscopic) rheology is limited to frequencies up to about 10 Hz [115]. The frequency behavior and time evolution of viscoelastic properties of Laponite suspensions is the subject of the next chapter of this thesis.

5.3 The Einstein relation in a hard sphere colloidal glass

Experimental details The experimental system mimicking a hard sphere system is a dispersion of poly-methyl methacrylate (PMMA) colloids sterically stabilized with a layer of 10 nm poly-12-hydroxystearic acid (kindly provided by Didi Derks) [178] in a refractive index and density matched solvent. The

solvent is a mixture of Cyclohexyle bromide (CHB, C_6H_11Br) and cis-decalin (Decahydronaphthalene) with weight ratio 3:1. Since CHB is a polar solvent, colloidal particles dissolved in it are charged. To screen the charges, the mixture is saturated with salt tetrabutyl ammonium bromide (TBAB) (around 300 μM/l).

The density of PMMA particles is ρ= 1.19 g/cm^3 and $n(\lambda = 500$ nm) =1.49 ($n(\lambda = 1064$nm) = 1.4184). The density and refractive index of decalin is $\rho_1 = 0.893$ g/cm^3 $n_1(\lambda = 500$ nm)= 1.481 and $n_1(\lambda = 1064$ nm)=1.470 and the corresponding values for CHB are $\rho_2 = 1.33$ g/cm^3, $n_2(\lambda = 500$nm)= 1.50. The refractive index of the mixture n_{12} can be estimated from the Lorentz-Lorenz mixing rule. This turns out to be the theoretical estimate that best matches the experimental results [179].

$$\frac{n_{12}^2 - 1}{n_{12}^2 + 2} = \frac{n_1^2 - 1}{n_1^2 + 2}\phi_1 + \frac{n_2^2 - 1}{n_2^2 + 2}\phi_2 \tag{5.4}$$

where $\phi_1 = 0.332$ and $\phi_2 = 0.668$ are the corresponding volume fractions of cis-decalin and CHB, respectively. This would lead to the refractive index of $n_{mix} = 1.493$ which is more or less the same as that of PMMA.

The mixture density is estimated as $1/\rho_{mix} = x_1/\rho_1 + x_2/\rho_2$, in which x_i are the mass fractions of each component. The resulting density is 1.185 gr/cm^3 very close to that of PMMA particles, so that no sedimentation takes place.

The viscosity of the solvent mixture was measured using the rheometer applying a shear rate and measuring the stress, yielding a Newtonian flow behavior with a viscosity $\eta_s = 2.47$ mPa.s.

The probe particles used for trapping are 1.1 μm melamine resin particles (micro-particles GmbH, Germany) with density $\rho = 1.51$ gr/cm^3 and refractive index of $n = 1.68$ allowing for convenient trapping (the main experimental problem here is that the probe particle must have a higher refractive index than the solution itself to allow for optical trapping.). A very small fraction of melamine particles $\phi < 10^{-4}$ are dissolved in the solvent before mixing it with the PMMA colloids which are received as a dry powder. The powder is dissolved in the solvent gradually and stirred vigorously using a spin-mixer. The radius of colloidal particles used in most of the experiments is $R = 197$nm while a few experiments are performed with larger colloids $R = 565$ nm. Since the density of solvent and colloid are equal, the samples are prepared in weight fraction, assuming this to be equal to the volume fraction. The sample volume fractions of interest are in the supercooled and glassy region ($\phi \approx 0.49 - 0.59$)(refer to Sec. 1.4.1 for the phase diagram of hard sphere suspensions). The samples in the supercooled region were measured within a couple of hours after preparation, since at later times, we observed the formation of crystals. The solution is introduced into a sample

chamber of about 50 μl volume, consisting of a coverslip and a microscope slide separated by a spacer of thickness 70 μm. This is sealed with epoxy glue to avoid evaporation of the sample. We then trap a single melamine bead and perform the active and passive experiments on it.

To measure the displacement of the probe particle more accurately at long times i.e. low frequencies $t > 1$ s, we also used video microscopy with sampling frequency of 25 Hz, in addition to the quadrant photodiode detection, used at all times.

Results

We would again like to test the validity of Einstein relation in the metastable supercooled colloidal fluids and glass phase as there have been reports of its violation for these systems [71, 41]. In the frequency range (0.1-100000 Hz), we investigate the Einstein relation by comparing the response functions obtained from active (direct) and passive (indirect) microrheology Eq. (5.1) performed on the same bead. We stress that the PSDs of several beads measured at different positions of samples were equal. In the measured frequency range, we did not see any effect of aging within 12h. We performed active and passive microrheology on different concentrations of $d = 394$ nm PMMA particles (C= 53, 58, 58.5 wt %) of which two are metastable colloidal fluids for which the FDR violation was reported by Bonn and Kegel [71] and the third one is a colloidal glass (See Sec. 1.4.1) for which deviations from FDR were reported by Song et. al. [41]. Note that the supercooled liquids are in principle ergodic systems and one does not expect to see deviations for the FDR in these. However, to resolve the apparent controversy existing in the literature, we have done experiments also on such supercooled liquids.

As demonstrated in Fig. 5.11 the agreement between active and passive response functions for all the samples is excellent showing that again no deviations are observed from FDR in this range of frequencies.

Furthermore, we did one set of active-passive experiments on a supercooled colloidal fluid with particles of diameter $d = 1.13\mu$m for which the probe particles and host particles have almost the same size (see Fig. 5.12). At $\phi = 0.55$, again excellent agreement is found.

In Fig. 5.13, we plot the resulting $T_{\rm eff}/T_{\rm bath} = \alpha''_{\rm passive}/\alpha''_{\rm active}$ as a function of frequency for the two glass samples and the supercooled fluids. This figure confirms again that to within the experimental uncertainty, the FDR is valid in the measured range of frequencies and the effective temperature does not differ from bath temperature, in agreement with the earlier experiments of Mason for $\phi \approx 0.56$ [173].

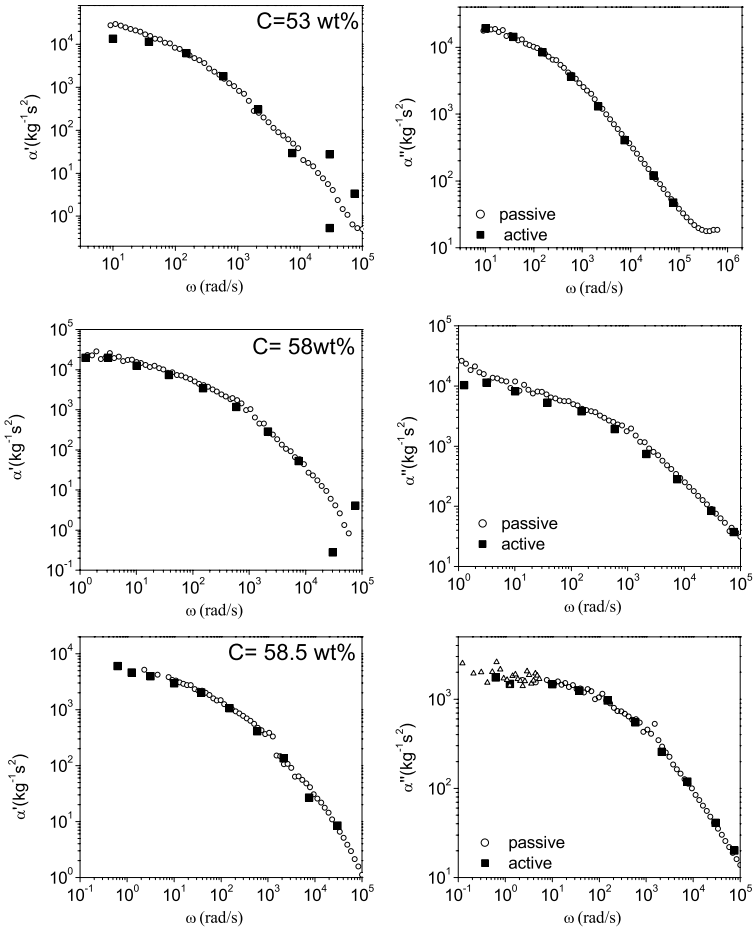

Figure 5.11: Real and imaginary parts α'' of the frequency-dependent response functions from active (solid symbols) and passive (open symbols) microrheology using 1.1 μm diameter melamine beads for 3 different concentrations of $d = 397$nm hard sphere colloids. The data are measured at 21 ^{0}C. Note, the data (shown by triangles) at low frequencies $\omega < 10$ rad/s in the glass sample with $\phi = 0.585$ are obtained from video microscopy to reduce the noise at low frequencies.

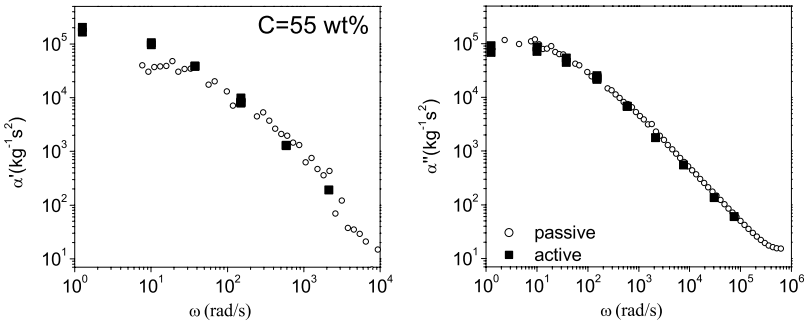

Figure 5.12: Real and imaginary parts α'' of the frequency-dependent response functions from active (solid symbols) and passive (open symbols) microrheology using 1.1 μm diameter melamine beads for 55 wt% concentration of $d = 1.13\mu$m hard sphere colloids. The data are measured at 21 ^{0}C.

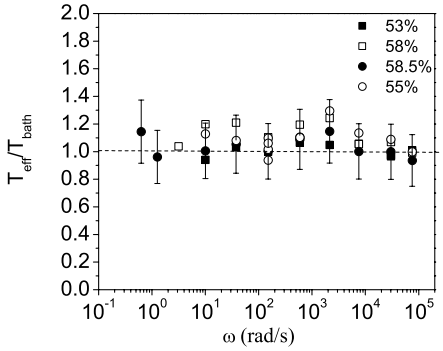

Figure 5.13: The effective temperature as a function of frequency for 53, 58 and 58.5 wt % d = 397nm colloids and 55 wt % concentration of $d = 1.13\mu$m colloids. The concentrations are shown in the legend.

It is necessary at this point to emphasize that we are in the same frequency region in which the plateau in structural relaxation is seen and deviations from FDR are possibly expected. This is more clear if we rescale the frequency with the Brownian time scale $\tau_B = \frac{R^2}{6D_0}$. For our colloidal glass with particle radius of 197 nm, $\tau_B = 1.46 \times 10^{-2}$ s. Therefore the range of dimensionless frequencies in

our measurements vary as $8.7 \times 10^{-3} < \omega\tau_B < 1.46 \times 10^3$. In the van Megen et. al. data [93] for a colloidal glass similar to ours the plateau of the intermediate scattering function is observed at time scales $1 < t/\tau_B < 10^5$ (see Fig. 5.14), which corresponds to $6 \times 10^{-5} < \omega\tau_B < 6$. Therefore, we are in the plateau; here one would already expect to see deviations from the FDR, if there are any.

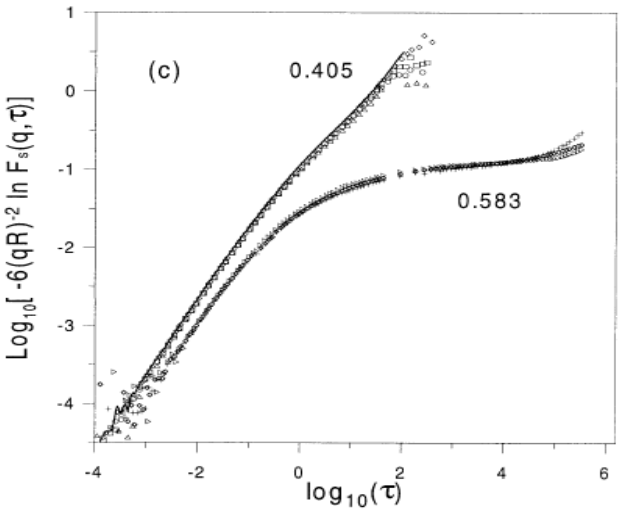

Figure 5.14: The mean-squared displacement of tracer particles in hard sphere suspensions obtained from the intermediate scattering function $(-6(qR)^{-2} ln F_s(q,t))$ vs the dimensionless time $\tau = t/\tau_B$, taken from reference [93].

5.4 Discussion

We have investigated the validity of the FDR in the form of the Einstein relation in colloidal glasses and gels of Laponite suspensions and a hard sphere glass in the frequency range $0.1 - 10^4$ Hz. We see a good quantitative agreement between the response function and the spontaneous thermal fluctuations, implying that we observe no violation of the FDR in any of these non-equilibrium systems. Equivalently, we find an effective temperature that does not differ from the bath temperature in the measured frequency range. It is important to note that these measurements provide a direct test of the FDR, since we directly mea-

sure the response and the *corresponding* fluctuations over the same wide range of frequencies.

The same experimental systems the as those studied here have been investigated by other groups, as we reviewed in the introduction. The rheological measurements of the Ciliberto group in a colloidal glass of Laponite are in agreement with our results [171], whereas their electrical measurements disagree [40]. It is necessary to note that in the electrical measurements, a different degree of freedom is measured. This could be the reason for the disagreement. On the other hand, simulations on a sheared binary Lennard-Jones fluid [158] have shown that the effective temperature is independent of the chosen observable, while it has been shown theoretically [151] that the effective temperature does depend on the observable in the glass phase of the Bouchauds trap model. Subsequent work of Ciliberto showed [25], however, that the measured FDR violations are due to the violent intermittent events, which cast some doubts on the measurements.

Abou et. al. [70] use a similar method as we do to investigate the validity of the Einstein relation during the aging of Laponite suspensions. However our method is more direct, since we are measuring the displacement and response on the same probe particle. They report slight violations from FDR, whereas our effective temperature is identical with the bath temperature. At this moment, it is not clear where this discrepancy comes from.

Also, in hard sphere glasses there have been reports of the violations of Stokes-Einstein relation. The large deviations from FDR reported by Bonn and Kegel [71] are likely to be due to the fact that they compared the rheological measurements and light scattering results of two different systems with different sizes of particles.

On the other hand, the Makse group [41] reports an effective temperature for a hard sphere glass that is twice the bath temperature for frequencies much lower than ours, corresponding to $t \sim 1000s$. However, also here some doubt can be cast on the method that they have used to determine the response function (mobility). In their experiments mobility is defined as the ratio of a constant force to the displacement of particle caused by the force at long times, which is not strictly true [41].

Although our results do not exclude the possibility of deviations from FDR at longer time scales, they do disagree with the simulation results which observe deviations from FDR in a binary Lennard–Jones mixture glass [38] and a fragile glass [143]. Our measurements are already in the time regime for which the models suggest that the FDR violations should be visible. In both of these systems the deviations from FDR have been observed by other groups at intermediate and long times, when the decay of correlation function is not exponential anymore.

To conclude, we remark that experimental works on this issue are still scarce,

owing to the difficulty of measuring the response function and the fluctuations simultaneously in experiments on soft materials or glasses. However, the technique used here offers a direct method for simultaneous measurements of response and correlation functions and shows no deviations from FDR.

6.

Viscoelastic Properties of Colloidal Gels and Glasses

6.1 Introduction

Soft glassy materials are ubiquitous in our everyday life. A common feature of all such materials is their relatively large response to small forces ('soft') and their disordered nature ('glassy'). Pertinent examples of such systems are foams, gels, slurries, concentrated polymer solutions and colloidal suspensions. These systems show interesting viscoelastic properties; depending on the frequency with which they are perturbed, they can behave like liquids or solids. However, the mechanical behavior of such soft glassy materials is still incompletely understood [20].

In recent decades, colloidal suspensions have been extensively used as model systems for the glass transition in simple liquids [42, 49, 50, 46] and gel formation [113, 118, 180]; since the diffusion of the particles can easily be measured using e.g. light scattering. In addition, they are good model systems in the sense that the interactions can be tuned to some extent by e.g. screening the electrostatic interactions between particles by adding salt. The viscoelasticity of such systems has received much less attention, especially during the aging of glassy systems or gel formation. Another issue which deserves more attention is differentiating between colloidal gels and glasses in terms of their rheological properties.

As an example of a soft glassy system, here we focus on studying the viscoelasticity of Laponite suspensions for which a very rich phase diagram has been

reported [62]. When dissolved in water, Laponite suspensions evolve from a liquid-like state to a non-ergodic state [49, 115, 63, 50, 112]. During this process both the diffusion slows down and the viscoelasticity develops. In chapter 3, we studied the evolution of translational and rotational diffusion of Laponite suspensions over a wide range of concentrations and salt content. Based on these studies, we could classify Laponite dispersions as gels and glasses. The main difference between colloidal gels and glasses stems from their structure. While the glass is a spatially homogenous structure with no long-range order, the gel has heterogenous structure whose length is set by the mesh size of its network.

Therefore we are interested to know

- How the viscoelastic properties of Laponite gels and glasses develop in time.
- Do the different structures of gel and glass lead to different dynamic viscoelastic properties and possibly position-dependent local shear moduli?

To reply to these questions, we take advantage of microrheology (Sec.2.3), that allows to measure the frequency-dependent shear moduli of colloidal suspensions over a wide range of frequencies. It is based on the detection of small displacements of probe particles inserted in the soft glassy material, and allows to obtain the mechanical properties of surrounding matrix. Considering the fragility of soft materials, it is interesting to use a technique that can be less invasive than conventional rheometry.

There are two broad classes of microrheology (MR) techniques: active and passive (see Sec.2.3). In a non-equilibrium system, application of any of active and passive methods appears difficult in principle. On the one hand, passive MR is based on the fluctuation-dissipation relation (FDR) the validity of which can not be taken for granted in non-equilibrium systems such as glasses. On the other hand, in active MR the response at every single frequency should be measured separately, contrary to passive MR for which the power spectrum of thermal fluctuations provides the information about the response function over the whole frequency range in a single shot [89, 181, 182]. Therefore, in the active method, collecting the data over the full range of frequencies is time-consuming and is limited to systems where the aging process is slow with respect to the time of measurement. However, in chapter 5, we have tested the validity of FDR in the same systems we intend to focus on here, and not only found that the FDR was obeyed at all times and for the frequency range we measured, but also found excellent agreement between active and passive methods. Therefore, in what follows we will use the much faster passive method.

Employing the microrheology technique has several advantages over conventional rheometry:

- The range of frequencies which can be measured by microrheology is much wider ($0.1 - 10^6$ Hz) relative to the classical rheometry methods. Most commercial rheometers are in general restricted to frequencies up to 10 Hz; beyond that, the inertia of the measurement geometry becomes important. The upper limit in microrheology experiments is equally set by inertial effects of the probe particle; however, since the particle is very small, we can go to much higher frequencies. The lowest frequencies which can be measured by conventional rheometers are also restricted in evolving systems (gels and glasses), which sets the lower limit of $f = 10^{-2} - 10^{-1}$Hz for fast evolving samples.

- Conventional rheometers provide us with average bulk properties and do not allow for local measurements in inhomogeneous systems, which could in principle be the case for colloidal gels and glasses. With microrheology technique, one measures the local viscoelastic properties of material at a length scale of the same order as the probe particle size. Therefore, by comparing the microrheology measurements performed with a single probe particle at different locations in the sample, we can detect possible inhomogeneities.

- We can use both one-particle and two-particle MR as explained in Sec. 2.3.4. One-particle MR extracts the rheological properties of the material from the displacement autocorrelation function of an individual embedded particle. Such measurements probe the dynamics of the medium on length scales of size of the probe particle [87, 181, 183, 182]. Two-particle microrheology [184, 183, 185, 186, 187, 188] on the other hand, uses the interparticle correlated fluctuations of two particles at a separation distance r larger than the probe particle size. Therefore, such measurements probe the viscoelastic properties of the medium on length scales comparable to the interparticle separation. These two measurements can yield different values for the apparent shear modulus, depending on the characteristic structural length scales of the complex fluid [89, 189, 188]. Thus, the combination of one and two-particle MR measurements can be used to probe inhomogeneities of the system under study.

Here we use the combination of one and two-particle MR measurements to probe the possible inhomogeneities of colloidal gels and glasses at length scales of the order of the particle size 1μm and separation distances of the order of 5-20 μm.

We measured the local shear moduli at several different positions of our colloidal gels and glasses at roughly equal aging times.

At early stages of aging the local shear moduli obtained from different positions of the sample are identical for both gel and glass samples. However, by progress of time, the local shear moduli of a gel turn out to vary from one point to another, while the shear moduli of a colloidal glass remain independent of the bead position at all stages of aging. The variation of shear moduli with position increases as the gel becomes more stiff with time. These findings suggest a heterogenous structure for the gel on the length scales on the order of 10 μm. Furthermore, shear moduli obtained from one- and two-particle MR are equal for the glass while for a gel the shear moduli obtained by two-particle MR are considerably lower than shear moduli extracted from single-particle MR. The relatively good agreement of shear moduli obtained from single bead MR with bulk rheology measurements provide another evidence for homogeneity of a glass.

In summary, our microrheology results confirm the homogeneity of glass and inhomogeneity of the gel, as suggested by the light scattering experiments in chapter 3.

Despite the different structure of gel and glass, we find that the time evolution of local shear moduli in gel and glass are qualitatively similar. During aging of Laponite colloidal suspensions around a certain time t_0 the complex shear modulus of the system shows a crossover from a single frequency-dependent component to a superposition of a strongly frequency-dependent viscoelastic component plus a weakly frequency dependent (elastic) component. Such a behavior was previously interpreted in the context of polymer networks as being due to a network, which is inhomogeneous [190], but our two-particle MR studies on a colloidal glass indicating homogeneity for a glass exclude this interpretation. It seems more plausible to interpret the observed power law behavior as a broad distribution of relaxation times as suggested in the context of soft glassy materials rheology [20, 191].

6.2 Microrheology of Laponite suspensions

We carried out the measurements on a variety of Laponite concentrations and salt contents (2.8, 3.2 wt%, in pure water, 3 wt% in pH=10, 1.5 wt %, 5mM NaCl, 0.8 wt %, 6mM NaCl, 0.8 wt %, 3mM NaCl). We have chosen these samples since their rate of aging is slow enough so that no significant aging happens during each measurement. On the other hand they evolve fast enough to allow us to follow the whole evolution within a few hours. The samples 2.8, 3.2 wt%, in pure water, 3 wt% in pH=10 and 1.5 wt %, 5mM NaCl are in the glass region of phase diagram and samples 0.8 wt %, 6mM NaCl, 0.8 wt %, 3mM NaCl behave like a colloidal gel (for details see chapter 3). Note that the pH=10 does not affect the aging

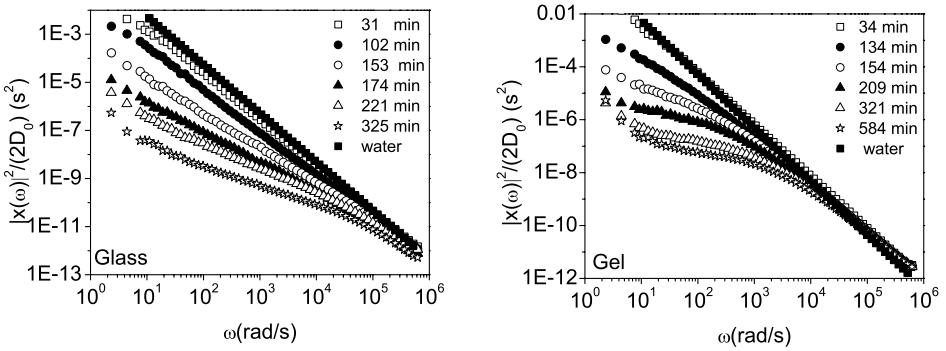

Figure 6.1: The normalized displacements power spectral densities $|x(\omega)|^2/2D_0$ of silica probe particles in a glass (3.2 wt% , bead diameter 1.16 μm) and a gel (0.8 wt%, 6mM, bead diameter 0.5 μ, in the x direction) with increasing age after preparing the sample. Waiting times are given in the legend. The filled squares show the PSD of a bead in pure water for comparison. All experiments were done at 21^oC.

dynamics. It merely acts as an electrolyte that slightly accelerates the aging. The same holds for Laponite 1.5 wt%, 5mM. In this case salt just accelerates the aging, but it does not change the underlying physics of the aging process, as demonstrated in chapter 3. the sample belongs to the glass region of the phase diagram.

We trapped a bead in a single laser trap and measured the displacement power spectral densities (PSD) as a function of waiting time.

Since the system evolves towards a non-ergodic state, the time average may not necessarily be equal to the ensemble average for the measured PSDs. However, in our range of frequencies ($1-10^5$ Hz) we confirm that our results do not depend on the time interval used to compute the time average. Thus, we can use the time-averaged PSD without averaging over several beads in our study.

Fig. 6.1 shows the measured displacement PSDs as a function of frequency during the aging of the glass and gel. We have normalized the PSDs with the diffusion coefficient ($D_0 = kT/(6\pi\eta_{water}R_{bead})$ of the same bead as measurements in water , so that PSDs will be independent of bead size. It is evident that in both systems the particle motion progressively slows down with increasing waiting time t_w, reflecting the increase of viscosity in the system. The PSDs in both sample start from a state similar with water, for which $|x(\omega)|^2/2D_0 = 1/\omega^2$, and gradually their magnitudes as well as their slopes decrease with time. There is a crossover

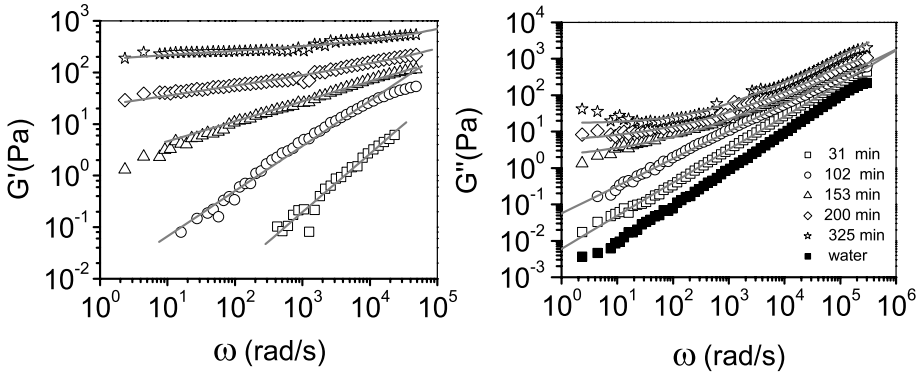

Figure 6.2: Glass data: The symbols show the shear moduli $G'(\omega)$ and $G''(\omega)$ as a function of frequency measured using 1.16 μm silica probe particles in a 3.2 wt% Laponite solution in pure water with increasing age after preparing the sample. Waiting times are given in the legend. The lines show the fits of $G'(\omega)$ and $G''(\omega)$ according to $C_1(i\omega)^a + C_2(i\omega)^b$ in which $C_2 = 0$ for waiting times $t_w < 120$ min.

time t_0 such that for $t_w < t_0$, the PSD can be described by a single power law. At longer waiting times $t_w > t_0$, two distinct slopes appear in the log-log plot (Fig. 6.1). For the gel, we have shown the PSDs only in one of the possible directions, since the PSDs in the x and y direction are not necessarily equal anymore. At late times, this leads to anisotropic local shear modulus. Measuring the PSDs of several beads, we did not find a preferred direction of anisotropy, for some of the beads, the PSD in the x direction was larger and for some others in the y direction.

Let us look at the evolution of the local shear moduli G^* obtained from PSDs. Fig. 6.2 (glass) and 6.3 (gel) present the elastic and shear moduli derived from single particle MR according to Eq. (2.94). As can be observed, the system evolves from an initially completely viscous liquid to a strongly viscoelastic fluid. At the early stages of aging, the loss modulus is much larger than the storage modulus ($G'' \gg G'$) and we have a more liquid-like state. With time it develops into a solid-like state in which the elastic modulus dominates the loss modulus ($G'' << G'$). Also we observe that the changes in G' are more dramatic than the changes in G''. While G'' almost saturates after 170 min for the glass and 100 min for the gel, G' continues to grow in time.

Visual inspection shows that gel is "softer" than the glass. When we tumble

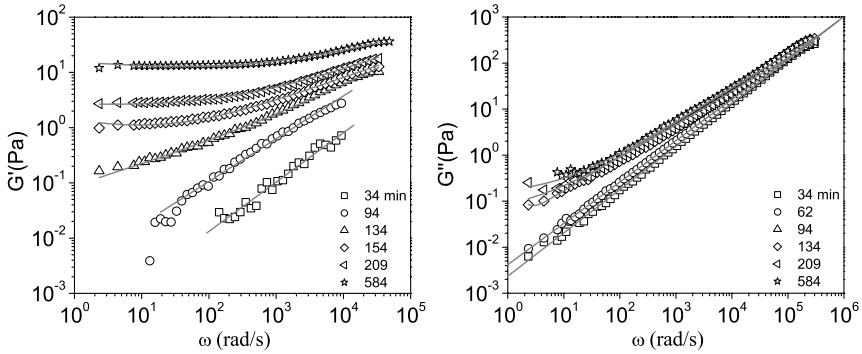

Figure 6.3: Gel data: The symbols show the shear moduli $G'(\omega)$ and $G''(\omega)$ as a function of frequency measured using a 0.5 μm silica probe particle in a 0.8 wt% Laponite solution in 6 mM NaCl water with increasing age after preparing the sample. Waiting times are given in the legend. The lines show the fits of $G'(\omega)$ and $G''(\omega)$ according to $C_1(i\omega)^a + C_2(i\omega)^b$ in which $C_2 = 0$ for waiting times $t_w < 100$ min.

similar tubes containing gel and glass, the gel fluidifies with a smaller force: it appears that gel has a lower yield stress compared to glass. Therefore it must have a lower viscoelastic modulus than the glass, as comparison of Fig. 6.2 and Fig. 6.3 confirms. Furthermore, at late stages of aging the ratio G'/G'' at low frequencies is higher in the gel ($G'/G'' = 30$ for Laponite 0.8 wt%, 6mM) compared to the glass ($G'/G'' = 12$ for Laponite 0.8 wt%), when G'' has almost saturated and G' evolves very slowly.

6.2.1 Heterogeneity

Single bead MR measures the local shear moduli, which in principle can be different from the average bulk shear modulus measured by a rheometer, if the material is heterogenous. Discrepancy between the shear moduli obtained from one- and two-particle MR can be used as an indicator of a heterogenous structure. The potential heterogeneities can be explored by measuring the PSDs of several beads at different positions in the sample. Further test of heterogeneity in a material is provided by comparison of MR with bulk rheology, as will be discussed in the next section. Therefore, we investigate here the potential inhomogeneities of colloidal gels and glasses of Laponite, combining one- and two-particle MR.

Glass

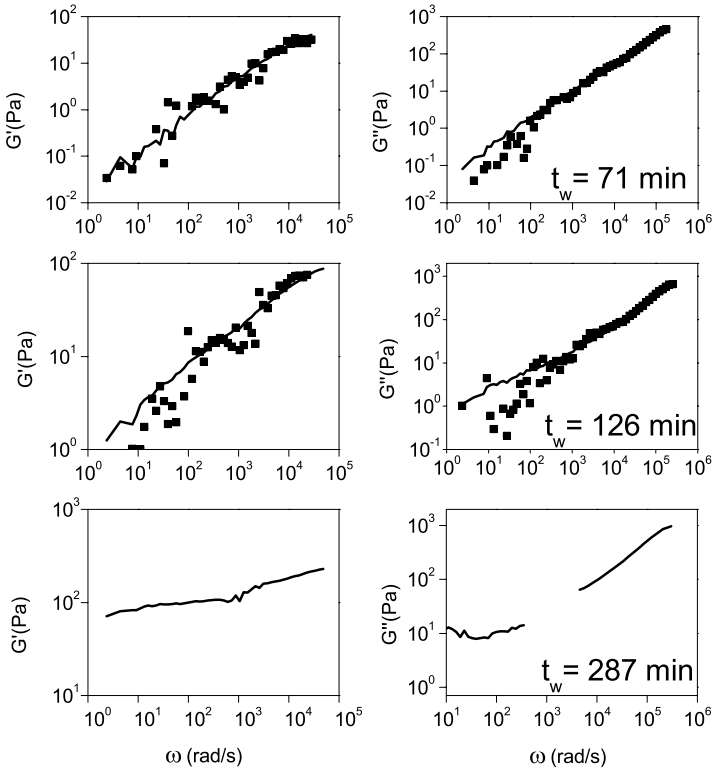

Figure 6.4: Glass data: The shear moduli $G'(\omega)$ and $G''(\omega)$ at different stages of aging in a 3 wt% Laponite in pH=10 solution derived from one (lines) and two-particle (symbols) MR of 1.16 μm silica probe particles. The distance between the two particles was 6 μm. The waiting times are shown on the figure. Note that in the late stages of aging material is too stiff to have a large enough signal for obtaining a proper cross correlation between the two beads.

For the glass samples the displacement PSDs turned out to be independent of the bead position, as was concluded from a comparison of simultaneous measurements of PSDs of two independent beads in two independent traps during aging. Furthermore, the comparison between one- and two-particle MR reveals

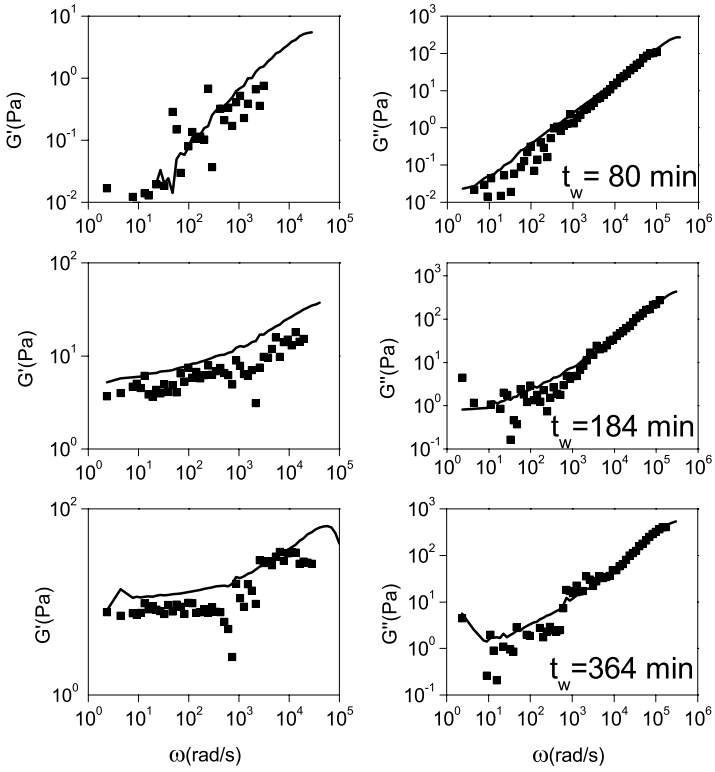

Figure 6.5: Glass data: The shear moduli $G'(\omega)$ and $G''(\omega)$ at different stages of aging in a 1.5 wt%,Laponite in 5mM salt derived from one (lines) and two-particle (symbols) MR of 1.16 μm silica probe particles. The distance between the two particles was 7.5 μm. The waiting times are shown on the figure.

that within the experimental error, the shear moduli are identical between the two methods for all stages of aging as demonstrated in Fig. 6.4 and Fig. 6.5. This was further verified by measuring the PSDs of several beads at different positions of an aged sample (see Fig. 6.6). Obviously, the resulting shear moduli were independent of position of the bead in the sample, verifying the homogeneity of glass as depicted in Fig. 6.8.

This suggests that the Laponite glass is homogenous on length scales larger than half a micrometer. If this were indeed true, an additional check on this can

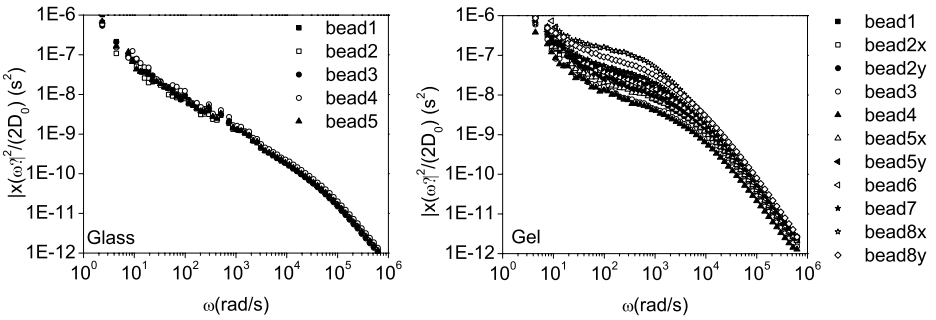

Figure 6.6: The displacement PSDs of 0.5 μm silica beads measured at different positions of an aged glass (Laponite 3.2 wt % in pure water, $t_w \approx 5$ h) and an aged colloidal gel (Laponite 0.8 wt% in 6mM NaCl solution, $t_w \approx 10$ h).

be obtained from a comparison between microrheology and macrorheology: these should yield the same results if the sample is homogeneous.

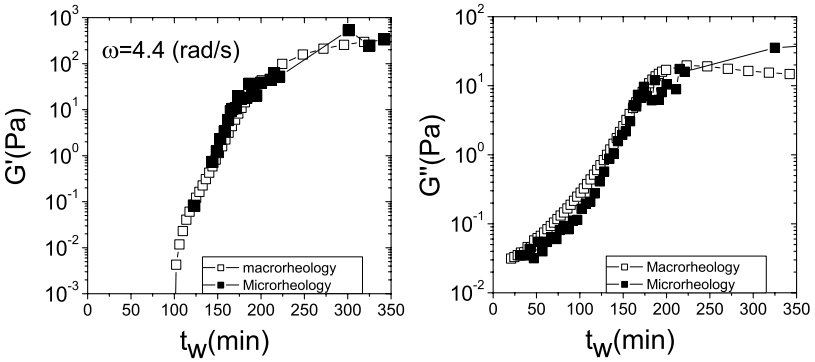

Figure 6.7: The elastic and loss modulus as a function of waiting time for a sample of Laponite 3.2 wt % in pure water obtained from macro and one-particle MR techniques.

Figure 6.7 depicts the shear moduli extracted from MR and bulk rheology experiments for a single frequency of ($f = 0.7$ Hz). The overall agreement between bulk rheology and MR is good. For the early stages of aging, the G'' measured by the rheometer appears slightly higher, but this can be attributed to the large

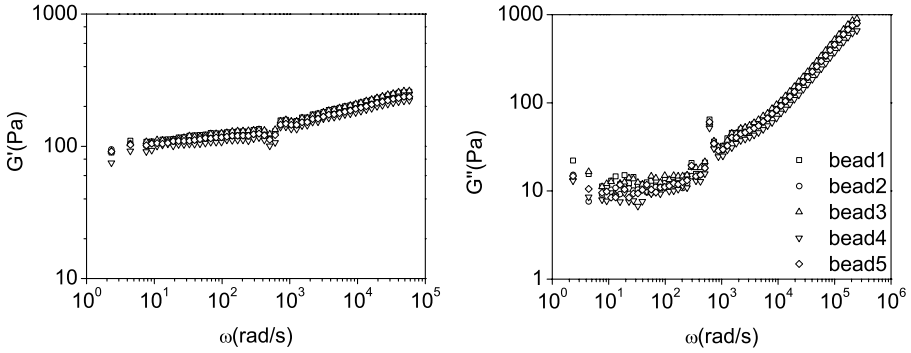

Figure 6.8: Local elastic modulus G' and loss modulus G'' measured at different positions in an aged glass sample of Laponite 3.2 wt % in pure water ($t_w \approx 5$h)

moment of inertia of the rheometer bob; macrorheology does not provide accurate measurements of the shear moduli, when $G^* < 1$ Pa. On the other hand, MR technique has other sources of error at low frequencies, especially for the late stages of aging, when the material becomes very elastic. In this case, the signal detected by the photodiode becomes so small that it can become comparable to the noise level; especially $1/f$ noise dominates the low frequencies. This is the most plausible explanation for the slight discrepancy between the two methods at long waiting times.

Gel

Note that the data in this section are about what we called attractive glasses in chapter 3 for which light scattering shows heterogeneity, although we use the term gel for them.

Measuring the displacement PSDs of several beads at different positions of a gel at the late stages of evolution reveals a considerable degree of inhomogeneity (Fig. 6.6). Not only the PSDs are position dependent, but also at some positions in the sample the measured PSDs are anisotropic.

This is consistent with the static light scattering measurements for this sample (see Chapter 3). Therefore, exploring a gel with a probe size smaller than the

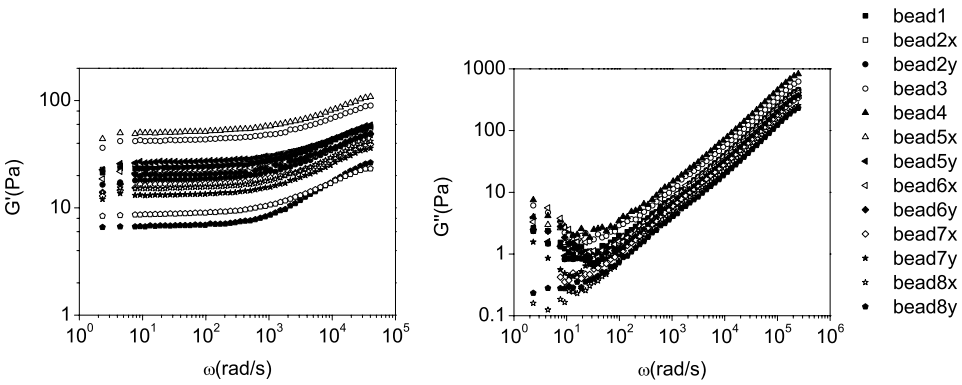

Figure 6.9: Gel data: local elastic modulus G' and loss modulus G'' measured at different positions in an aged gel sample of Laponite 0.8 wt % in 6mM NaCl solution ($t_w \approx 10$h)

mesh size of the network, would detect the inhomogeneities. In order to know how the observed heterogeneity in the PSDs translates into the inhomogeneity in the local shear moduli, we have plotted the shear moduli of the bead at different positions (Fig. 6.9). As can be seen there is an order of magnitude difference between the smallest and largest elastic moduli measured.

The question which arises is whether the heterogeneity exists from the very beginning, after sample preparation, or it appears as a network-like structure is building up in the gel. To answer this question, we measured the PSDs of two beads at different positions of a gel as a function of waiting time. We performed two sets of experiments: in the first one the two beads were chosen at a relatively close distance $r = 4.66\mu$m (Fig. 6.10) and at the other one $r = 19\mu$m (Fig. 6.11).

In both experiments, in the early stages of aging the PSDs at different positions were equal. However, as time progresses, some inhomogeneity appeared and the PSDs measured at different positions were not equal anymore. Interestingly, at later stages of aging, the displacement PSDs measured for some of the beads became anisotropic, meaning that the PSDs in the x and y directions were not equal anymore. In one case the anisotropy survived the latest measurement (Fig. 6.11). For another one, the appeared anisotropy disappeared after some time (Fig. 6.10). This suggests that the building up of structure in the gel is a dynamic process; at some points and times more particles join to the network and at some other points and times some particles disintegrate from the network.

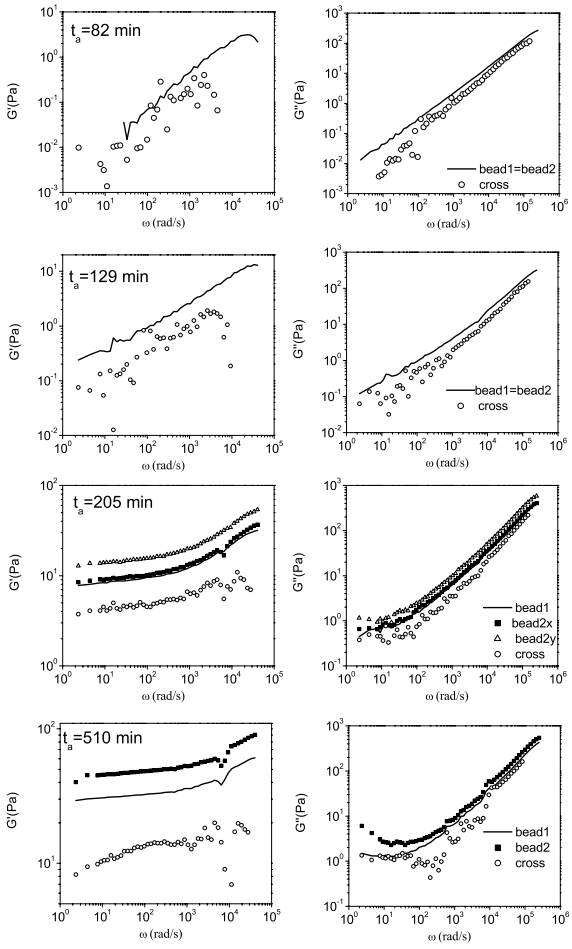

Figure 6.10: Gel data: The shear moduli $G'(\omega)$ and $G''(\omega)$ at different stages of aging derived from one and two-particle MR of 0.5 μm silica probe particles in a gel of Laponite 0.8 wt % in 6mM NaCl solution.The distance between the two beads was 4.66 μm. The waiting times are shown on the figures.

Now, let us investigate how the shear moduli obtained from correlated motion of the two-particle MR compare to the single particle MR. As explained before,

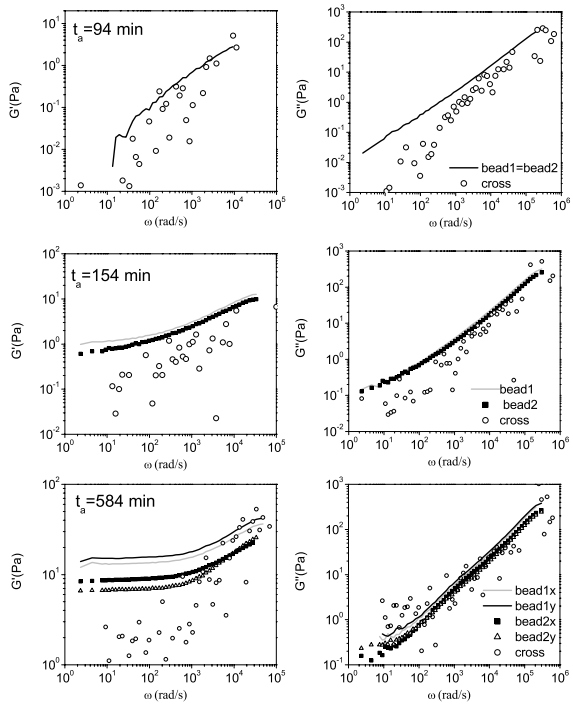

Figure 6.11: Gel data: The shear moduli $G'(\omega)$ and $G''(\omega)$ at different stages of aging derived from one and two-particle MR of 0.5 μm silica probe particles in a gel of Laponite 0.8 wt % in 6mM NaCl solution. The distance between the two beads was 19 μm. The waiting times are shown on the figures.

two-particle MR measures the shear moduli on a length scale comparable to the distance between the two particles and is a better representative of the bulk properties in contrast to single particle microrheology which is sensitive to the local properties. Our experiments show that immediately after preparation, shear moduli obtained from two-particle MR and one-particle MR are equal. But, at relatively early stages of aging, the two-particle MR differ from 1PMR as demonstrated in Fig. 6.10 and Fig. 6.11. This deviation appears long before the local shear moduli of the two beads in one-particle MR start differing. Therefore the heterogeneity is more important for longer length scales.

6.2.2 Model for the viscoelastic behavior

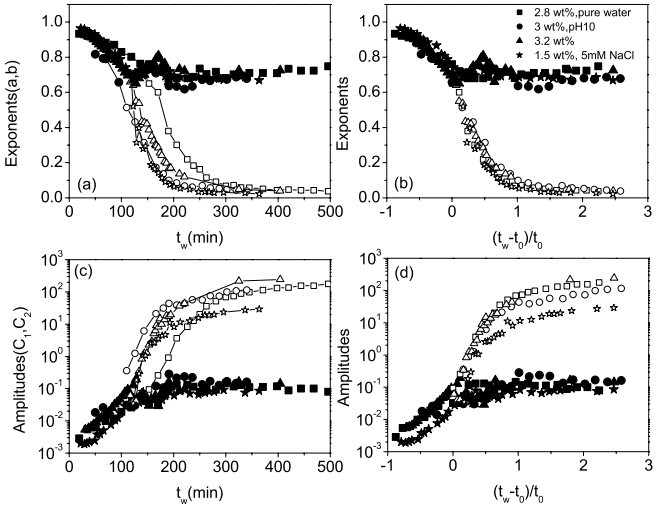

Figure 6.12: The complex shear moduli of Laponite suspensions can be described as the sum of two power laws $C_1(i\omega)^a + C_2(i\omega)^b$ in which $C_2 = 0$ for waiting times $t_w < t_0$. The crossover times are $t_0 = 155, 95, 120, 105, 95$ min for Laponite concentrations 2.8 wt%, 3 wt%,pH=10, 3.2 wt% , 1.5 wt%, 5mM NaCl and 0.8 wt%, 6mM NaCl, respectively. (a) The evolution of exponents a (filled symbols) and b (empty symbols) as a function of waiting time for different concentrations of Laponite. (b) The exponents a (filled symbols) and b (empty symbols) as a function of scaled waiting time (c) The amplitude of viscoelastic contributions C_1 (filled symbols) and C_2 (empty symbols) as a function of aging for different samples. (d) The same as panel (c) but versus scaled waiting time. The samples concentrations are shown in the legend.

As shown before, the combination of one- and two-particle MR can differentiate in the mechanical properties between gel and glass. It is also interesting to investigate if there are similarities between gel and glasses.

Looking at Fig. 6.2 and Fig. 6.3 we see that the complex shear modulus of both gel and glass is observed to cross over from a single power law to a superposition of two power laws around a certain waiting time t_0 depending on the sample ($t_0 \approx 155min$ for the glass sample of Laponite 3.2 wt % and $t_0 \approx 95min$ for the gel sample of Laponite 0.8 wt %,6mM NaCl) [190]. The local shear moduli of both samples turn out to be well-described by the following:

$$G(\omega) = G'(\omega) + iG''(\omega) \equiv \begin{cases} C_1(i\omega)^a & : \quad t_w < t_0 \\ C_1(i\omega)^a + C_2(i\omega)^b & : \quad t_w > t_0 \end{cases} \tag{6.1}$$

The exponent of the single power law decreases from 1 to a value about 0.7 before the second component becomes visible. The exponent and amplitude of the first component does not change with waiting time for $t_w > t_0$ while the amplitude of the other one grows appreciably for the same waiting times.

Indeed, we find a very similar behavior for the other samples measured. In Fig. 6.12(a) and (c), we have plotted the evolution of the fitting parameters as a function of waiting time for different samples. As can be seen the development of the two viscoelastic components for different samples are qualitatively similar, although the rate of change depends on the sample concentration and salt content.

Interestingly, the exponents a and b of the different samples coincide if we scale the waiting time as $t'_a = (t_w - t_0)/t_0$. The crossover times are $t_0 = 155, 95, 120, 105, 95$ min for Laponite concentrations 2.8 wt%, 3 wt%, pH10, 3.2 wt%, 1.5 wt%, 5mM and 0.8 wt%, 6mM NaCl, respectively. For the amplitudes on the other hand, the data do not collapse. Especially the amplitudes of the second (viscoelastic) component systematically decrease as the Laponite content is reduced. Furthermore for the gel we can see some fluctuations in the amplitude of the second component C_2, at later stages of evolution. This can be understood in terms of the dynamic process of gel formation in which Laponite particles still can join or detach from the network.

6.3 Discussion and Conclusion

We have studied the evolution of the viscoelastic properties of a variety of Laponite suspensions including both gel and glass over a wide range of frequencies using MR.

The one-particle microrheology provides us with the possibility of studying the local shear moduli of colloidal gels and glasses at length scales of the order of the probe particle size. On the other hand, two-particle microrheology measures the viscoelastic properties of the system at length scales of the separation distances between two probe particles which can vary between a few microns to a few tens of micrometers. Therefore the combination one and two-particle microrheology can be used as a strong tool to detect the potential inhomogeneities in gels and glasses.

Our microrheology measurements reveal the differences between gel and glasses from the rheological point of view : while glass is homogenous on all length scales

probed in our experiments ($l > 0.5\mu$m), the colloidal gels show a considerable degree of inhomogeneity that increases as the gel develops into a solid-like state.

Moreover, in the glass, we checked the homogeneity of our system on even larger length scales, by comparing microrheology and conventional rheology results. We find that measurements at different scales all give the same results. Thus, there is no evidence for spatial inhomogeneity, neither in our system, nor in glassy systems in general.

In the gel, however, along the evolution from a liquid-like state to a viscoelastic state, inhomogeneities develop in time, as was detected by measuring the local shear moduli at different positions of the sample at nearly equal waiting times. Our measurements on several beads at different distances suggest that these inhomogeneities extend over a range of 100 micrometer. Therefore the macroscopic bulk shear modulus is not necessarily equal to that measured by single particle MR. In Fig. 6.13, we compare the shear moduli obtained from one- and two-particle MR with the results of bulk rheology at late stages of aging ($t_w \approx 8.5$ h) when the changes of loss and elastic moduli are slow. As can be seen the local shear modulus of one of the positions in the sample is equal to its bulk value, while the other has a considerably lower shear modulus. Notably, the shear modulus obtained from the cross correlation of two-particles is lower than both bulk and local shear moduli. This suggests two-particle MR can be used to detect inhomogeneities. However, it still does not reflect bulk properties.

In addition, we find that the local viscoelastic moduli for both gel and glass around a certain time t_0 cross over from a single power law to the sum of two power laws. These results demonstrate the existence of two distinct contributions in the viscoelasticity of the system in the later stages of aging. In addition to a strongly frequency-dependent viscoelastic shear modulus at high frequencies $\cong \omega^{0.7}$, we also observe the slow development of a more elastic (only weakly frequency-dependent) shear modulus during the aging. The exponents of the power laws have exactly the same trend of evolution for different concentrations if we scale the waiting time as $t'_a = (t_w - t_0)/t_0$. This result is truly independent from the sample being a gel or a glass.

The crossover from a single frequency-dependent component to a superposition of a strongly frequency-dependent viscoelastic component plus a weakly frequency dependent (elastic) component was previously interpreted in the context of polymer networks as being due to large inhomogeneities [190, 192, 193, 174, 175].

Here the sum of two power-laws describes both gel (heterogenous) and glass (homogenous) local shear moduli, suggesting that locally the underlying physical process responsible for the evolution of gels and glasses is similar. This poses the rather puzzling question where the two power-laws in the viscoelasticity come

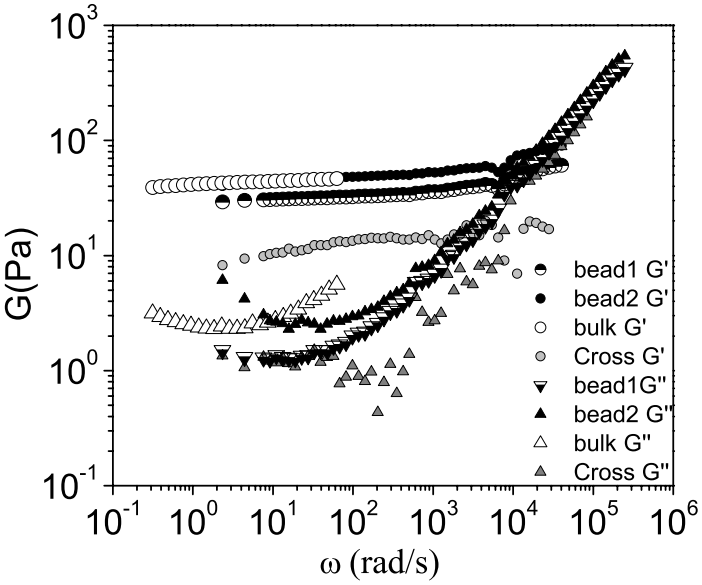

Figure 6.13: The complex shear modulus at a late stage of aging $t_w \approx 8.5$h obtained from different methods of single-particle MR at two different positions of the sample, two-particle MR and bulk rheology in a sample of Laponite 0.8 wt%, 6mM NaCl. The circles show G' and triangles show G'' values.

from. One phenomenological interpretation of power law frequency-dependence of shear moduli is a broad distribution of relaxation times as can be obtained from a sum of a large number of Maxwell fluids with different relaxation times whose distribution obeys a power law behavior. This is makes sense, as we showed in the previous chapter that the correlation functions of both gels and glasses at long times can be described by a stretched exponential which corresponds to a broad distribution of relaxation times.

At this point it is also tempting to believe that t_0 has a relation with the onset of the glass transition or the gel formation. In light scattering experiments the characteristic transition point is when a transition from ergodic to a non-ergodic state occurs, i.e. ergodicity-breaking point t_{eb} . It is interesting to see how t_0 is related to t_{eb}. We have performed simultaneous DLS (at scattering vector $q = 1.87 \times 10^7 m^{-1}$) and microrheology experiments on the same sample of Laponite 3.2 wt % (chapter 3). We found that the ergodicity-breaking point $t_{eb} \approx$

450 min occurs much later than the time we see dramatic changes in rheological properties, the time $t_0 \approx 120$ min. A similar trend can be seen if we compare the ergodicity-breaking points t_{eb} obtained for other samples (see Fig. 3.3 and 3.9) with t_0 obtained from microrheology, although they have not been measured simultaneously. The values of ergodicity-breaking and mechanical transition times are $t_{eb} \approx 750, 150, 900, 180, 450$ min and $t_0 \approx 105, 95, 155, 95, 120$ min for the samples Lap 0.8 wt%, 6mM, Lap 1.5 wt%, 5mM, Lap 2.8 wt%, Lap 3 wt% pH=10, Lap 3.2 wt%, respectively.

An analogous observation has been reported before [194], in which the mechanical transition occurs before ergodicity-breaking point. Although there the mechanical transition point is defined differently. Cocard et. al. have defined the mechanical transition point [194] as the time for which G' and G'' become equal at low frequencies. They observe that for a sample of Laponite 1 wt %, 5 mM, this point is well before t_{eb} [194]. They attribute it to the fact that in DLS experiments, they are looking at different length scales. DLS experiments are performed at a typical wave vector $q = 2 \times 10^7 m^{-1}$ corresponding to a length scale of the order of 350 nm. The motion at this length scale is prohibited only when the material has become stiff enough. In summary, we think that characteristic points of transition from different experiments occur at different waiting times because we are looking at different frequency and length scales (wave vector windows). Furthermore, in light scattering experiments, we measure the density fluctuations which are longitudinal modes, whereas in microrheology, the thermal response of the bead embedded in the viscoelastic medium mainly excites the transverse shear modes.

Another point which deserves discussion is the different role of ergodicity-breaking point and mechanical transition point in the classifying of gels and glasses. We saw in chapter 3, that the slow relaxation times and the non-ergodicity parameters of all Laponite suspensions in a wide range of concentrations and salt contents fell into two classes (gel and glass) when scaling the waiting time with t_{eb}. Here, scaling the waiting time with t_0 does not lead to a classification of distinct groups of samples. Nonetheless, microrheology, measuring the local shear moduli of material, is used as a powerful tool to detect the inhomogeneities and therefore differentiating the gel and the glass.

A.

Viscoelastic Properties of Hard Sphere Colloids

Hard sphere colloids are a very simple model system for molecular systems in which the interaction potential is solely determined by excluded volume. Understanding their behavior can be an insightful first step in understanding either molecular systems or more complex suspensions of technological importance. The phase diagram of hard sphere suspensions has consequently been studied extensively by numerous simulations [195, 196] and experiments [44, 42] (see Fig. 1.3).

Highly monodisperse particles with hard- sphere-like interactions undergo an entropically driven fluid-solid transition to form crystals and glass [44](See Sec. 1.4.1). Here, we are interested in understanding the viscoelastic behavior of the hard sphere suspensions at volume fractions approaching the glass transition (supercooled liquids) and in the glass region of phase diagram. The frequency-dependent shear moduli of hard sphere systems have been studied using classical rheometry techniques by several groups for wide ranges of concentrations [197, 198, 199], among which van der Werff et. al. [197] have done high frequency measurements using a high torsion oscillator.

There have been a few microrheology experiments on hard spheres based on diffusive wave spectroscopy [86, 173] and dynamic light scattering [200] techniques. Here, we use the microrheology based on optical trapping of probe particles to study the viscoelasticity of concentrated hard sphere suspensions and compare our results with existing ones in the literature.

The experimental system used to mimic the hard spheres is (d = 397 nm) PMMA particles in an index and density-matched solvent. Melamine beads (1.1

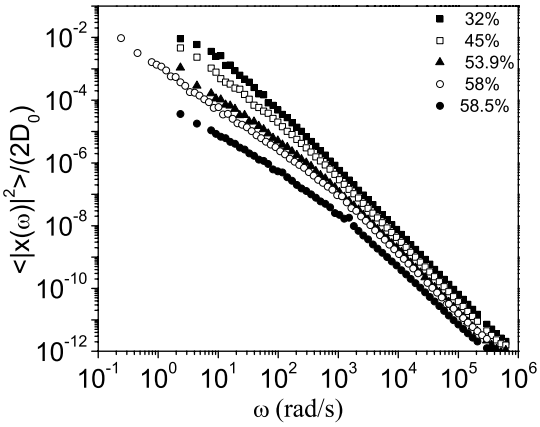

Figure A.1: The normalized displacement power spectral densities of several concentrations of hard spheres with diameter 397 nm.

and 1.3 μm diameter) are used as probe particles. For more details on sample preparation, we refer to Sec. 5.3.

Fig. A.1 shows the displacement PSDs normalized to the free diffusion constant of the probe particle in the solvent for a few concentrations of PMMA. As can be observed the higher the concentration of the host particles, the more difficult it is for the probe particle to diffuse, therefore the slower the motion. This in turn leads to increasing values of the viscoelastic moduli with concentration. We obtain the shear moduli from the response function as explained in Sec. 2.3.4, assuming that Stokes relation is valid.

In Fig. A.2, we have plotted the frequency-dependent shear moduli of hard sphere suspensions. The viscoelastic moduli are seen to increase by several orders of magnitude at volume fractions around ϕ_g, as expected approaching the glass transition.

Now let us see what is the origin of viscoelastic behavior. The contributions to the shear stress come from (1) the Brownian motion of the particles, (2) their hydrodynamic interactions and (3) structural relaxations (caging effect). By exerting a shear, we disturb the particles from their equilibrium configuration. The Brownian motion of the particles acts as a restoring force, which tends to restore to equilibrium configuration. Thus it leads to a weak elasticity of the suspension. The applied shear, also influences the flow field around each particle which in turn

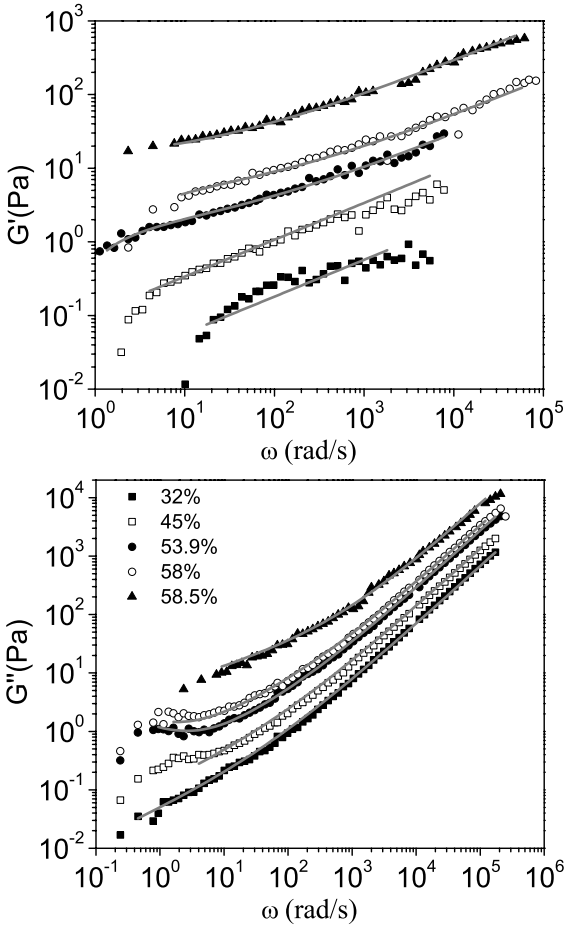

Figure A.2: The shear moduli of several concentration of hard spheres with diameter 397 nm. The complex shear moduli are fitted according to Eq. (A.9)

affects the particles motion (hydrodynamic interactions). The hydrodynamic interactions become important specially when the particles come close together, since expelling the fluid from the gap between two colloids costs energy.

Using Stokesian computer simulations of hard spheres, Brady and coworkers [201] have shown that at high frequencies the Brownian motion does not have

sufficient time to contribute to the shear stress. Therefore the high frequency viscosity consists only of the hydrodynamic contribution. The disappearance of the Brownian contribution leads to a viscosity reduction and therefore shear thinning.

At very short times the localized motion of individual spheres (with the full details of hydrodynamic interactions) determines the high frequency viscoelastic behavior, while at relatively long times for high enough volume fractions particles are trapped in 'cages' by their neighbors. The changes in the configuration of these cages provides a mechanism for energy storage and dissipation, contributing to the shear moduli.

Mason et. al. [199] have suggested to add up these contributions of different mechanisms of energy storage and dissipation, to determine the frequency behavior of the shear moduli. The contribution due to hydrodynamic interactions and Brownian motion has been calculated by Brady [202] using a 'free drainage' approximation for the hydrodynamic interactions which ignores lubrication effects. Taking into account lubrication effects causes G' to reach a constant plateau at high frequencies as ω increases[203]. Our data do not show a saturated G' at high frequencies, therefore, we can use the Brady approximation [202]:

$$G^*(\omega) = i\omega\eta'_\infty + G_1(i\omega\tau_D)^{1/2} \tag{A.1}$$

$$G_1 = \frac{3}{5\pi}\frac{k_BT}{R^3}\phi^2 g(2R,\phi) \tag{A.2}$$

where $\tau_D = R^2/D_s$ is determined by the ϕ-dependent short time diffusion coefficient and $g(2R,\phi) = 0.78/(0.64-\phi)$ is the radial distribution function at contact, consistent with the simulations, which show a divergence of $g(2R,\phi)$ at random close packing [195].

To describe the viscoelasticity originating from caging effects in dense suspensions $\phi \geq 0.50$, we take advantage of the mode coupling theory (MCT) formalism, as suggested in [199]. MCT successfully describes the light scattering data from the hard spheres at volume fractions near the glass transition [199]. Assuming that the stress autocorrelation function has the same form as the density correlation function Eq. (A.3), we can get the form of shear moduli at low frequencies. The lowest frequencies measured for our experiments are 0.1 Hz. Hence, we only need to take into account the β relaxation regime. In the β regime the density correlation function is described as [204]:

$$f(q,t) = f_c(q) + h(q)(t/\tau_0)^{-a} \qquad \tau_0 \ll t \ll \tau_\beta \tag{A.3}$$

$$f(q,t) = f_c(q) - Bh(q)(t/\tau_0)^{b} \qquad \tau_\beta \ll t \ll \tau_\alpha \tag{A.4}$$

$$\tau_0 = \frac{S(q)}{D_0 q^2} \tag{A.5}$$

$$\tau_\beta = \tau_0[\frac{\phi - \phi_g}{\phi_g}]^{-\frac{1}{2a}} \tag{A.6}$$

where $a = 0.301$, $b = 0.545$ and $B = 0.963$ are determined from MCT for hard spheres and $f_c(q)$ represents the amplitude of arrested state at ϕ_g. $f_c(q)$ as well as the critical amplitude $h(q)$ are independent of concentration fixed by MCT.

Taking $\tau_0 \approx 10^{-3}s$ as estimated from light scattering experiments on particles of nearly the same as ours ($R = 200$nm) [205], we can estimate the values of τ_β and τ_α. Of course these values are concentration-dependent and are diverging at ϕ_g. For our range of concentrations ($0.5 < \phi < 0.6$), we have $\tau_\beta \succeq 0.02$s and $\tau_\alpha \succeq 8$s. The lowest frequency in our microrheology measurements 0.1 Hz corresponds to 10s.

The suggested form for the stress autocorrelation, assumed to be proportional to the density correlations, is then [199]

$$C_{\sigma\sigma}(t) = f_{\sigma\sigma} + h_{\sigma\sigma}[(t/\tau_0)^{-a} - B(t/\tau_0)^{b}] \tag{A.7}$$

Near the glass transition, contribution of structural relaxation to the complex shear modulus is given by $G_g(\omega) = G_0[i\omega C_{\sigma\sigma}(\omega)]$, where $C_{\sigma\sigma}(\omega)$ is the unilateral complex Fourier transform of the stress autocorrelation function. This leads to

$$G_g(\omega) = G_0 + G_2[\Gamma(1-a)(i\omega\tau_0)^a - B\Gamma(1-b)(i\omega\tau_0)^b] \tag{A.8}$$

Taking the sum of all these contributions, we get the following form for the complex shear modulus of dense hard sphere suspensions

$$G_{total}(\omega) = G_0 + i\omega\eta'_\infty + G_1(i\omega\tau_D)^{1/2} + G_2[\Gamma(1-a)(i\omega\tau_0)^a - B\Gamma(1-b)(i\omega\tau_0)^b] \tag{A.9}$$

The above form describes the viscoelastic behavior of semi-dilute suspensions taking $G_0 = G_2 = 0$.

This is a function with 4 fitting parameters $G_0, G_2, D_s, \eta'_\infty$. In order to reduce the number of fitting parameters, we determine the high frequency viscosity η'_∞ independently from $\lim_{\omega\to\infty} \frac{G''(\omega)}{\omega}$, as demonstrated in Fig. A.3a. In panel b we

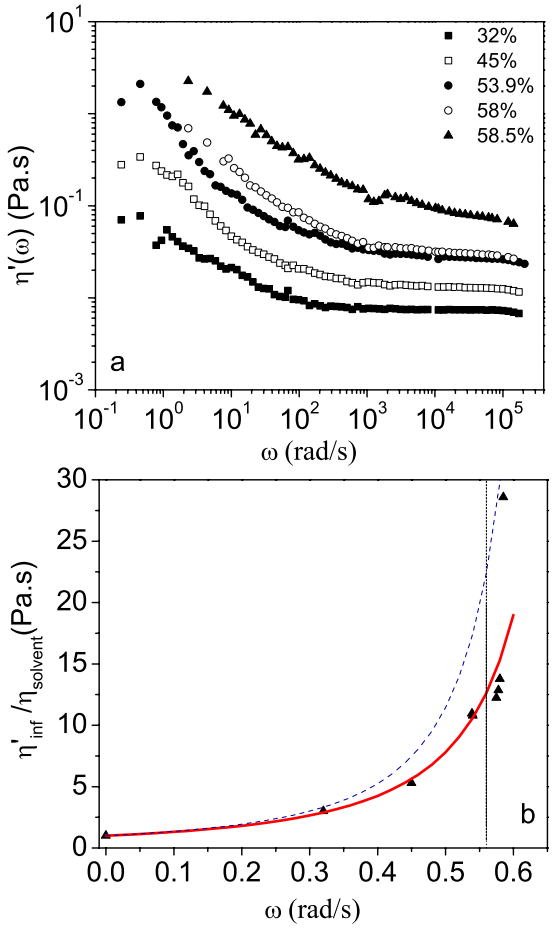

Figure A.3: High frequency shear viscosity as a function of concentration. The dashed and solid line show the Krieger-Dougherty expression Eq. (A.10) and Sierou and Brady formula Eq. (A.11), respectively.

have plotted the reduced high frequency viscosity $\eta'_\infty/\eta_{solvent}$ as a function of volume fraction.

Different equations have been suggested to describe the concentration dependence of high frequency viscosity, here we mention two of them. The first one is

the phenomenological Krieger-Dougherty expression:

$$\eta_\infty = (1 - \phi/0.71)^{-2} \tag{A.10}$$

which fits the experimental data not so well. The more accurate expression is derived by Sierou and Brady [201] which is consistent both with the known exact results in the dilute limit and fits the experimental data on concentrated dispersions.

$$\eta'_\infty/\eta_{solvent} = \begin{cases} \frac{1+\frac{3}{2}\phi[1+\phi(1+\phi-2.3\phi^2)]}{1-\phi[1+\phi(1+\phi-2.3\phi^2)]} & : \quad 0 \leq \phi \leq 0.56 \\ 15.78 \ln \frac{1}{1-1.160\phi^{1/3}} - 42.47 & : \quad 0.60 \leq \phi \leq 0.64 \end{cases} \tag{A.11}$$

We have plotted both expressions in Fig. A.3b. As can be seen from our experimental data, there is a better agreement with Sierou- Brady expression. The small deviations near the glass transition are expected since this expression is not valid for $\phi > 0.56$.

Note that in our data both G' and G'' are increasing functions of frequency in the measured range of frequencies and G' does not reach a saturation value G_∞. This is consistent with the bulk rheology measurements of Van der Werff et. al. [206] and microrheology measurements of Mason et. al. [173] but in contradiction with the bulk rheology results of Shikata et. al. [198] and microrheology measurements of [200]. While the first two groups [206, 173] see a power law behavior for G' at high frequencies, the other two groups [198, 200] see a plateau for G' at high frequencies. Theoretically, the power law behavior at high frequencies is expected if the hydrodynamic interactions between the particles are negligible [207]. Dissimilar high frequency behaviors for different experiments probably originate from the details of interactions between two spheres at close distances; it is likely that not in all experiments the systems behave like hard spheres. Lionberger and Russel [203] have suggested that the stabilizing layers on spheres produce different lubrication forces, therefore hydrodynamic interactions.

The fits according to Eq. (A.9) are shown in Fig. A.2. They describe the data reasonably well, leaving G_0 and G_2 as free parameters. Fig. A.4, shows the concentration dependence of amplitudes and the ratio of short time diffusion to the free diffusion coefficient D_s/D_0 extracted from the fits. We have compared this ratio with the inverse of high frequency relative viscosity, i. e. η_s/η'_∞. They show a similar behavior.

Another phenomenological fit along the same lines used for Laponite suspensions is the simpler form of

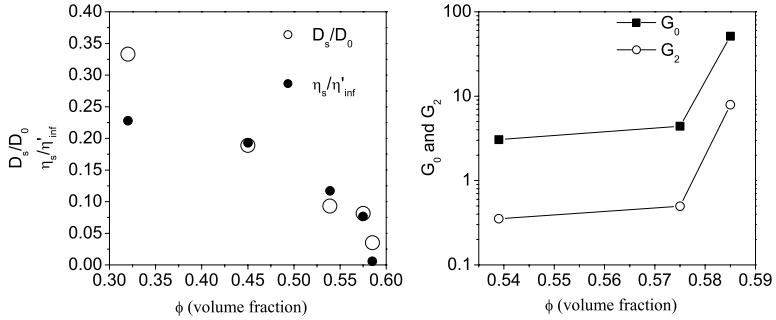

Figure A.4: The concentration-dependence of parameters obtained by the fit according to the equation Eq. A.9

$$G(\omega) = i\omega\eta'_\infty + C_1(i\omega\tau)^a \tag{A.12}$$

which is a special case of the form of Eq. (6.1) with b=1.

The exponent a here changes from 0.5 for the semi-dilute samples to 0.3 for the glass samples. The concentration dependence of the fitting parameters are plotted in Fig. A.5.

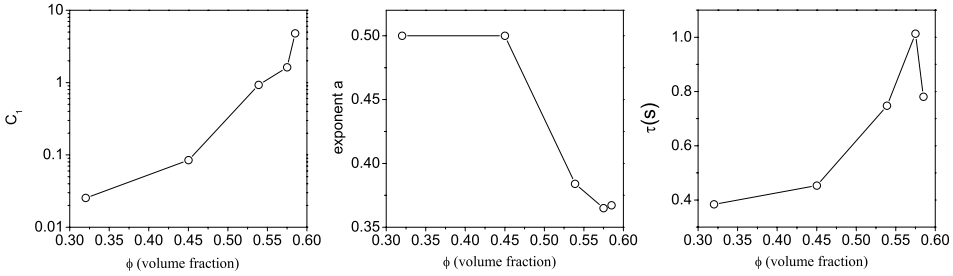

Figure A.5: The concentration-dependence of parameters obtained by the fit according to the equation Eq. (A.12)

This form suggests a superposing of a purely viscous liquid and a viscoelastic fluid. The power law frequency behavior can be interpreted as the sum of a large number of Maxwell modes with different relaxation times [20, 191].

Bibliography

[1] A. J. Liu and S. R. Nagel, *Jamming and Rheology: Constrained Dynamics on Microscopic and Macroscopic Scales*, London: Taylor and Francis, 2000.

[2] M. Cates and M. Evans, *Soft and Fragile Matter: Nonequilibrium Dynamics, Metastability and Flow,*, Institute of Physics Publishing,, 2000, Scottish Universities Summer School in Physics, 53.

[3] L. Cugliandolo, J. Kurchan, and L. Peliti, *Energy flow, partial equilibration, and effective temperatures in systems with slow dynamics*, Phys. Rev. E **55**, 3898 (1997).

[4] R. Kubo, *The fluctuation-dissipation theorem*, Reports on Progress in Physics **29**, 255 (1966).

[5] E. Donth, *The glass transition*, Springer, 2001.

[6] P. A. Egelstaff, *An Introduction to the liquid state*, Academic press, 1967.

[7] H. Vogel, *The law of relation between the viscosity of liquids and the temperature*, Phys. Z. **22**, 645 (1921).

[8] G. S. Fulcher, *Analysis of recent measurements of the viscosity of glasses*, J. Am. Ceram. Soc. **8**, 339 (1925).

[9] G. Tamman and W. Z. Hesse, *The dependence of viscosity upon the temperature of supercooled liquids*, Anorg. Allg. Chem. **156**, 245 (1926).

[10] G. Heuberger and H. Silescu, *Size dependence of tracer diffusion in supercooled liquids*, J. Phys. Chem. **100**, 15255 (1996).

[11] I. Chang, F. Fujara, B. Geil, G. Heuberger, T. Mangel, and H. Sillescu, *Translational and rotational molecular motion in supercooled liquids studied by NMR and forced Rayleigh scattering*, J. Non-Crystal Solids **172**, 248 (1994).

[12] F. Alberici-Kious, J. P. Bouchaud, L. F. Cugliandolo, P. Doussineau, and A. Levelut, *Aging in $K_{1-x}Li_xTaO_3$: A Domain Growth Interpretation*, Phys. Rev. Lett. **81**, 4987 (1998).

[13] L. F. Cugliandolo and J. Kurchan, *On the out-of-equilibrium relaxation of the Sherrington-Kirkpatrick model*, J. Phys. A: Math Gen. **27**, 5749 (1994).

[14] D. B. B. Abou and J. Meunier, *Aging dynamics in a colloidal glass*, Phys. Rev. E **6402** (2001), Part 1 021510.

[15] E. Vincent, J. Hammann, M. Ocio, J.-P. Bouchaud, and L. Cugliandolo, *Complex Behaviour of Glassy Systems*, volume 492, pages 184–219, Springer Verlag Lecture Notes in Physics, 1997, M. Rubi Editor.

[16] P. D. F. Alberici and A. Levelut, *New results about aging in an orientational glass*, Europhys. Lett **39**, 329 (1997).

[17] J. P. Bouchaud, *Weak ergodicity breaking and aging in disordered systems*, J. Phys. I France **2**, 1705 (1992).

[18] P. D. S. Sastry and F. Stillinger, *Signatures of distinct dynamical regimes in the energy landscape of a glass-forming liquid*, Nature **393**, 554 (1998).

[19] G. Biroli and R. Monasson, *From inherent structures to pure states: Some simple remarks and examples*, Europhys. Lett. **50**, 155 (2000).

[20] P. H. P. Sollich, F. Lequeux and M. E. Cates, *Rheology of Soft Glassy Materials*, Phys. Rev. Lett. **78**, 2020 (1997).

[21] H. Sillescu, *Heterogeneity at the glass transition: a review*, J. Non-Crystal. Solids **243**, 81 (1999).

[22] M. D. Ediger, *Spatially heterogeneous dynamics in supercooled liquids*, Annu. Rev. Phys. Chem. **51**, 99 (2000).

[23] R. Richert, *Heterogeneous dynamics in liquids: fluctuations in space and time*, J. Phys.: Condens. Matter **14**, R703 (2002).

[24] L. F. Cugliandolo, *Heterogeneities and local fluctuations in glassy systems*, Noise as a tool for studying materials" (SPIE), Santa Fe, New Mexico (2003), [cond-mat/0401506].

[25] S. C. L. Buisson, L. Bellon, *Intermittency in ageing*, J. Phys.: Condens. Matter **15**, S1163 (2003).

[26] P. Habdas and E. Weeks, *Video microscopy of colloidal suspensions and colloidal crystals*, Curr. Opin. Colloid Interface Sci. **7**, 196 (2002).

[27] L. Cipelletti, H. Bissig, V. Trappe, P. Ballesta, and S. Mazoyer, *Time-resolved correlation: a new tool for studying temporally heterogeneous dynamics*, J. Phys.: Condens. Matter **15**, S257 (2003).

[28] W. K. Kegel and A. van Blaaderen, *Direct observation of dynamical heterogeneities in colloidal hard-sphere suspensions*, Science **287**, 290 (2000).

[29] H. Bissig, S. Romer, L. Cipelletti, V. Trappe, and P. Schurtenberger, *Intermittent dynamics and hyperaging in dense colloidal gels*, Phys. Chem. Comm. **6**, 21 (2003).

[30] H. S. F. Fujara, B. Geil and G. Fleischer, *Translational and rotational diffusion in supercooled orthoterphenyl close to the glass transition*, Z. Phys. B **88**, 195 (1992).

[31] I. Chang and H. Sillescu, *Heterogeneity at the glass transition: translational and rotational self-diffusion*, J. Phys. Chem. B **101**, 8794 (1997).

[32] M. T. Cicerone, P. A. Wagner, and M. D. Ediger, *Translational diffusion on heterogeneous lattices: a model for dynamics in glass forming liquids*, J. Phys. Chem. B **101**, 8727 (1997).

[33] D. B. Hall, A. Dhinojwala, and J. M. Torkelson, *Translationrotation paradox for diffusion in glass-forming polymers: the role of the temperature dependence of the relaxation time distribution*, Phys. Rev. Lett. **79**, 103 (1997).

[34] L. Onsager, *Reciprocal Relations in Irreversible Processes*, Phys. Rev. **37**, 405 (1931).

[35] H. B. Callen and T. A. Welton, *Irreversibility and Generalized Noise*, Phys. Rev. **83**, 34 (1951).

[36] T. M. Nieuwenhuizen, *Thermodynamics of the Glassy State: Effective Temperature as an Additional System Parameter*, Phys. Rev. Lett. **80**, 5580 (1998).

[37] F. R.-T. E. Marinari, G. Parisi and J. J. Ruiz-Lorenzo, *Violation of the fluctuation-dissipation theorem in finite-dimensional spin glasses*, Journal of Physics A **31**, 2611 (1998).

[38] W. Kob and J. L. Barrat, *Fluctuation-dissipation ratio in an aging Lennard-Jones glass*, Europhys. Lett. **46**, 5 (1999).

[39] T. S. Grigera and N. E. Israeloff, *Observation of Fluctuation-Dissipation-Theorem Violations in a Structural Glass*, Phys. Rev. Lett. **83**, 5038 (1999).

[40] S. C. L. Bellon and C. Laroche, *Violation of the fluctuation-dissipation relation during the formation of a colloidal glass*, Europhys. Lett. **53**, 511 (2001).

[41] P. Wang, C. M. Song, and H. A. Makse, *Dynamic particle tracking reveals the ageing temperature of a colloidal glass*, Nature Physics **2**, 526 (2006).

[42] P. N. Pusey and W. van Megen, *Observation of a glass transition in suspensions of spherical colloidal particles*, Phys. Rev. Lett. **59**, 2083 (1987).

[43] R. E. Courtland and E. R. Weeks, *Direct visualization of ageing in colloidal glasses*, J. Phys.: Condens. Matter **15**, S359 (2003).

[44] P. Pusey and W. van Megen, *Phase behavior of concentrated suspensions of nearly hard colloidal spheres*, Nature **320**, 340 (1986).

[45] T. Eckert and E. Bartsch, *Re-entrant Glass Transition in a Colloid-Polymer Mixture with Depletion Attractions*, Phys. Rev. Lett. **89**, 125701 (2002).

[46] K. N. Pham, S. U. Egelhaaf, P. N. Pusey, and W. C. K. Poon, *Glasses in hard spheres with short-range attraction*, Phys. Rev. E **69**, 011503 (2004).

[47] S. H. Chen, W. R. Chen, and F. Mallamace, *The glass-to-glass transition and its end point in a copolymer micellar system*, Science **300**, 619 (2003).

[48] A. Mourchid, A. Delville, and P. Levitz, *Sol-gel transition of colloidal suspensions of anisotropic particles of laponite*, Faraday Discussions **101**, 275 (1995).

[49] M. Kroon, G. H. Wegdam, and R. Sprik, *Dynamic light scattering studies on the sol-gel transition of a suspension of anisotropic colloidal particles*, Phys. Rev. E **54**, 6541 (1996).

[50] D. Bonn, H. Kellay, H. Tanaka, G. Wegdam, and J. Meunier, *Laponite: What is the difference between a gel and a glass?*, Langmuir **15**, 7534 (1999).

[51] T. Nicolai and S. Cocard, *Dynamic light-scattering study of aggregating and gelling colloidal disks*, J. Colloid Interface Sci. **244**, 51 (2001).

[52] B. Ruzicka, L. Zulian, and G. Ruocco, *Routes to Gelation in a Clay Suspension*, Phys. Rev. Lett. **93**, 258301 (2004).

[53] F. Schosseler, S. Kaloun, M. Skouri, and J. P. Munch, *Diagram of the aging dynamics in laponite suspensions at low ionic strength*, Phys. Rev. E **73** (2006), Part 1, 021401.

[54] J. Bergenholtz and M. Fuchs, *Nonergodicity transitions in colloidal suspensions with attractive interactions*, Phys. Rev. E **59**, 5706 (1999).

[55] L. Fabbian, W. Götze, F. Sciortino, P. Tartaglia, and F. Thiery, *Ideal glass-glass transitions and logarithmic decay of correlations in a simple system*, Phys. Rev. E **59**, R1347 (1999).

[56] K. Dawson, G. Foffi, M. Fuchs, W. Götze, F. Sciortino, M. Sperl, P. Tartaglia, T. Voigtmann, and E. Zaccarelli, *Higher-order glass-transition singularities in colloidal systems with attractive interactions*, Phys. Rev. E **63**, 011401 (2000).

[57] F. Sciortino, *Disordered materials - One liquid, two glasses*, Nat. Mater. **1**, 145 (2002).

[58] W. C. K. Poon, *Colloidal glasses*, MRS Bulletin **29**, 96 (2004).

[59] K. A. Dawson, *The glass paradigm for colloidal glasses, gels, and other arrested states driven by attractive interactions*, Curr. Opin. Colloid Interface Sci. **7**, 218 (2002).

[60] S. Tawari, D. Koch, and C. Cohen, *Electrical Double-Layer Effects on the Brownian Diffusivity and Aggregation Rate of Laponite Clay Particles*, J. Colloid Interface Sci. **240**, 54 (2001).

[61] D. W. Thompson and J. T. Butterworth, *The nature of Laponite and its aqueous dispersions*, J. colloid interface sci. **151**, 236 (1992).

[62] P. Levitz, E. Lecolier, A. Mourchid, A. Delville, and S. Lyonnard, *Liquid-solid transition of Laponite suspensions at very low ionic strength: Long-range electrostatic stabilisation of anisotropic colloids*, Europhys. Lett. **49**, 672 (2000).

[63] D. Bonn, H. Tanaka, H. Kellay, G. Wegdam, and J. Meunier, *Aging of a colloidal "Wigner" glass*, Europhys. Lett. **45**, 52 (1998).

[64] A. Mourchid, A. Delville, J. Lambard, E. Lecolier, and P. Levitz, *Phase-Diagram Of Colloidal Dispersions Of Anisotropic Charged-Particles - Equilibrium Properties, Structure, And Rheology Of Laponite Suspensions*, Langmuir **11**, 1942 (1995).

[65] H. Tanaka, J. Meunier, and D. Bonn, *Nonergodic states of charged colloidal suspensions: Repulsive and attractive glasses and gels*, Phys. Rev. E **69**, 031404 (2004).

[66] H. Tanaka, S. Jabbari-Farouji, J. Meunier, and D. Bonn, *Kinetics of ergodic-to-nonergodic transitions in charged colloidal suspensions: Aging and gelation*, Phys. Rev. E **71** (2005).

[67] P. Mongondry, J. F. Tassin, and T. Nicolai, *Revised state diagram of Laponite dispersions*, J. Colloid Interface Sci. **283**, 397 (2005).

[68] B. Ruzicka, L. Zulian, and G. Ruocco, *Ergodic to non-ergodic transition in low concentration Laponite*, J. Phys.: Condens. Matter **16**, S4993 (2004).

[69] G. W. S. Jabbari-Farouji and D. Bonn, *Experimental observation of the intricate free-energy landscape for a soft glassy system*, cond-mat/0611546, submitted to Phys. Rev. Lett.

[70] B. Abou and F. Gallet, *Probing a Nonequilibrium Einstein Relation in an Aging Colloidal Glass*, Phys. Rev. Lett. **93**, 160603 (2004).

[71] D. Bonn and W. K. Kegel, *Stokes-Einstein relations and the fluctuation-dissipation theorem in a supercooled colloidal fluid*, J. Chem. Phys. **118**, 2005 (2003).

[72] J. D. Jackson, *Classical Electrodynamcis, third edition*, John Wiley and Sons, 1999.

[73] H. C. van de Hulst, *Light Scattering by Small Partciles*, Dover, 1981.

[74] B. J. Berne and R. Pecora, *Dynamic Light Scattering*, Dover, 2000.

[75] J. K. G. Dhont, *An Introduction to Dynamics of Colloids*, Elsevier, 1996.

[76] M. Born and E. Wolf, *Principles of Optics*, Pergamon, sixth edition edition, 1980.

[77] J. S. Pedersen, *Analysis of small-angle scattering data from colloids and polymer solutions: modeling and least square fitting*, Adv. Colloid Interface Sci. **70**, 171 (1997).

[78] M. R. I. Weiner and T. D. Donnelly, *Particle size determination: An undergraduate lab in Mie scattering*, Am. J. Phys. **69**, 129 (2001).

[79] F. Perrin, J. de Phys. et Rad. **V**, 497 (1934).

[80] H. Shimizu, *Effect of molecular shape of nuclear magnetic relaxation*, J. Chem. Phys. **62**, 765 (1962).

[81] P. N. Pusey and W. Van Megen, *Dynamic Light-Scattering By Non-Ergodic Media*, Physica A **157**, 705 (1989).

[82] W. van Megen, S. M. Underwood, and P. N. Pusey, *Nonergodicity parameters of colloidal glasses*, Phys. Rev. Lett. **67**, 1586 (1991).

[83] C. Macosko, *Rheology: principles, measurements, and applications*, VCH, New York, 1994.

[84] R. Larson, *The structure and rheology of complex fluids*, Oxford University, New York, 1999.

[85] J. Ferry, *Viscoelastic properties of polymers*, Wiley, New York, 1980.

[86] T. G. Mason and D. A. Weitz, *Optical Measurements of Frequency-Dependent Linear Viscoelastic Moduli of Complex Fluids*, Phys. Rev. Lett. **74**, 1250 (1995).

[87] F. Gittes, B. Schnurr, P. D. Olmsted, F. C. MacKintosh, and C. F. Schmidt, *Microscopic viscoelasticity: Shear moduli of soft materials determined from thermal fluctuations*, Phys. Rev. Lett. **79**, 3286 (1997).

[88] L. Hough and H. D. Ou-Yang, *Correlated motions of two hydrodynamically coupled particles confined in separate quadratic potential wells*, Phys. Rev. **E 65**, 021906 (2001).

[89] J. C. Crocker, M. T. Valentine, E. R. Weeks, T. Gisler, P. D. Kaplan, A. G. Yodh, and D. A. Weitz, *Two-Point Microrheology of Inhomogeneous Soft Materials*, Phys. Rev. Lett. **85**, 888 (2000).

[90] A. D. Dinsmore, E. R. Weeks, V. Prasad, A. C. Levitt, and D. A. Weitz, *Three-dimensional confocal microscopy of colloids*, Applied Optics **40**, 4152 (2001).

[91] E. R. Weeks, J. C. Crocker, A. C. Levitt, A. Schofield, and D. A. Weitz, *Three-dimensional direct imaging of structural relaxation near the colloidal glass transition*, Science **287**, 627 (2000).

[92] T. G. Mason, K. Ganesan, J. H. van Zanten, D. Weitz, and S. C. Kuo, *Particle Tracking Microrheology of Complex Fluids*, Phys. Rev. Lett. **79**, 3282 (1997).

[93] W. van Megen, T. C. Mortensen, and S. R. Williams, *Measurement of the self-intermediate scattering function of suspensions of hard spherical particles near the glass transition*, Phys. Rev. E **58**, 6073 (1998).

[94] M. Gardel, M. Valentine, and D. Weitz, *Microscale Diagnostic Techniques*, chapter Microrheology, Springer, 1st edition, 2003, ed. K. Breuer.

[95] F. C. MacKintosh and C. F. Schmidt, *Microrheology*, Current Opinion In Colloid Interface Science **4**, 300 (1999).

[96] M. J. Solomon and Q. Lu, *Rheology and dynamics of particles in viscoelastic media*, Current Opinion In Colloid Interface Science **6**, 430 (2001).

[97] A. Mukhopadhyay and S. Granick, *Micro- and nanorheology*, Current Opinion In Colloid Interface Science **6**, 423 (2001).

[98] M. Atakhorrami, J. I. Sulkowska, K. M. Addas, G. H. Koenderink, J. X. Tang, A. J. Levine, F. C. MacKintosh, and C. F. Schmidt, *Correlated fluctuations of microparticles in viscoelastic solutions: Quantitative measurement of material properties by microrheology in the presence of optical traps*, Phys. Rev. E **73** (2006), Part 1 061501.

[99] F. C. M. D. Mizuno and C. F. Schmidt, *Active and Passive Microrheology*, preprint (2006).

[100] A. Ashkin, *Forces Of A Single-Beam Gradient Laser Trap On A Dielectric Sphere In The Ray Optics Regime*, Biophysical Journal **61**, 569 (1992).

[101] A. Ashkin, *Optical trapping and manipulation of neutral particles using lasers*, Proceedings Of The National Academy Of Sciences Of The United States Of America **94**, 4853 (1997).

[102] A. Ashkin, *Forces of a single-beam gradient laser trap on a dielectric sphere in the ray optics regime*, in *Methods In Cell Biology*, volume 55, pages 1–27, 1998.

[103] P. A. M. Neto and H. M. Nussenzveig, *Theory of optical tweezers*, Europhys. Lett. **50**, 702 (2000).

[104] D. Vossen, *Optical tweezers in concentrated colloidal dispersions*, Ph.d. thesis, University of Utrecht, 2004.

[105] F. Gittes and C. F. Schmidt, *Interference model for back-focal-plane displacement detection in optical tweezers*, Optics Letters **23**, 7 (1998).

[106] M. Atakhorrami, *High bandwidth microrheology of complex fluids and biopolymer networks*, Phd thesis, Vrije Universiteit Amsterdam, 2006.

[107] A. J. Levine and T. C. Lubensky, *Two-point microrheology and the electrostatic analogy*, Phys. Rev. E **65** (2002), Part 1 011501.

[108] E. D. Zanotto, *Do cathedral glasses flow?*, Am. J. Phys. **66**, 392 (1998).

[109] E. D. Zanotto, *Do cathedral glasses flow?Additional remarks*, Am. J. Phys. **67**, 260 (1999).

[110] L. Leuzzi and T. M. Nieuwenhuizen, *Inherent structures in models for fragile and strong glass*, Phys. Rev. E **64**, 066125 (2001).

[111] F. S. C. Donati and P. Tartaglia, *Role of Unstable Directions in the Equilibrium and Aging Dynamics of Supercooled Liquids*, Phys. Rev. Lett. **85**, 1464 (2000).

[112] M. Bellour, A. Knaebel, J. L. Harden, F. Lequeux, and J. P. Munch, *Aging processes and scale dependence in soft glassy colloidal suspensions*, Phys. Rev. E **67** (2003), Part 1 031405.

[113] D. A. Weitz, J. S. Huang, M. Y. Lin, and J. Sung, *Limits of the Fractal Dimension for Irreversible Kinetic Aggregation of Gold Colloids*, Phys. Rev. Lett. **54**, 1416 (1985).

[114] T. Nicolai and S. Cocard, *Light scattering study of the dispersion of laponite*, Langmuir **16**, 8189 (2000).

[115] D. Bonn, P. Coussot, H. T. Huynh, F. Bertrand, and G. Debregeas, *Rheology of soft glassy materials*, Europhys. Lett. **59**, 786 (2002).

[116] B. Ruzicka, L. Zulian, and G. Ruocco, *More on the phase diagram of laponite*, Langmuir **22**, 1106 (2006).

[117] T. Nicolai and S. Cocard, *Structure of gels and aggregates of disk-like colloids*, European Physical Journal E **5**, 221 (2001).

[118] M. Carpineti and M. Giglio, *Spinodal-type dynamics in fractal aggregation of colloidal clusters*, Phys. Rev. Lett. **68**, 3327 (1992).

[119] L. Cipelletti, s. Manley, R. C. Ball, and D. A. Weitz, *Universal Aging Features in the Restructuring of Fractal Colloidal Gels*, Phys. Rev. Lett. **84**, 2275 (2000).

[120] F. Pignon, A. Magnin, J. M. Piau, B. Cabane, P. Lindner, and O. Diat, *Yield stress thixotropic clay suspension: Investigations of structure by light, neutron, and x-ray scattering*, Phys. Rev. E **56**, 3281 (1997).

[121] W. van Ketel, C. Das, and D. Frenkel, *Structural Arrest in an Ideal Gas*, Phys. Rev. Lett. **94**, 135703 (2005).

[122] J. Israelachvili, *Intermolecular and surface forces*, Academic Press, 2 edition, 1997.

[123] L. Li, L. Harnau, S. Rosenfeldt, and M. Ballauff, *Effective interaction of charged platelets in aqueous solution: Investigations of colloid Laponite suspensions by static light scattering and small-angle x-ray scattering*, Phys. Rev. E **72**, 051504 (2005).

[124] F. Sciortino, S. Mossa, E. Zaccarelli, and P. Tartaglia, *Equilibrium Cluster Phases and Low-Density Arrested Disordered States: The Role of Short-Range Attraction and Long-Range Repulsion*, Phys. Rev. Lett. **93**, 055701 (2004).

[125] P. N. Segrè, V. Prasad, A. B. Schofield, and D. A. Weitz, *Glasslike Kinetic Arrest at the Colloidal-Gelation Transition*, Phys. Rev. Lett. **86**, 6042 (2001).

[126] A. Mourchid, E. Lecolier, H. V. Damme, and P. Levitz, *On viscoelastic, birefringent, and swelling properties of Laponite clay suspensions: Revisited phase diagram*, Langmuir **14**, 4718 (1998).

[127] A. Mourchid and P. Levitz, *Long-term gelation of laponite aqueous dispersions*, Phys. Rev. E **57**, R4887 (1998), Part A.

[128] N. Willenbacher, *Unusual Thixotropic Properties of Aqueous Dispersions of Laponite RD*, J. Colloid Interface Sci. **182**, 501 (1996).

[129] A. Knaebel, M. Bellour, J.-P. Munch, V. Viasnoff, F. Lequeux, and J. L. Harden, *Aging behavior of Laponite clay particle suspensions*, Europhys. Lett. **52**, 73 (2000).

[130] R. Bandyopadhyay, D. Liang, H. Yardimci, D. A. Sessoms, M. A. Borthwick, S. G. J. Mochrie, J. L. Harden, and R. L. Leheny, *Evolution of Particle-Scale Dynamics in an Aging Clay Suspension*, Phys. Rev. Lett. **93**, 228302 (2004).

[131] M. Dijkstra, J.-P. Hansen, and P. A. Madden, *Statistical model for the structure and gelation of smectite clay suspensions*, Phys. Rev. E **55**, 3044 (1997).

[132] S. Kutter, J.-P. Hansen, M. Sprik, and E. Boek, *Structure and phase behavior of a model clay dispersion: A molecular-dynamics investigation*, J. Chem. Phys. **112**, 311 (2000).

[133] S. Mossa, C. D. Michele, and F. Sciortino, *Aging in a Laponite colloidal suspension: A Brownian dynamics simulation study*, J. Chem. Phys. **126**, 014905 (2007).

[134] N. Olivi-Trana, P. Lenormand, A. Lecomte, and A. Dauger, *Molecular Dynamics approach of solgel transition:Comparison with experiments*, Physica A **354**, 10 (2005).

[135] M. T. A. Bos and J. H. J. van Opheusden, *Brownian dynamics simulation of gelation and aging in interacting colloidal systems*, Phys. Rev. E **53**, 5044 (1996).

[136] M. E. C. A. M. Puertas, M. Fuchs, *Aging in attraction-driven colloidal glasses*, cond-mat/0603666.

[137] S. Jabbari-Farouji, E. Eiser, G. H. Wegdam, and D. Bonn, *Ageing dynamics of translational and rotational diffusion in a colloidal glass*, J. Phys.: Condens. Matter **16**, L471 (2004).

[138] W. Gotze and L. Sjogren, *Relaxation Processes In Supercooled Liquids*, Reports On Progress In Physics **55**, 241 (1992).

[139] E. Levitz and J.-P. Korb, *Probing glass transition of clay colloids by NMR relaxometry: Interplay between fluid Brownian dynamics and particle jamming*, Europhys. Lett. **70**, 684 (2005).

[140] S. C. Glotzer, *Spatially heterogeneous dynamics in liquids: insights from simulation*, Journal of Non-Crystalline Solids **274**, 342 (2000).

[141] D. Chakrabarti and B. Bagchi, *Decoupling Phenomena in Supercooled Liquids: Signatures in the Energy Landscape*, Phys. Rev. Lett. **96**, 187801 (2006).

[142] L. Berthier, *Time and length scales in supercooled liquids*, Phys. Rev. E **69**, 020201 (2004).

[143] G. Parisi, *Off-Equilibrium Fluctuation-Dissipation Relation in Fragile Glasses*, Phys. Rev. Lett. **79**, 3660 (1997).

[144] L. F. Cugliandolo and J. Kurchan, *Analytical solution of the off-equilibrium dynamics of a long-range spin-glass model*, Phys. Rev. Lett. **71**, 173 (1993).

[145] A. Annibale and P. Sollich, *Spin, bond and global fluctuationdissipation relations in the non-equilibrium spherical ferromagnet*, J. Phys. A: Math. Gen. **39**, 2853 (2006).

[146] I. P. A. Garriga, P. Sollich and F. Ritort, *Universality of fluctuation-dissipation ratios: The ferromagnetic model*, Phys. Rev. E **72**, 056114 (2005).

[147] P. Mayer and P. Sollich, *Observable dependent quasiequilibrium in slow dynamics*, Phys. Rev. E **71**, 046113 (2005).

[148] N. Andrenacci, F. Corberi, and E. Lippiello, *Fluctuation-dissipation relation in an Ising model without detailed balance*, Phys. Rev. E **73**, 046124 (2006).

[149] S. Fielding and P. Sollich, *Observable Dependence of Fluctuation-Dissipation Relations and Effective Temperatures*, Phys. Rev. Lett. **88**, 050603 (2002).

[150] P. Mayer, S. Lonard, L. Berthier, J. P. Garrahan, and P. Sollich, *Activated Aging Dynamics and Negative Fluctuation-Dissipation Ratios*, Phys. Rev. Lett. **96**, 030602 (2006).

[151] S. M. Fielding and P. Sollich, *Equivalence of driven and aging fluctuation-dissipation relations in the trap model*, Phys. Rev. E **67**, 011101 (2003).

[152] Y. Shokef, G. Bunin, and D. Levine, *Fluctuation-dissipation relations in driven dissipative systems*, Phys. Rev. E **73**, 046132 (2006).

[153] N. Xu and C. S. O'Hern, *Effective Temperature in Athermal Systems Sheared at Fixed Normal Load*, Phys. Rev. Lett. **94**, 055701 (2005).

[154] C. S. O'Hern, A. Liu, and S. R. Nagel, *Effective Temperatures in Driven Systems: Static Versus Time-Dependent Relations*, Phys. Rev. Lett. **93**, 165702 (2004).

[155] L. Berthier and J. Barrat, *Fluctuation-dissipation relation in a sheared fluid*, Phys. Rev. E **63**, 012503 (2000).

[156] I. Ono, C. S. O'Hern, D. J. Durian, S. A. Langer, A. J. Liu, and S. R. Nagel, *Effective Temperatures of a Driven System Near Jamming*, Phys. Rev. Lett. **89**, 095703 (2002).

[157] L. Berthier and J. Barrat, *Shearing a Glassy Material: Numerical Tests of Nonequilibrium Mode-Coupling Approaches and Experimental Proposals*, Phys. Rev. Lett. **89**, 095702 (2002).

[158] L. Berthier and J. L. Barrat, *Nonequilibrium dynamics and fluctuation-dissipation relation in a sheared fluid*, The Journal of Chemical Physics **116**, 6228 (2002).

[159] P. Calabrese and A. Gambassi, *Ageing properties of critical systems*, J. Phys. A: Math. Gen. **38**, R133 (2005).

[160] P. Calabrese and A. Gambassi, *On the definition of a unique effective temperature for non-equilibrium critical systems*, J. Stat. Mech.: Theory and Experiment **2004**, P07013 (2004).

[161] T. Harada and S. Sasa, *Equality Connecting Energy Dissipation with a Violation of the Fluctuation-Response Relation*, Phys. Rev. Lett. **95**, 130602 (2005).

[162] P. Ilg and J. L. Barrat, *Effective temperatures in a simple model of non-equilibrium, non-Markovian dynamics*, J. Phys.: Conference Series (Statistical Physics of Ageing Phenomena and the Glass Transition) **40**, 76 (2000).

[163] A. Garriga and F. Ritort, *Mode-dependent nonequilibrium temperature in aging systems*, Phys. Rev. E **72**, 031505 (2005).

[164] G. Diezemann, *Fluctuation-dissipation relations for Markov processes*, Phys. Rev. E **72**, 011104 (2005).

[165] M. Sellitto, *Effective temperature of an aging powder*, Phys. Rev. E **63**, 060301 (2001).

[166] A. Perez-Madrid, D. Reguera, and J. M. Rubi, *Origin of the violation of the fluctuation-dissipation theorem in systems with activated dynamics*, Physica A **329**, 357 (2003).

[167] D. Hérisson and M. Ocio, *Fluctuation-Dissipation Ratio of a Spin Glass in the Aging Regime*, Phys. Rev. Lett. **88**, 257202 (2002).

[168] F. Q. Potiguar and H. A. Makse, *Effective temperature and jamming transition in dense, gently sheared granular assemblies*, European Physical Journal E **19**, 171 (2006).

[169] P. W. C. M. Song and H. A. Makse, *Experimental measurement of an effective temperature for jammed granular materials*, Proceedings Of The National Academy Of Sciences Of The United States Of America **102**, 2299 (2005).

[170] G. D'Anna, P. Mayor, A. Barrat, V. Loreto, and F. Nori, *Observing Brownian motion in vibration-fluidized granular matter*, Nature **424**, 909 (2003).

[171] L. Bellon and S. Ciliberto, *Experimental study of the fluctuation dissipation relation during an aging process*, Physica D **168**, 325 (2002).

[172] B. Abou, P. M. F. Gallet, and N. Pottier, *Fluctuation-dissipation relation in a colloidal glass: frequency and aging time dependence*, cond-mat/0605111.

[173] H. G. T. G. Mason and D. A. Weitz, *Diffusing-wave-spectroscopy measurements of viscoelasticity of complex fluids*, J. Opt. Soc. Am. **A 14**, 139 (1997).

[174] V. Trappe and D. A. Weitz, *Scaling of the Viscoelasticity of Weakly Attractive Particles*, Phys. Rev. Lett. **85**, 449 (2000).

[175] M. L. Gardel, J. H. Shin, F. C. MacKintosh, L. Mahadevan, P. A. Matsudaira, and D. A. Weitz, *Scaling of F-Actin Network Rheology to Probe Single Filament Elasticity and Dynamics*, Phys. Rev. Lett. **93**, 188102 (2004).

[176] W. Hess and R. Klein, *Generalized hydrodynamics of systems of Brownian particles*, Adv. Phys. **32**, 173 (1983).

[177] D. R. Strachan, G. C. Kalur, and S. R. Raghavan, *Size-dependent diffusion in an aging colloidal glass*, Phys. Rev. E **73**, 041509 (2006).

[178] D. Derks, *Colloidal suspensions in shear flow*, PhD thesis, University of Utrecht, 2006.

[179] R. Mehra, *Application of refractive index mixing rules in binary systems of hexadecane and heptadecane with n-alkanols at different temperatures*, Proc. Indian Acad. Sci. (Chem. Sci.) **115**, 147 (2003).

[180] A. H. Krall and D. A. Weitz, *Internal Dynamics and Elasticity of Fractal Colloidal Gels*, Phys. Rev. Lett. **80**, 778 (1998).

[181] M. Buchanan, M. Atakhorrami, J. F. Palierne, and C. F. Schmidt, *Comparing macrorheology and one- and two-point microrheology in wormlike micelle solutions*, Macromolecules **38**, 8840 (2005).

[182] K. M. Addas, C. F. Schmidt, and J. X. Tang, *Microrheology of solutions of semiflexible biopolymer filaments using laser tweezers interferometry*, Phys. Rev. E **70** (2004), Part 1 021503.

[183] M. Buchanan, M. Atakhorrami, J. F. Palierne, F. C. MacKintosh, and C. F. Schmidt, *High-frequency microrheology of wormlike micelles*, Phys. Rev. E **72** (2005), Part 1 011504.

[184] A. J. Levine and T. C. Lubensky, *One- and two-particle microrheology*, Phys. Rev. Lett. **85**, 1774 (2000).

[185] M. Atakhorrami and C. F. Schmidt, *High-bandwidth one- and two-particle microrheology in solutions of wormlike micelles*, Rheologica Acta **45**, 449 (2006).

[186] M. Atakhorrami, G. H. Koenderink, C. F. Schmidt, and F. C. MacKintosh, *Short-time inertial response of viscoelastic fluids: Observation of vortex propagation*, Phys. Rev. Lett. **95** (2005), 208302.

[187] G. H. Koenderink, M. Atakhorrami, F. C. MacKintosh, and C. F. Schmidt, *High-frequency stress relaxation in semiflexible polymer solutions and networks*, Phys. Rev. Lett. **96** (2006), 138307.

[188] L. Starrs and P. Bartlett, *One- and two-point micro-rheology of viscoelastic media*, Journal Of Physics-Condensed Matter **15**, S251 (2003).

[189] D. T. Chen, E. R. Weeks, J. C. Crocker, M. F. Islam, R. Verma, J. Gruber, A. J. Levine, T. C. Lubensky, and A. G. Yodh, *Rheological Microscopy: Local Mechanical Properties from Microrheology*, Phys. Rev. Lett. **90**, 108301 (2003).

[190] S. Jabbari-Farouji, D. Mizuno, M. Atakhorrami, F. C. MacKintosh, C. F. Schmidt, E. Eiser, G. H. Wegdam, and D. Bonn, *Fluctuation-dissipation theorem in an aging colloidal glass*, [cond-mat /0511311], to appear in Phys. Rev. Lett.

[191] S. M. Fielding and M. C. P. Sollich, *Aging and rheology in soft materials*, J. Rheology **44**, 323 (2000).

[192] S. T. Milner, *Dynamical theory of concentration fluctuations in polymer solutions under shear*, Phys. Rev. E **48**, 3674 (1993).

[193] F. Brochard and P. de Gennes, *Dynamical Scaling for Polymers in Theta Solvents*, Macromolecules **10**, 1157 (1977).

[194] S. Cocard, J. F. Tassin, and T. Nicolai, *Dynamical mechanical properties of gelling colloidal disks*, Journal Of Rheology **44**, 585 (2000).

[195] L. V. Woodcock, *Glass transition in the hard-sphere model and Kauzmanns paradox*, Ann. N. Y. Acad. Sci. **37**, 274 (1981).

[196] C. A. Angell, J. H. R. Clarke, and L. V. Woodcock, *Interaction Potentials and Glass Formation: A Survey of Computer Experiments*, Adv. Chem. Phys. **48**, 397 (1981).

[197] C. B. J. Mellema, C. G. de Kruif and A. Vrij, *Hard sphere colloidal dispersions. Mechanical relaxation pertaining to thermodynamic forces*, Rheol. Acta **26**, 40 (1987).

[198] T. Shikata and D. S. Pearson, *Viscoelastic Behavior Of Concentrated Spherical Suspensions*, Journal Of Rheology **38**, 601 (1994).

[199] T. G. Mason and D. A. Weitz, *Linear Viscoelasticity of Colloidal Hard Sphere Suspensions near the Glass Transition*, Phys. Rev. Lett. **75**, 2770 (1995).

[200] I. S. Sohn and R. Rajagopalan, *Microrheology of model quasi-hard-sphere dispersions*, Journal Of Rheology **48**, 117 (2004).

[201] A. Sierou and J. F. Brady, *Accelerated Stokesian Dynamics simulations*, Journal Of Fluid Mechanics **448**, 115 (2001).

[202] J. Brady, *The rheological behavior of concentrated colloidal dispersions*, J. Chem. Phys. **99**, 567 (1993).

[203] R. A. Lionberger and W. Russel, *High-Frequency Modulus of Hard-Sphere Colloids*, Journal of Rheology **38**, 1885 (1994).

[204] W. Götze and L. Sjogren, *Relaxation processes in supercooled liquids*, Rep. Prog. Phys. **55**, 241 (1992).

[205] W. van Megen and S. M. Underwood, *Glass transition in colloidal hard spheres: Measurement and mode-coupling-theory analysis of the coherent intermediate scattering function*, Phys. Rev. E **49**, 4206 (1994).

[206] J. C. van der Werff, C. G. de Kruif, C. Blom, and J. Mellema, *Linear viscoelastic behavior of dense hard-sphere dispersions*, Phys. Rev. A **39**, 795 (1989).

[207] B. Cichocki and B. U. Felderhof, *Linear viscoelasticity of semidilute hard-sphere suspensions*, Phys. Rev. A **43**, 5405 (1991).

Summary

Materials such as slurries, pastes, gels, clay suspensions, foams, emulsions and granular media are ubiquitous in our everyday life. These materials, despite their very different appearance, share many physical properties from a physicist's point of view. Common features of such substances are the absence of flow, their relatively large response to small forces ('soft') and their disordered nature ('glassy'). Therefore, the paradigm of *soft glassy materials* has been used to describe such widely differing materials. Mesoscopic rearrangements due to thermal fluctuations occur rather slowly in such substances. As a result, these systems can show aging meaning that the system properties depend on time; notably the relaxation time of the density fluctuations grows in time.

We aim here to get a deeper insight into the dynamics and non-equilibrium behavior (aging) of soft glassy materials. The soft glassy system investigated in this thesis is a synthetic clay called Laponite. To a good approximation Laponite particles can be considered as rigid disks of 15 nm radius and 1 nm thickness. Laponite is a white powder that dissolves easily in water and evolves from an initially liquid-like ergodic state to a final non-ergodic solid-like state, which looks like a transparent gel.

Here, we have studied the aging dynamics of the translational degrees of freedom of Laponite particles over a wide range of concentrations and salt content using light scattering. The speed of evolution in these system turns out to be a very strong function of the Laponite concentration. The lower the concentration, the longer it takes for the Laponite samples to become non-ergodic. In the free energy landscape picture of glassy systems, the slow dynamics characteristic of these systems is believed to be due to the existence of a complicated free-energy landscape with many local minima. Our studies reveal that there are different paths of evolution through the free energy landscape. However, these paths lead to only two different non-ergodic states at the late stages of aging that we identify as gel (the route mainly taken by low concentration samples) and glass (the route mainly taken by high concentration samples). For the concentrations in between the transition to non-ergodicity can occur in either direction (gel or glass), the system 'hesitates' between two non-ergodic states. It shows that the route towards the gel and glass may wander through an intricate free energy landscape. Furthermore, we provide clear experimental evidence for the distinction of gel and glassy states in the system.

Studying the aging dynamics of rotational degrees of freedom of colloidal gels

and glasses of Laponite, we find that rotational diffusion slows down at a faster rate than translational diffusion in both cases. Furthermore, the rotational degree of freedom evolves in a distinctly different manner in gel and glassy samples, providing us further indications for the distinction between gels and glasses of Laponite suspensions.

We then turn to the question whether a statistical mechanical description of non-equilibrium systems can be developed. In non-equilibrium systems such as aging materials, the validity of the fluctuation-dissipation relation (FDR) can not be taken for granted, as it is strictly valid only in equilibrium. It has been predicted theoretically that the FDR is violated in glasses and suggested that the deviations from the FDR can be quantified with a time-scale-dependent effective temperature. We have studied the validity of the FDR in the form of the Einstein relation in aging colloidal gels and glasses of Laponite and hard sphere colloidal glasses. The use of combined active and passive microrheology allows us to independently measure both the correlation and response functions in a non-equilibrium situation. Contrary to previous reports, we find no deviations from the FDR over several decades in frequency and various aging times for both systems. The effective temperature is simply the bath temperature.

The validity of the FDR allows us to take advantage of the passive microrheology technique to study the viscoelastic properties of colloidal gels and glasses over a wide range of frequencies. Furthermore, by measuring the local shear moduli at different positions of the sample, we can investigate the presence of heterogeneity. Our microrheology measurements reveal differences between gel and glasses from the rheological point of view. While the glass is homogenous on all length scales probed in our experiments ($l > 0.5\mu$m), the colloidal gels show a considerable degree of inhomogeneity that increases as the gel develops into a solid-like state. Thus the picture obtained on the basis of our earlier light scattering experiments is confirmed. In addition, the shear moduli of both colloidal gels and glasses obey a similar frequency behavior which can be described as the sum of two power laws. The origin of this frequency behavior, however, remains an open question.

Samenvatting

Materialen als slurries, pasta's, gelen, klei suspensies, schuimen, emulsies en granulaire materialen zijn alom tegenwoordig in ons dagelijkse leven. Deze materialen, hoewel op het eerste gezicht zeer verschillend, hebben bezien door de bril van de wetenschapper vele eigenschappen gemeenschappelijk. Deze materialen vloeien niet, vertonen een grote response op een relatief kleine mechanische kracht (zachte materie), en bezitten een wanordelijke structuur (glasachtig). Het epitheton zachte glasachtige materialen wordt daarom gebruikt om deze zo verschillende materialen te beschrijven. Herrangschikking op mesoscopische schaal door thermische fluctuaties verloopt zeer langzaam in deze systemen. Zij vertonen daarom verouderingsverschijnselen : de eigenschappen veranderen op een tijdschaal lang ten opzichte van de natuurlijke thermische fluctuaties van de bouwstenen. De relaxatietijd van de dichtheidsfluctuaties wordt verlengd naarmate het verouderingsproces voortschrijdt.

In dit proefschrift bestuderen wij het verouderingsproces van de translationele vrijheidsgraden van Laponiet deeltjes (klei) gesuspendeerd in water met behulp van lichtstrooiing, voor een groot aantal concentraties en enkele concentraties toegevoegd zout. Het tempo van de evolutie blijkt in deze systemen sterk af te hangen van de Laponiet concentratie. Hoe lager de concentratie des te langer is de tijdsduur tot de niet-ergodische toestand. De "trage dynamica" in deze systemen wordt, zoals ook in glazen, toegeschreven aan het gecompliceerde vrije energie landschap met vele locale minima gescheiden door passen met variabele hoogte. Onze studie laat zien dat verschillende paden gevolgd kunnen worden door dit vrije energie landschap. Deze paden leiden echter tot slechts twee niet-ergodische toestanden, die wij identificeren als gel (de route die voornamelijk door de lage concentraties gevolgd wordt) en glas (de route die die voornamelijk door de hoge concentraties gevolgd wordt). Voor de concentraties tussen deze limieten kan de overgang naar de niet-ergodische toestand op twee manieren plaats vinden, deze systemen "aarzelen" tussen beide toestanden. Hoe ingewikkeld de weg door het vrije energie landschap ook kan zijn, het systeem komt de niet-ergodische toestand binnen of als glas of als gel, beiden met een karakteristiek verouderingsproces. Op grond van de experimenten kunnen we een duidelijk experimenteel onderscheid maken tussen gel en glas.

Gedurende het verouderingsproces van de Laponiet suspensies, verloopt het vertagings proces van de rotationele diffusie sneller dan de translationele diffusie. De evolutie van de rotationele vrijhiedsgraden is duidelijk verschillend in de glas

en gel. Dit resultaat is een bevestiging van het verschil in veroudering in gel en glas.

Vervolgens hebben wij bekeken of een statistisch mechanische beschrijving toepasbaar is op deze niet-evenwichtssystemen. In systemen uit evenwicht is de geldigheid van het fluctuatie-dissipatie theorema niet a priori duidelijk. Er zijn theoretische beschouwingen dat het fluctuatie-dissipatie theorema verbroken wordt in glazen. Introductie van een effectieve tijdsafhankelijke temperatuur zou de geldigheid kunnen herstellen. Wij hebben op experimentele wijze getracht de geldigheid van het theorema te toetsen. Twee onafhankelijke metingen van de Einstein relatie in colloidale gelen en glazen van Laponiet en spherische deeltjes. De combinatie van actieve en passieve microrheologie stelde ons in staat om de correlatie- en response-functies te meten in een niet-evenwichtssituatie.. In tegenstelling tot eerdere metingen vinden wij geen afwijkingen van het fluctuatie-dissipatie theorema in een frekwentiegebied van verscheidene decades en voor wachttijden die zich uitstreekken tot in het niet ergodische regime. De effectieve temperatuur blijft gelijk aan de badtemperatuur.

De geldigheid van het fluctuatie-dissipatie theorema stelt ons in staat om met passieve microrheologie de visco-elastische eigenschappen van colloidale glazen en gelen te meten over een groot frekwentiegebied. Omdat deze metingen lokaal zijn , kunnen we de eventuele aanwezigheid van heterogeniteit in het systeem op het spoor komen. In dit aspect laten de microrheologie metingen verschillen zien tussen glas en gel. Glazen zijn homogeen op alle gemeten lengte-schalen ($l > 0.5\mu$m). De gelen daarentegen laten een aanzienlijke inhomogeniteit zien, die toeneemt als de gel vast wordt. Dit bevestigt het beeld dat verkregen is uit de lichtstrooiingsmetingen. De shear moduli van glazen en gelen hebben eenzelfde frekwentie-afhankelijkheid : de som van twee algebrasche machtswetten. De oorsprong van deze frekwentie-afhankelijkheid is nog onduidelijk.

List of Publications

1. *Calculation of four-point correlation function of logarithmic conformal field theory using AdS/CFT correspondence*, S. Jabbari-Farouji, S. Rouhani, Phys. Lett. B. **548**, 237 (2002) [hep-th/0205016].

2. *Ageing dynamics of translational and rotational diffusion in a colloidal glass*, S. Jabbari-Farouji, E. Eiser, G. H. Wegdam, D. Bonn, J. Phys. : Condens. Matter **16**, L471 (2004).

3. *Kinetics of ergodic-to-nonergodic transitions in charged colloidal suspensions: Aging and gelation*, H. Tanaka, S. Jabbari-Farouji; J. Meunier; D. Bonn, Phys. Rev. E **71**, 021402 (2005)

4. *Fluctuation-dissipation theorem in an aging colloidal glass*, S. Jabbari-Farouji, D. Mizuno, M. Atakhorrami, F. C. MacKintosh, C. F. Schmidt, E. Eiser, G. H. Wegdam, D. Bonn, [cond-mat/0511311], accepted for publication in Phys. Rev. Lett. .

5. *Experimental evidence for the intricate free-energy landscape for a soft glassy system*, S. Jabbari-Farouji, G. H. Wegdam, D. Bonn, [cond-mat/0611546] submitted to Phys. Rev. Lett. .

6. *Comparison of viscoelastic properties in colloidal gels and glasses of Laponite* , S. Jabbari-Farouji, M. Atakhorrami, D. Mizuno, E. Eiser, F. C. MacKintosh, G. H. Wegdam, D. Bonn, C. F. Schmidt, manuscript in preparation.

7. *Short-time diffusion dynamics of charged colloidal disks*, S. Jabbari-Farouji, E. Eiser, G. H. Wegdam, D. Bonn, manuscript in preparation.

8. *Experimental study of effective temperature in hard sphere colloidal glasses and colloidal gels*, S. Jabbari-Farouji, D. Mizuno, F. C. MacKintosh, G. H. Wegdam, D. Bonn, C. F. Schmidt, manuscript in preparation.

9. *Gels, Glasses and attractive glasses in Laponite; a phase diagram*, S. Jabbari-Farouji, G. H. Wegdam, D. Bonn, manuscript in preparation.

10. *Rotational dynamics of aging colloidal gels and glasses* , S. Jabbari-Farouji, G. H. Wegdam, D. Bonn, manuscript in preparation.

Acknowledgments

Finally my PhD journey with its all ups and downs has come to an end and has found a metastable state to relax for a while, and now is the time to acknowledge all the people who have helped me on this way and have contributed to the happy moments of my life.

Four and a half years ago, when I met Daniel in Iran, I could not imagine that I would end up doing a PhD in experimental physics. When I heard his talk on "Turbulent drag reduction" I was quite fascinated and thought it might be a good idea to switch from mathematical physics to experimental work and experience a whole new and more realistic world. During my PhD, I have enjoyed discussing science with him, usually coming up with new and creative ideas, and I have learnt a lot from him. Gerard has often been helpful and supportive. He has always been ready to discuss my data and help to make my PhD path smoother. Erika was very helpful with showing me how to work as an experimentalist, especially since I had no experience with working in the lab.

The results presented in this thesis are to a great deal due to very fruitful interactions with my collaborators: Christoph Schmidt, Fred Mackintosh, Maryam Atakhorrami and Daisuke Mizuno at Complex systems group at Vrije Universiteit of Amsterdam. I enjoyed discussing my results with them a lot. First of all I would like to thank Christoph to give me the opportunity to work in his lab and with his fabulous and exciting microrheology setup that I enjoyed a lot. I am also indebted to Maryam and Daisuke for making me familiar with the microrheology technique and teaching me the data analysis and most important of all helping me with performing the experiments. I do especially appreciate the efforts of Daisuke who stayed with me in the lab until midnight and over the weekends in the last days of finishing the experiments. It has been a great pleasure to discuss with Fred, who has always been open and enthusiastic to discuss and helpful for getting a deeper understanding of the data. I would also like to thank Didi for her providing us the PMMA colloids and showing me how to prepare the samples.

I have also enjoyed the occasional discussions with Daan Frenkel, which have been inspiring. I always got excited after talking to him, and I appreciate that despite his busy schedule he allocated some time for me.

My special thanks to Ben who taught me using Mathematica and was always eager to help me to solve my Mathematica problems. I have also found discussing with Rudolf, Theo, Salima, Gerardo and Yves, pretty helpful. I also like to thank peter Verschuren for his guidance and help in the chemistry lab.

Finishing this thesis would not have been possible without encouragements and supports of my supervisors and friends in hectic moments of writing my thesis. I appreciate the availability of Gerard and Daniel to discuss my thesis whenever I needed them and especially Daniel for going through revising my manuscript over and over. I am particularly grateful to my wonderful friends during the tough working days of finishing my thesis. Salima, Grazyna, Sarah, Sharareh and Antje thanks for all your mental support and encouragements to keep on going during those days.

I also would like to thank the committee members of my thesis for their patience to read the preliminary version of my thesis and their valuable and insightful comments. I am especially grateful to Leticia for her extensive list of comments. I benefited a lot from them and it helped me to improve my thesis.

My special thanks the proof-reading team of my friends for their invaluable help in the last stressful moments of finishing my thesis. Antje, Behnaz, Kuba, Maryam and Piotr and Salima I am really glad that I have such nice friends around. Also thanks to Sharareh for the help with some of the figures and Mirjam and Srdjan for the thesis template and Gerard for translating the summary of my thesis. My deepest thanks to kind Kuba, Stan, Salima and Nazly for the help with the cover.

Working in WZI would not have been possible without having a friendly atmosphere. I would like to thank Mark Golden for his good management and the idea of organizing the social club that definitively was very effective to change the atmosphere of WZI after the Asbestos crisis. I remember when I started my PhD here, there were hardly PhD students around. Thanks to Jeroen coming up with the nice idea of international cooking party. I am also very grateful to Rita, Mariet, Roos and Luuk for all their help with the paper work and many other practical matters.

I would like to thank all of my friends and colleagues whom I have had fun and shared my concerns with. First my thanks to the people in the soft matter group that I have shared many of my days with: Asmae, Javier, Kuba, Nazly, Noushine, Oleg, Peter, Rose, Salima and Tracy and people from the ITS: Blandine, Dion, Hakon, Marko and Javier. I am especially grateful to Tracy and Asmae who have always been ready to help and has tried to cheer me up whenever I have been upset, and Salima for her enduring mental support and advice that has been of very great value to me.

I also spent enjoyable moments with my friends at WZI and ITFA during lunch times, Kriterion, movies, parties and many other fun activities: that I would like to mention them in a chaotic order: Alessia, Jérémie, Pasquale (the spiritual leader of the fun activities), Gerardo, Salima, Piotr, Antje, Srdjan, Salvo, Nacho, Nazly,

Mischa, David, Raoul, Kuba, Javier, Rob, Bahar, Sanli, Phil, Sacha, Xerxes, Lisa, Sebastian, Dennis, Inge, Stan, Leonid and Gianni.

Living in a foreign county especially in first years would not be so easy without the presence of fantastic and helpful friends who have helped me at different times and stages of my life. The friends whom I have spent memorable days and shared my concerns and worries with. These friends have always been helpful no matter where they are and how far we are from each other. Farzaneh, I would like to thank you for your supportive presence in my life, especially during hard days. These four and a half years have not made us farther apart but have revealed to me what a treasure you are. Thanks to Sarah for being always kind, sympathetic and supportive to me. If it was not for your persistence, I would not have found you after 7 years, again.

My friends in Amsterdam have also been of a great value to me for all their help and mental support. My warmest thanks to Maryam, whose presence in the airport in my first day of life outside of Iran, was such a big comfort to me. Since then she has always been a good and sympathetic friend and has been available whenever I have needed her support and consultation.

I am deeply grateful to Sharareh and Behaz who filled the greatest parts of my lonely moments in Holland, with all the fun we had together. Sharareh has always been ready to help no matter where she is. I also learnt a lot from her either in preparing a good presentation or cooking and organizing matters. Behnaz has been a great friend to spend time with and share your happy feelings and concerns.

I am very glad that I had such nice flat mates during all these years. I spent pleasant nights and dinners with Ania and Grazyna chatting and talking about our happy and unhappy days.

I would also like to thank my good friends Azadeh, Fatemeh, Leili, Maryam, Neda, Maniya, Saloumeh, Parvaneh, Parastoo, Zahra and Zohreh with whom I have had great time with in Iran and traveling around in Europe. And the last but not the least important ones are my dear parents who have always been supportive and have done their best to provide for me a nurturing environment to follow my wishes. I am grateful to my sister Samaneh and my brothers Sadegh and Saber who have always been thinking of me and have helped whenever they could. Also, I appreciate my uncles and their families who helped me whenever I needed them and especially, when I wanted to leave Iran and come to Holland.

Reviewing the period of my PhD to remember all the people who had a role in my life, I see that lots of people have come and gone and I could list a couple of more pages of names. But, I stop here, and thank and apologize all those whom I have not mentioned.

Abbreviations

Acronym	complete form
AOD	Acousto-Optical Deflector
CCD	Charged-Coupled Device
CHB	Cyclohexyle Bromide
DDLS	Depolarized Dynamic Light Scattering
DIC	Differential Interference Contrast
DLCA	Diffusion-Limited Cluster Aggregation
DLS	Dynamic Light Scattering
FDR	Fluctuation-Dissipation Relation
FDT	Fluctuation-Dissipation Theorem
ICF	Intensity Correlation Function
MCT	Mode Coupling Theory
MR	Microrheology
MSD	Mean Squared Displacement
NMR	Nuclear Magnetic Resonance
PMMA	Poly-Methyl Methacrylate
PSD	Power Spectral Density
QPD	Quantum Photodiode
SLS	Static Light Scattering
VCO	Voltage-Controlled Oscillator
VH	Vertical-Horizontal (polarization vectors)
VV	Vertical-Vertical (polarization vectors)